

# **Chapter 6: Extratropical Stratosphere–troposphere Coupling**

---

## **Chapter Leads:**

Edwin P. Gerber (Courant Institute of Mathematical Sciences, New York University, New York NY, United States)

Patrick Martineau (Research Center for Advanced Science and Technology, The University of Tokyo, Japan)

## **Chapter Co-Authors:**

Blanca Ayarzagüena (Departamento de Física de la Tierra y Astrofísica, Universidad Complutense de Madrid, Madrid, Spain; Instituto de Geociencias (CSIC, UCM), Madrid, Spain)

David Barriopedro (Departamento de Física de la Tierra y Astrofísica, Universidad Complutense de Madrid, Madrid, Spain; Instituto de Geociencias (CSIC, UCM), Madrid, Spain)

Thomas J. Bracegirdle British Antarctic Survey, Cambridge, United Kingdom()

Amy H. Butler (National Oceanic and Atmospheric Administration/Chemical Sciences Laboratory)

Natalia Calvo (Departamento de Física de la Tierra y Astrofísica, Universidad Complutense de Madrid, Madrid, Spain)

Steven C. Hardiman (Met Office Hadley Centre, Exeter, United Kingdom)

Peter Hitchcock (Cornell University, Ithaca NY, United States)

Maddalen Iza (Departamento de Física de la Tierra y Astrofísica, Universidad Complutense de Madrid, Madrid, Spain)

Ulrike Langematz (Institut für Meteorologie, Freie Universität Berlin, Germany)

Hua Lu (British Antarctic Survey, Cambridge, United Kingdom)

Gareth Marshall (British Antarctic Survey, Cambridge, United Kingdom)

Andrew Orr (British Antarctic Survey, Cambridge, United Kingdom)

Froila M. Palmeiro (Departamento de Física de la Tierra y Astrofísica, Universidad Complutense de Madrid, Madrid, Spain; Barcelona Supercomputing Center, Barcelona, Spain)

Seok-Woo Son (School of Earth and Environmental Sciences, Seoul National University, Seoul, South Korea)

Masakazu Taguchi (Department of Earth Science, Aichi University of Education, Kariya, Japan)

## Abstract

This chapter assesses the representation of the two-way coupling between the troposphere and the stratospheric polar vortices in the reanalysis products. This coupling is evaluated over a broad range of time scales, from sub-seasonal to decadal, with a particular emphasis on Sudden Stratospheric Warming (SSW) events, which are among the clearest manifestations of coupling between the tropospheric and stratospheric circulations. Coupled variability on synoptic to seasonal time scales is evaluated by comparing the timing, evolution, and dynamical consistency of SSW events and Final Warming events, and the representation of the Annular Mode indices. Variability on interannual time scales is evaluated by comparing the modulation of sub-seasonal stratosphere-troposphere coupling by El Niño-Southern Oscillation (ENSO) and the Quasi-Biennial Oscillation (QBO). Finally, variability on decadal time scales is evaluated by comparing atmospheric circulation trends driven by the depletion of stratospheric ozone over Antarctica.

As the large scale circulation cannot easily be characterized from direct observations, this chapter has largely focused on the consistency between the reanalyses, asking the question: would the characterization of stratosphere-troposphere coupling provided by a given reanalysis differ from that provided by another? The internal self consistency of reanalyses has also been evaluated, allowing for more objective grading of the reanalyses. In the satellite era, there is generally good agreement among full-input reanalyses (which assimilate all available observations, including satellite measurements) on stratosphere-troposphere coupling on synoptic to interannual time scales. In addition, conventional-input reanalyses (which exclude satellite observations, and hence full-input reanalyses before the introduction of satellites) are fairly consistent as far back as 1958 in the Northern Hemisphere. There is, however, demonstrable evidence of improvement in the more recent reanalyses. While results in prior studies based on older reanalyses will generally not be significantly different from comparable results based on the modern reanalyses, due to large sampling uncertainty, *we strongly recommend that users discontinue use of older reanalyses such as NCEP-R1, NCEP-R2 and ERA-40 since they provide limited data (i.e., lower model top) and are biased with respect to modern products.*

The dominance of sampling uncertainty implies that our assessment of stratosphere-troposphere coupling is limited by the length of the reanalysis records. Consequently, the availability of high quality pre-satellite era reanalysis in the Northern Hemisphere reduces our uncertainty in the tropospheric response to SSWs by approximately 20%.

Among the more modern reanalyses, a consistent trend in the coupled stratosphere-troposphere circulation is found, associated with ozone loss in the Southern Hemisphere. Caution should always be employed in the assessment of decadal variations and trends in stratosphere-troposphere coupling, however, due to changes in the observational network. It is also shown that uncertainties in older and conventional-input reanalyses increase with height, particularly above 10 hPa, and that satellite observations appear to be critical for an assessment of stratosphere-tropospheric coupling in the austral hemisphere. Finally, surface-input reanalyses have also been evaluated. While they should not be used in place of a full-input reanalysis, there is evidence that ERA-20C captures a substantial fraction of the variability between the troposphere and stratosphere, and so may be valuable for research into low frequency variations in stratospheric-troposphere coupling.

# 73 **Contents**

74 <b>6 Extratropical Stratosphere–troposphere Coupling</b>	<b>1</b>
75 <b>Contents</b>	<b>1</b>
76    6.1 Introduction and Key Points . . . . .	2
77    6.2 Context and Background . . . . .	5
78    6.3 Reanalysis Datasets . . . . .	7
79    6.4 Sudden Stratospheric Warming Events . . . . .	8
80      6.4.1 Identifying SSW Events . . . . .	8
81      6.4.2 Characterizing SSW Events . . . . .	11
82      6.4.3 Sampling Uncertainty vs. Reanalysis Uncertainty . . . . .	17
83      6.4.4 Assessing the Internal Consistency of SSW Events in Reanalyses . . . . .	19
84    6.5 Annular Modes . . . . .	22
85      6.5.1 Consistency of the annular mode index across reanalyses in the post and 86                pre-satellite periods . . . . .	22
87      6.5.2 Sampling Uncertainty vs. Reanalysis Uncertainty . . . . .	27
88    6.6 Stratospheric Final Warming Events . . . . .	29
89    6.7 Modulation of Stratosphere-Troposphere Coupling by ENSO and QBO . . . . .	30
90      6.7.1 Troposphere-stratosphere coupling through ENSO . . . . .	32
91      6.7.2 Blocking patterns associated to SSWs and the modulation of ENSO . . . . .	34
92      6.7.3 Nonlinear modulation of the extratropical stratosphere by ENSO and QBO	36
93    6.8 Stratosphere-Troposphere Coupling through the Antarctic Ozone Hole . . . . .	40
94    6.9 Conclusions and Future Work . . . . .	45
95    Detection and classification of major SSW events . . . . .	48
96    List of Acronyms . . . . .	53
97 <b>Bibliography</b>	<b>54</b>

98 **6.1 Introduction and Key Points**

99 In this chapter, we assess the representation of coupling between the troposphere and stratosphere  
100 across all reanalyses, with a focus on interaction through the stratospheric polar vortices. While  
101 this coupling is primarily manifested on daily to seasonal time scales, low frequency modulation  
102 by other modes of internal variability (e.g., the Quasi-Biennial Oscillation) and external forcings  
103 (e.g., stratospheric ozone loss) require an analysis across a wide range of time scales. The global  
104 nature of these low frequency changes also requires consideration of links between variability in  
105 the tropics and extratropics.

106 Our focus on the influence of the stratosphere on tropospheric weather and variability presented  
107 two challenges to this chapter. First, this report has sought to evaluate reanalyses against direct  
108 measurements, ideally measurements that are not assimilated into the reanalyses themselves. The  
109 large scale weather and variability of the troposphere, however, is not easily characterized or veri-  
110 fied with single measurement records. We have attempted to compare with observation-constrained  
111 measures where available, but generally, this chapter evaluates the *consistency of the reanalyses*,  
112 or lack thereof, as opposed to verifying them against some objective standard.

113 A second challenge that we face in this chapter are limitations to our understanding imposed  
114 by the natural variability of the atmosphere. A common theme is the relative importance of sam-  
115 pling errors, associated with the finite length of the reanalysis records, compared to the differences  
116 between the reanalyses themselves. We term the latter a "reanalysis uncertainty", to differentiate  
117 it from the sampling uncertainty. While we find evidence for an improvement in more recent re-  
118 analysis products, overall we find that our characterization of stratosphere-troposphere coupling  
119 is dominated by sampling uncertainty. As such, the choice of one reanalysis over another would  
120 not affect the scientific conclusions of a particular study, with certain exceptions, e.g., the use of  
121 restricted input reanalyses, as documented below.

122 Sampling uncertainty can appear in subtle ways. Stratosphere-troposphere coupling is often  
123 evaluated through the analysis of events that are identified by threshold criteria, e.g., a Sudden  
124 Stratospheric Warming (SSW) is identified by a reversal of the winds at 10 hPa and 60°. As  
125 a result, subtle differences between reanalyses can lead to the identification and examination of  
126 different events. This effectively aliases sampling error into a comparison of reanalyses, giving a  
127 false impression of disagreement between different reanalysis products. To address this concern,  
128 we suggest the use of a uniform set of events when evaluating different reanalysis products.

129 After a brief introduction to stratosphere-troposphere coupling (Section 6.2), we describe the  
130 reanalysis datasets in Section 6.3. We then present our methodology for identifying, character-  
131 izing, and evaluating SSW events in Section 6.4. Stratosphere-troposphere coupling on daily to  
132 seasonal time scales is further evaluated in Sections 6.5 and 6.6, where we evaluate the represen-  
133 tation of the annular modes and final warming events, respectively. Section 6.7 then examines the  
134 modulation of stratosphere-troposphere coupling on interannual time scales by El Niño-Southern  
135 Oscillation (ENSO) and the Quasi-Biennial Oscillation (QBO). Finally, Section 6.8 compares the  
136 representation of the vertical coupling forced by ozone depletion over interdecadal time scales.

137 To aid the reader seeking a quick summary of our chapter, we provide a compact summary  
138 of our key points and recommendations below. For a more detailed summary, we refer the reader  
139 to Section 6.9, where we provide guidelines for future studies making use of reanalysis and offer  
140 suggestions for the development of future reanalysis products.

141 **Key findings**

- In the satellite era (1979-onward), the representation of large scale stratosphere-troposphere circulation is very consistent across all full-input (including satellite observations) reanalyses. On finer scales, the more recent reanalyses (ERA-Interim, JRA-55, MERRA 1 and 2, and to a slightly lesser extent, CFSR/CFSv2) become more clearly superior.
- Our ability to assess and understand stratosphere-troposphere coupling is primarily limited by sampling uncertainty, that is, by the comparatively large natural variability of the circulation relative to the length of the satellite record. As an example, various efforts have sought to characterize the break-down of the polar vortex during a Sudden Stratospheric Warnings (SSW) as a split or displacement event. Methodological differences among the classifications proposed in the literature, however, result in a partial agreement (for two-thirds of SSW events). In contrast, applying the same definition to different reanalyses yields nearly identical results.
- Although measures of stratosphere-troposphere coupling determined from earlier reanalyses are generally not statistically distinct from results obtained with a more recent reanalysis, the more recent products show demonstrable improvement, particularly with respect to internal consistency (e.g., the momentum budget) and at higher levels (10 hPa and above).
- Reanalysis datasets broadly agree on temperture, wind, and wave forcing trends in the austral polar vortex related to ozone depletion from 1979 to 2001. In contrast, there are no discernible trends in Northern Hemisphere polar vortex variability over the same period.
- Pre-satellite era reanalyses (1958-1978) appear to be of good quality in the Northern Hemisphere, and therefore can be used to reduce sampling uncertainty in measures of stratosphere-troposphere coupling by approximately 20%. We emphasize that this represents a more significant reduction in uncertainty than achieved by shifting from an earlier generation reanalysis to a more recent reanalysis.
- Pre-satellite era reanalyses of the Southern Hemisphere are generally of poor quality, and can only be used to reduce sampling uncertainty with great caution.
- A conventional-input (excluding satellite observations) reanalysis of the Northern Hemisphere (JRA-55C) matches full-input reanalyses well up to 10 hPa, supporting the validity of pre-satellite reanalysis products in this hemisphere. JRA-55C's representation of the Southern Hemisphere is not as accurate, suggesting that satellite measurements are more critical in this hemisphere due to the reduced density of conventional observations.
- Surface-input reanalyses have also been evaluated. ERA-20C captures not only the correct statistical climatology of the Northern Hemisphere stratospheric polar vortex, but also much of its actual variability (correctly representing the timing of about half of observed SSWs). This suggests it may be suitable for exploring low-frequency variability of the stratosphere-troposphere coupled system. The representation of the stratospheric vortex in NOAA 20CR v2/v2c, however, is demonstrably poor.

## 180     Recommendations

- We recommend the use of more recent reanalysis products. As a matter of best practice, we urge all users to avoid the use of earlier reanalyses unless there is a specific need. In particular, we note for users that modern reanalyses can be obtained, in addition to their native high-resolution grids, at a coarser resolution that is comparable to that of earlier reanalyses and thus more manageable in size, but which still captures the best representation of the large scale circulation.
- One must exercise great caution in the interpretation of trends in the reanalyses, as they can be spuriously caused by changes in the observations assimilated over time.
- When an extended record is needed to reduce sampling uncertainty, we recommend the use of pre-satellite era reanalyses (1958-1978) in the Northern Hemisphere, but caution against their use in the Southern Hemisphere.
- Due to significant biases in the mean state and variability of the polar vortex in the NOAA 20CR surface-input reanalysis, we do not recommend it for the purpose of investigating stratosphere-troposphere coupling.
- ERA-20C may be suitable, with caution, for exploring the low-frequency variability of the stratosphere-troposphere coupled system.
- As our ability to quantify the large scale coupling between the stratosphere and troposphere is primarily limited by sampling uncertainty, we recommend that future reanalysis products, including ERA5, extend their analysis prior to the satellite era.

200 **6.2 Context and Background**

201 The troposphere and the stratosphere, the two lowermost layers of the Earth's atmosphere, contain  
202 together about 99% of the atmospheric mass. The troposphere is the portion of the atmosphere in  
203 close contact with Earth's surface. It is the region where day-to-day weather systems evolve and  
204 impact human life; in this sense it could be viewed as a boundary layer, albeit one that occupies  
205 roughly 80-90% of the atmospheric mass. The stratosphere is found from about 10-16 km, de-  
206 pending on the latitude, to about 50 km above the surface (Andrews et al., 1987). What sets these  
207 two layers apart is mainly the stability of the layers: whereas temperature decreases with height in  
208 the troposphere at a rate of about 7 K per kilometer – making it nearly neutral to moist convection  
209 – stratospheric temperatures increase with height owing to the absorption of ultraviolet radiation  
210 by ozone. This stratification gave the "sphere of layers" its name.

211 The stratosphere's large stability sets it dynamically apart from the troposphere as it pre-  
212 vents the penetration of atmospheric convection from the surface, and inhibits the propagation  
213 and growth of baroclinic disturbances that make up a great fraction of tropospheric weather. Yet,  
214 depending on the season, it can be a dynamically active region subject to large variability. Large  
215 pole-to-pole temperature gradients favor the formation of strong westerly vortices in the winter  
216 stratosphere (Waugh et al., 2017). These strong westerlies act as a window for the propagation  
217 of tropospheric disturbances, allowing planetary-scale waves to go through while preventing the  
218 propagation of synoptic-scale systems (Charney and Drazin, 1961).

219 When planetary-scale waves propagate vertically from the troposphere to the stratosphere, they  
220 interact with the mean flow and sometimes break (McIntyre and Palmer, 1983, 1984) causing an  
221 irreversible mixing of potential vorticity leading to a long-lasting weakening of the westerly winds.  
222 One of the most extreme examples of stratospheric variability, Sudden Stratospheric Warming  
223 (SSW) events, which are characterized by an abrupt deceleration and reversal of the zonal-mean  
224 zonal wind, are the result of such interactions between planetary-scale waves and the stratospheric  
225 vortex (Matsuno, 1971; Limpasuvan et al., 2004; Polvani and Waugh, 2004).

226 The vortices in the Northern Hemisphere and Southern Hemisphere are known to behave quite  
227 differently. While the Northern Hemisphere vortex is often disturbed by SSW events in December-  
228 January-February, the Southern Hemisphere vortex is more quiescent. These differences are at-  
229 tributable mainly to differences in topography and land-sea temperature contrasts which are known  
230 to generate stronger planetary-scale waves in the Northern Hemisphere (Plumb, 1989, 2010; Ran-  
231 del, 1988). Because of the comparatively weaker wave drag in the Southern Hemisphere, zonal  
232 winds are too strong to allow vertical propagation of waves which limit wave-mean flow interac-  
233 tions and the variability of the vortex (Plumb, 1989).

234 As mentioned earlier, a large fraction of stratospheric variability is the result of temporal fluc-  
235 tuations in planetary-scale wave propagation from the troposphere to the stratosphere. It is there-  
236 fore of great importance to understand how these waves are amplified or reduced in the tropo-  
237 sphere. Garfinkel and Hartmann (2010) has shown that the intensification of wavenumber-1 and  
238 wavenumber-2 waves in the Northern Hemisphere are important precursors of stratospheric polar  
239 vortex weakening. One specific tropospheric circulation pattern, atmospheric blocking, has gar-  
240 nered particular attention due to its ability to modulate planetary-scale wave fluxes. Nishii et al.  
241 (2011), for instance, have shown that there are preferred regions where upward-propagating wave  
242 packets from blocking events can interfere constructively with stationary waves to produce large  
243 bursts of upward-propagating wave activity, ultimately causing SSW events. The role of such in-

terference in modulating stratospheric variability was also discussed in Smith and Kushner (2012).

The coupling between the stratosphere and the troposphere is not limited to an upward coupling where the evolution of the stratosphere is influenced by upward-propagating waves. The coupling is actually two-way. Events of weak stratospheric vortex anomalies, such as SSW events, were shown to affect weather at the surface by, notably, favoring the negative phase of the related North Atlantic Oscillation (NAO) and Northern Annular Mode (NAM) patterns, and shifting the storm track southward (Baldwin and Dunkerton, 2001). This coupling, which is often attributed to balance arguments (e.g., Haynes et al., 1991; Black, 2002) and eddy feedback mechanisms (e.g., Kushner and Polvani, 2004; Song and Robinson, 2004), has implications for the predictability of tropospheric weather. Mounting evidence suggests that the state of the stratosphere influences the skill of numerical weather forecasts (e.g., Baldwin et al., 2003; Sigmond et al., 2013; Tripathi et al., 2015; Domeisen et al., 2019b).

Although the extratropical stratosphere itself has no interannual memory, essentially due to the opacity to wave propagation of the summertime easterly circulation which resets the state of the vortex every year, it does vary on interannual time scales because of dynamical linkages with other modes of atmospheric variability. A clear example of such influence is the connection between ENSO and the fluxes of planetary-scale waves from the troposphere to the stratosphere which can modulate the frequency of SSW events (Cagnazzo and Manzini, 2009; Calvo et al., 2017; Song and Son, 2018; Domeisen et al., 2019a; Weinberger et al., 2019). In fact, the stratosphere can play a significant role in setting the extratropical response to ENSO events (Butler et al., 2015b; Iza and Calvo, 2015; Polvani et al., 2017). Unlike the extratropics, the equatorial stratosphere does possess an intrinsic interannual memory which manifests itself as the Quasi-Biennial Oscillation (QBO). The QBO is characterized by a seesaw between westerly and easterly winds which occurs approximately every 28 months (Baldwin et al., 2001). The QBO can induce interannual variability in the extratropical stratosphere through the modulation of upward fluxes of planetary-scale wave activity in the extratropics (Holton and Tan, 1980) and influence atmospheric circulation at the surface (Gray et al., 2018).

On interdecadal to longer time scales, the stratospheric state is influenced by modes of sea surface temperature variability such as the Atlantic Multidecadal Oscillation (Omrani et al., 2014) and the Pacific Decadal Oscillation (Woo et al., 2015) and anthropogenic forcing. Perhaps the clearest example of human influence to date is the destruction of ozone which cools the polar stratosphere. This perturbation of the stratosphere has in turn affected the tropospheric circulation by inducing a poleward shift of the storm track and jet through changes in wave forcing and wave mean-flow interactions (Orr et al., 2012; Son et al., 2018). Finally, increasing greenhouse gas concentrations continue to cool the stratosphere (e.g., Ramaswamy et al., 2001) (Steiner et al. 2020 in review????), and may ultimately have the largest impact as the ozone hole recovers over the next decades.

A substantial fraction of the progress made in understanding these features of the stratospheric circulation and its coupling to the troposphere is owed to the development of reanalysis data sets which have greatly facilitated the study of the dynamical phenomena that regulate the coupling. Reanalysis systems integrate both forecasts from numerical models and observations through data assimilation to produce a best guess of the true state of the atmosphere. However, as discussed in Chapter 2 (see also Fujiwara et al., 2017), reanalysis data sets differ by the models, observations and assimilation techniques they utilize. As such, they produce different versions of the thermodynamic and kinematic properties of the atmosphere.

As a notable example of the differences in the representation of the stratosphere among reanalyses, Charlton and Polvani (2007), and more recently Butler et al. (2017), have highlighted discrepancies in the onset dates of SSW events between NCEP-NCAR and ERA-40 data sets. However, subsequent studies have revealed that the depiction of the evolution of SSW events is fairly similar among data sets (Martineau and Son, 2010; Palmeiro et al., 2015; Butler et al., 2015a; Martineau et al., 2018b). The biases among reanalyses are limited enough as to not significantly alter our understanding of the physical processes regulating the evolution of SSWs. More generally, vortex variability was also shown to be similar among reanalyses during both strong and weak stratospheric vortex states (Martineau et al., 2016). On interannual time scales, Mitchell et al. (2015) recently compared reanalysis datasets and found a remarkable consistency between them in the context of the variability of the circulation associated with volcanic eruptions, ENSO, QBO and the solar cycle. Despite these recent findings, there is a growing need to better quantify and understand the differences in the representation of atmospheric processes among reanalyses as the number of available data sets grows with the development of more sophisticated reanalyses incorporating advanced modeling and assimilation components.

### 6.3 Reanalysis Datasets

The reanalyses assessed in this chapter are listed in Table 6.1. The reader is referred to Fujiwara et al. (2017) and Chapter 2 for an exhaustive description of reanalyses. Variables analyzed include geopotential height, temperature and three-dimensional wind components, all of which are analyzed on pressure levels.

**Table 6.1:** List of reanalysis data sets compared.

Name	type	Reference
ERA-40	full-input	Uppala et al. (2005)
ERA-Interim	full-input	Dee et al. (2011)
ERA-20C	surface-input	Poli et al. (2016)
JRA-25	full-input	Onogi et al. (2007)
JRA-55	full-input	Kobayashi et al. (2015)
JRA-55C	conventional-input	Kobayashi et al. (2014)
JRA-55AMIP	SSTs only	Kobayashi et al. (2014)
MERRA <sup>b</sup>	full-input	Rienecker et al. (2011)
MERRA-2 <sup>b</sup>	full-input	Gelaro et al. (2017)
NCEP-R1	full-input	Kalnay et al. (1996)
NCEP-R2	full-input	Kanamitsu et al. (2002)
CFSR	full-input	Saha et al. (2010)
CFSv2	full-input	Saha et al. (2014)
20CR v2	surface-input	Compo et al. (2011)
20CR v2c	surface-input	Compo et al. (2011)

<sup>b</sup> For MERRA and MERRA-2, only the assimilated state (ASM) products are used (see discussion in Chapter 2 and Fujiwara et al., 2017).

In order to facilitate the comparison of zonal-mean quantities, a standardized data set of zonal mean dynamical and thermodynamical variables, the S-RIP: Zonal-mean dynamical variables of

311 global atmospheric reanalyses on pressure levels (Martineau, 2017; Martineau et al., 2018c), was  
312 prepared for this chapter and made public at <http://dx.doi.org/10.5285/b241a7f536a244749662360bd7839312>. Details about the variables archived, the grids and numerical methods are provided  
313 in Martineau et al. (2018c). Analyses of the zonal mean circulation in this chapter made use of  
314 this data, with the exception of Section 6.6. Sections 6.4.2, 6.7.1 and 6.7.2, involved additional  
315 analysis of the full three-dimensional circulation.  
316

## 317 6.4 Sudden Stratospheric Warming Events

318 A Sudden Stratospheric Warming is a dramatic breakdown of the climatological stratospheric polar  
319 vortex in the winter hemisphere, first observed in post-war Berlin by Scherhag (1952). The name  
320 itself encapsulates the essential features of these events. They are sudden, or, in the original lan-  
321 guage of Scherhag, explosive: the entire vortex breaks down in a few days, being associated with a  
322 remarkable warming of the winter pole, typically on the order of 10s of degrees Celsius at 10 hPa,  
323 sometimes exceeding 50 or 60. They are primarily a Northern Hemisphere phenomenon, and only  
324 one (in 2002) has been observed in the Southern Hemisphere. We therefore focus exclusively on  
325 SSWs in the Northern Hemisphere.

326 SSWs tend to come in two flavors, splits and displacements. In the former, the climatological  
327 vortex splits into two vortices of similar size at the time of the warming, while in the latter, the  
328 vortex shifts off the pole. In both cases, the vortex(ices) are ultimately sheared apart, leading to  
329 an irreversible mixing of potential vorticity and the deceleration of the polar vortex. Equivalently,  
330 splits are associated with comparatively more wavenumber-2 activity, while displacements are  
331 primarily associated with wavenumber-1. Recent work has suggested that the type of warming  
332 may have significant implications to the mechanism of the warming and its impact on the surface  
333 (Matthewman and Esler, 2011; Esler and Matthewman, 2011; Mitchell et al., 2013) although this  
334 sensitivity is not observed in all studies (Maycock and Hitchcock, 2015; White et al., 2019). While  
335 many SSWs can be characterized unambiguously (e.g., 22 February 1979 is a classic split), a non-  
336 trivial number (roughly 1/3, as we will see) are not so easy to classify. There are also substantial  
337 sampling uncertainty issues, particularly when assessing the influence of anthropogenic forcing  
338 (e.g., Maycock and Hitchcock, 2015).

339 A key result of this section is shown in Table 6.2 and Figure 6.2, where a standardized list  
340 of SSW event dates and classifications for the period 1957 to 2011 are provided. We refer the  
341 reader to the SSW compendium (Butler et al., 2017) for an up-to-date list of SSW events (<https://www.esrl.noaa.gov/csd/groups/csd8/sswcompendium/majorevents.html>). Results of SSW  
342 classification performed independently for each reanalysis are listed in the Appendix, Tables 6.4-  
343 6.7.  
344

### 345 6.4.1 Identifying SSW Events

346 A number of definitions have been proposed to characterize SSWs in reanalyses and models, all  
347 ultimately establishing a key threshold to define the onset of an event. This threshold nature of  
348 SSWs makes them sensitive to subtle differences between the reanalyses (Butler et al., 2015b). For  
349 example, the most commonly used criteria, as adopted by the World Meteorological Organization  
350 (WMO; McInturff, 1978), requires that the zonal mean zonal wind reverses at  $60^\circ$  and 10 hPa. If the  
351 zonal mean winds drop just below zero in one reanalysis, but to only  $+0.1 \text{ ms}^{-1}$  in another, only one  
352 would count as an event (Kim et al., 2017). Given the large variation between SSW events, this can

353 alias sampling error into a comparison of events across reanalyses. In our hypothetical case above<sup>1</sup>,  
354 a trivial difference in the reanalysis winds ( $0.1 \text{ ms}^{-1}$  compared to a climatological variability on the  
355 order of  $10 \text{ ms}^{-1}$ ) could mistakenly imply a large difference between two products that are actually  
356 very similar.

357 To account for this issue, we identify a standardized set of SSW dates for use across all re-  
358 analyses. This was obtained by first identifying events for each reanalysis individually, similarly  
359 to Butler et al. (2017), based on a reversal of the daily mean, zonal mean zonal wind at  $60^\circ\text{N}$  and  
360  $10 \text{ hPa}$  from November to April, as listed in Table 6.4. The central date is defined by the day the  
361 daily mean wind first reverses, not necessarily the date on which the instantaneous zonal mean  
362 wind first reverses. Two criteria to ensure events are independent, and not the final reversal of the  
363 polar vortex to its summertime state, are also imposed. Following Charlton and Polvani (2007),  
364 the winds must return to a westerly direction for at least 20 consecutive days between independent  
365 events, and for at least 10 consecutive days prior to April 30.

366 The standard WMO definition also requires a reversal of the temperature gradient at  $10 \text{ hPa}$ .  
367 This gradient reversal is not well defined. Commonly it is interpreted that the zonal-mean temper-  
368 ature at the pole [here,  $87.5^\circ\text{N}$  is used to avoid the singular nature of the zonal mean at  $90^\circ\text{N}$ ] must  
369 exceed the zonal-mean temperature at  $60^\circ\text{N}$ , but this puts a great deal of weight on the temperature  
370 near the pole. In practice, this criterion rarely matters; the stratosphere remains in geostrophic bal-  
371 ance during an SSW, such that a reversal of the  $10 \text{ hPa}$  winds implies a reversal in the temperature  
372 gradients below  $10 \text{ hPa}$ , which are highly correlated with the  $10 \text{ hPa}$  temperatures. Only a few  
373 events would be excluded (two from NCEP R1, and just one from JRA-55, as delineated by the  
374 green boxes in table 6.4). We therefore omit the temperature gradient criterion for classifying SSW  
375 events in this work.

376 To establish the standard set of dates listed in Table 6.2, events were defined when a majority  
377 of the reanalyses identify a SSW around the same time, i.e., prior to 1979, 2 out of 3 reanalyses  
378 must detect the event and post 1979, at least 4 reanalyses must detect the event. The onset date  
379 was then set by taking the median across the dates given by each reanalysis. In recent decades,  
380 the dates rarely vary by more than a day or two across reanalyses, but there are a few events at the  
381 beginning of the reanalysis record, as in December 1965, where the spread was more than a week.  
382 In this case the date was set by the average of the two more modern reanalyses.

383 The frequency and seasonality of SSWs determined from each reanalysis separately were ex-  
384 amined, as detailed in Ayarzagüena et al. (2019). In both periods, historical (1958-1978) and  
385 satellite (1979-2012), there is a good agreement in the mean frequency of SSWs between all re-  
386 analyses. This frequency is very similar in both eras, with 5.9 events per decade for the historical  
387 period and 6.5 events per decade for the satellite period.

388 In contrast, larger differences are found for the seasonality of SSWs. Figure 6.1 shows the  
389 SSW decadal frequency distribution within  $\pm 10$ -day periods. The historical period shows the  
390 largest spread. ERA-40 and JRA-55 display an increasing SSW occurrence from early winter  
391 that maximizes in January and decreases by late winter (Figure 6.1a). On the contrary, the intra-  
392 seasonal distribution of SSWs for NCEP-NCAR shows three sharp maxima in early, mid and late  
393 winter, in agreement with the evolution of the standard deviation of the polar night jet (PNJ) for  
394 this reanalysis.

<sup>1</sup>This case is actually not hypothetical; a similar situation, for example, occurred in February 2002, when MERRA missed an event detected by MERRA2 by only  $0.07 \text{ ms}^{-1}$ .

**Table 6.2:** Sudden Stratospheric Warming dates and classifications, according to the four schemes: D refers to a displacement, S to a split, and U, for an event that was unclassifiable, while W1 and W2 refer to events preceded by wave forcing at that number. The symbol \* indicates that there was disagreement between the reanalyses; a † indicates that only a single reanalysis disagreed (after 1979 only).

date	Seviour	Shibata	Lehtonen	Barriopedro and Calvo
30-Jan-58	D	S	S	W1
17-Jan-60	S*	D*	D*	W1
29-Jan-63	S	S	D*	W2
17-Dec-65	D	D*	D	W1
23-Feb-66	D*	D	S	W1
7-Jan-68	S	S	S	W2
28-Nov-68	D	D	D	W1
13-Mar-69	S*	D	D	W1
2-Jan-70	S	D	D*	W1
18-Jan-71	S	S	S	W2
20-Mar-71	D	D	D	W1
31-Jan-73	S	S	S	W1
9-Jan-77	S	D	S	W1
22-Feb-79	S	S	S	W2
29-Feb-80	D	D	D	W1
4-Mar-81	D	D	D	W1
4-Dec-81	U	D†	D	W1
24-Feb-84	D	D	D	W1
1-Jan-85	S	S*	S	W2
23-Jan-87	D	D	D	W1
8-Dec-87	S	S*	S	W1
14-Mar-88	S	S	S	W1
21-Feb-89	S†	S	S	W2
15-Dec-98	D*	S	D	W1
26-Feb-99	S	S	S	W1
20-Mar-00	U*	D†	D	W2
11-Feb-01	S	D†	S*	W1
31-Dec-01	S	D	D	W1
18-Jan-03	S	S†	S	W1
5-Jan-04	D	D	D	W1
21-Jan-06	D	D	D	W1
24-Feb-07	D	D	D	W1
22-Feb-08	D	D	D	W2
24-Jan-09	S	S	S	W2
9-Feb-10	U*	S	S	W1
24-Mar-10	D	D	D	W1

In the satellite period, the results are similar across reanalyses (Figure 6.1b). For this time period, the maximum occurrence is shifted to late winter in all datasets, unlike the distributions of ERA-40 and JRA-55 in the historical period. Similar differences in the intra-seasonal distribution of events were already documented by Gómez-Escolar et al. (2012) for the pre/post 1979 periods. The distribution of events in the two periods were compared with a two-sample Kolmogorov-Smirnov test: the null hypothesis that both samples came from the same probability distribution can be rejected. This may indicate low frequency variations in the seasonality of SSWs, although we have less confidence in the pre-satellite distribution given differences between reanalyses.

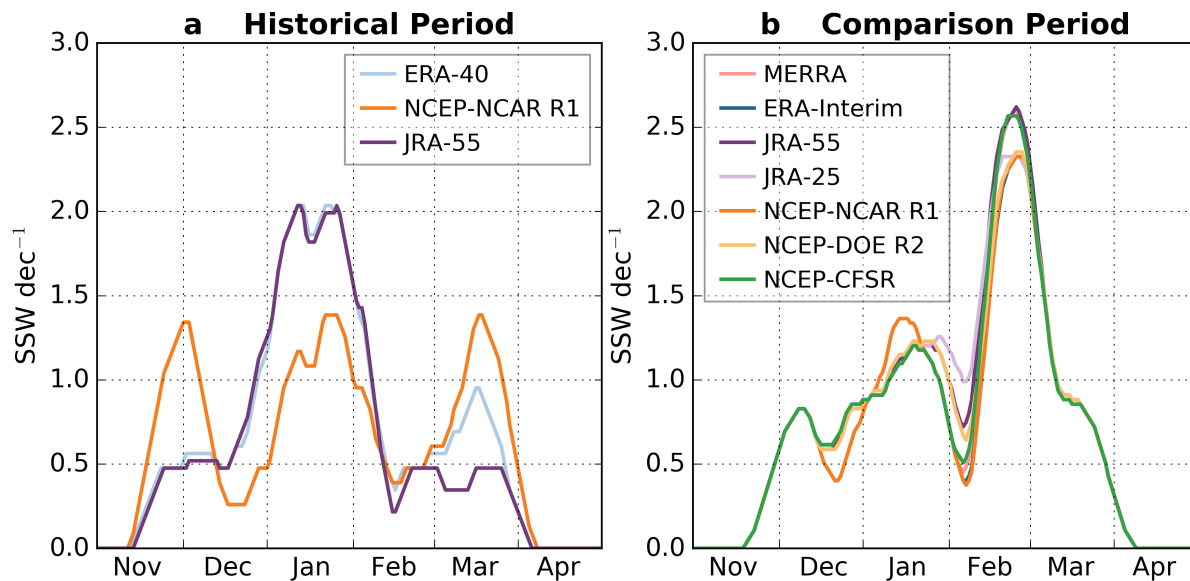


**Figure 6.1:** Decadal frequency distribution of SSW events within  $\pm 10$  day-periods from the date displayed in the axis for: (a) the historic period (1958-1978) and (b) the satellite period (1979-2012). Data was smoothed with a 10-day running mean.

#### 6.4.2 Characterizing SSW Events

Recent work has suggested that there may be fundamental differences between the two types of sudden warmings. For instance, Matthewman et al. (2009) have shown that while split events typically have deep equivalent-barotropic structures, vortex displacement events have clear baroclinic structures. In addition, the impact of the event on the troposphere may differ between the two types of events (e.g., Mitchell et al., 2013). The limited sample size, however, leads to large uncertainty, such that alternative studies come to differing conclusions (e.g., Maycock and Hitchcock, 2015). The topic is further muddled by the fact that different studies have utilized alternative definitions of SSWs, leading to a proverbial apples vs. oranges situation.

To provide greater clarity, while acknowledging that the topic is still an area of active research, we have taken the following approach. First, we consider only wind reversal events: classification schemes were applied to the 36 SSWs identified in the previous subsection. Second, we have applied four alternative classification schemes, described in more detail below, chosen to capture the range of ideas in the current literature. We provide a standardized classification of each event, listed in Table 6.2, based on the agreement of the classification applied separately to each reanalysis.

418 We compare three schemes designed to characterize whether the polar vortex is split (S) or  
419 displaced (D) during the warming event with another classification scheme that focuses primarily  
420 on the wave activity that precedes the vortex breakdown. The three schemes have been tuned to  
421 produce approximately the same rates of S and D events, all three reporting slightly more displace-  
422 ments than splits. The wave based diagnostic is different in that it focuses on the period leading  
423 up to the warming, as opposed to the evolution of the warming itself. It reflects the climatological  
424 dominance of wavenumber 1, classifying a clear majority of the events as wave 1-type. All the  
425 schemes are detailed below.

426 **(1) The Seviour et al. (2013) classification scheme** is based on geometric moment diagnostics  
427 of the geopotential height field at 10 hPa. The use of 10 hPa geopotential heights, which is output  
428 from all reanalyses, makes the scheme more practical than previous moment diagnostic techniques  
429 which rely on isentropic tracers, such as N<sub>2</sub>O or potential vorticity (Waugh, 1997; Waugh and  
430 Randel, 1999; Mitchell et al., 2011, 2013). The Seviour et al. (2013) approach was originally  
431 designed to characterize event dates as well; e.g., a split event was triggered when the aspect  
432 ratio of the vortex remained higher than 2.4 for 7 days or more. However, only half of the major  
433 splits/displacements using this method are in common with those detected using the zonal-mean  
434 zonal wind reversal.

435 We therefore adapted the method to classify reversal events. We apply the same methodology  
436 as in Seviour et al. (2013), but only to days -10 to +10 surrounding the wind reversal. The  
437 diagnostic is based on both the aspect ratio of the vortex (the number of days the aspect ratio is  
438 above 2.4) and the displacement of the centroid (the number of days the centroid of the vortex  
439 stays below 66 degrees latitude). If the latter is greater than the former, then the event is classified  
440 as a displacement. Conversely, if the former is greater than the latter, the event is classified as  
441 a split. If the numbers are equal (or both are zero) we consider the event “unclassifiable”. Note  
442 that if this adapted technique is applied to the events of Seviour et al. (2013), it yields identical  
443 classifications (W. Seviour, personal communication). Table 6.5 shows results based on analysis  
444 of each individual reanalysis.

445 **(2) The "Shibata" scheme** was originally developed by Kiyotaka Shibata, and first described  
446 in Ayarzagüena et al. (2019). It focuses on non-zonal anomalies in the absolute vorticity at 10 hPa  
447 over a 16 day period starting 5 days before the central date of the SSW and ending 10 days later.  
448 Application of this scheme to each reanalysis is listed in 6.6.

449 The method is based on the algorithm suggested by Charlton and Polvani (2007), but with a few  
450 important modifications, as detailed in Ayarzagüena et al. (2019). Briefly, the algorithm identifies  
451 a local maximum in the vorticity. If two vorticity maxima are detected in diametrically opposing  
452 sectors, and the secondary maximum is at least half as strong as the first, the event is classified  
453 as a split. Otherwise it is a displacement. The main differences with the strategy of Charlton and  
454 Polvani (2007) consist in the definition of the sector around the strongest vorticity maximum, and  
455 the fact that the second sector must be located diametrically opposed to the first one.

456 **(3) The Lehtonen and Karpechko (2016) classification**, applied to all reanalyses in table 6.7,  
457 shares features with both of the previous methods. It is based on a analysis of geopotential height  
458 at 10 hPa (as with the Seviour method), but with a goal similar to that of the Shibata approach: to  
459 separate cases where there are two independent vortices (as in a split event) from cases where there  
460 is essentially one vortex at any given time (as in a displacement).

461 The algorithm seeks out the two minima in the 10 hPa geopotential height, spaced apart by at  
462 least 1500 km in the horizontal and separated by a ridge of at least 375 m. If this condition is met

463 on at least three consecutive days over the period -5 to 10 days relative to the event onset, then  
464 the SSW is classified as a split. Otherwise, it is classified as a displacement. These parameters in  
465 the classification were selected to give the best agreement with the classification of major SSWs  
466 during 1958–2002 presented by Charlton and Polvani (2007).

467 Finally, the **(4) Barriopedro and Calvo (2014) method** classifies SSWs into W1 and W2  
468 types by focusing on wave activity over just the period leading up to the SSW. The method, based  
469 on earlier work by Bancalá et al. (2012). It was applied to all reanalyses (with the exception  
470 of MERRA2), and there was universal agreement on the classification of all 36 warmings across  
471 all the datasets. Briefly, this approach considers a Fourier decomposition of geopotential height  
472 anomalies at 50 hPa and 60°N over an 11 day period, days -10 to 0 relative to onset. An SSW is  
473 classified as a wave-2 (W2) event if the amplitude mean over the 11-day period associated with  
474 wave 2 is equal or larger than that of wave 1, or if the wave 2 amplitude mean exceeds that of  
475 wave 1 by 200 m or more for at least one day of the period. Otherwise, the SSW is classified  
476 as a wave-1 (W1) event. In most cases, the former condition determines the type of SSW. The  
477 latter was included because the build up of W2 events is generally more abrupt than W1 events.  
478 The 50-hPa pressure level was chosen because wave 2 reaches its climatological maximum at this  
479 level.

480 As shown in Figure 6.2, 11 of the 36 SSWs observed between 1958 and 2011 are unanimously  
481 classified as splits by all three schemes, and 12 unanimously as displacements. The remaining 13  
482 events differ depending on the classification scheme. These events, however, are more likely to be  
483 classified as a displacement: 8 events were displacements according to 2 of the 3 schemes, while  
484 only 5 were splits according to 2 of the 3 schemes.

485 We find that more than half of split events are preceded by enhanced wavenumber-2 activity  
486 (see the Barriopedro and Calvo (2014) method described above), as one might expect but the rest  
487 do not have prominent wavenumber-2 precursors. These events may correspond to wavenumber-  
488 2 events that are preconditioned by wavenumber-1 forcing (Labitzke, 1977; Bancalá et al., 2012)  
489 which reduces the necessity for large wavenumber-2 forcing prior to the onset in comparison to  
490 “pure” wavenumber-2 events. . Perhaps more surprisingly, 2 displacement events (20-Mar-2000  
491 and 22-Feb-2008) – one that was unambiguous across all classification schemes (the latter) – were  
492 also preceded by enhanced wavenumber-2 forcing.

493 Compared to the timing of event dates, there is more spread in the classification analysis be-  
494 tween different reanalysis products. In a few instances, a tie had to be broken, in which case we  
495 gave greater weight to more modern reanalyses. In addition, the Seviour scheme considers a few (3  
496 of 36) events to be “unclassifiable”, as they reflect too much of a mixture of properties of splits and  
497 displacements. In some cases, an event was unclassifiable for the individual reanalyses; in others,  
498 there was so much spread between products that we felt “unclassifiable” was the most reasonable  
499 designation. The classification schemes were applied to the wind reversal SSW events as follows.

500 There are a number of small differences in the dates and classifications based on individual  
501 reanalyses, as detailed in Tables 6.4, 6.5, 6.6 and 6.7. Hence two studies based exclusively on two  
502 different reanalyses will not find the same SSW frequency, or produce the same composite fields.  
503 We find, however, that these differences are generally not significant if one accounts for sampling  
504 error. That is to say, the differences in the SSW frequency, or event composites, based on the two  
505 different reanalyses, would not be statistically significant.

506 As an example, consider a comparison of the dynamical evolution of W1 and W2 SSWs, clas-  
507 sified with the Barriopedro and Calvo (2014) method, across different reanalyses. Key character-

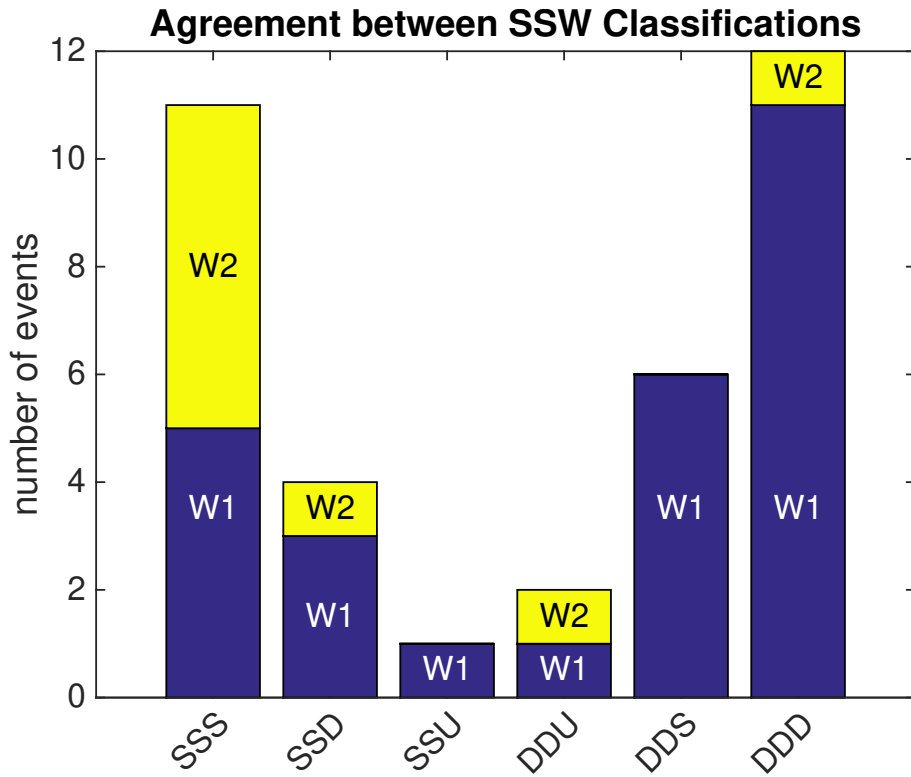


**Figure 6.2:** Agreement between the SSW classification approaches. SSS and DDD refer to cases where all three schemes identified a split, displacement, respectively. SSD refers to cases where two schemes indicate the event is a split while one characterizes it as a displacement, SSU refers to a similar case, but where the third scheme was unable to classify the event, and so forth. Each bar is then divided into cases where the wave amplitude at 50 hPa over the 11 days preceding the event (see the Barriopedro and Calvo (2014) method for more detail) was primarily wave 1 (blue) or 2 (yellow).

istics of SSWs, such as the warming of the lower and middle polar stratosphere, the deceleration of the polar vortex, and the injection of tropospheric wave activity, were compared across reanalyses by Ayarzagüena et al. (2019) based on the diagnostic benchmarks by Charlton and Polvani (2007). Common events were considered to avoid possible discrepancies between reanalyses due to a different sampling. In both the pre- and post satellite periods of comparison, the agreement between datasets is very high. Only small discrepancies are found for the deceleration of the polar vortex at 10hPa in the case of NCEP-R1, particularly in the historical period. These discrepancies are probably related to the lowest model top and vertical resolution of the NCEP-R1 model, since other SSW properties computed at lower levels do not present discrepancies between reanalyses.

As shown in Figure 6.3, anomalous meridional eddy heat flux (HF), averaged between 45° N and 75° N, and its different contributing terms (Nishii et al., 2009) have been computed as a function of height about the onset date of SSWs. Since some previous studies have shown differences in mechanisms triggering different types of SSWs (e.g., Smith and Kushner, 2012; Barriopedro and Calvo, 2014), the heat flux analysis is shown separately for WN1 and WN2 SSWs in the comparison period. The results of the Reanalysis Ensemble Mean (REM) resemble very much those by Smith and Kushner (2012) for D and S events, respectively, despite the lack of a one-to-one correspondence between WN1 (WN2) and D (S) SSWs.

## WN1 SSWs

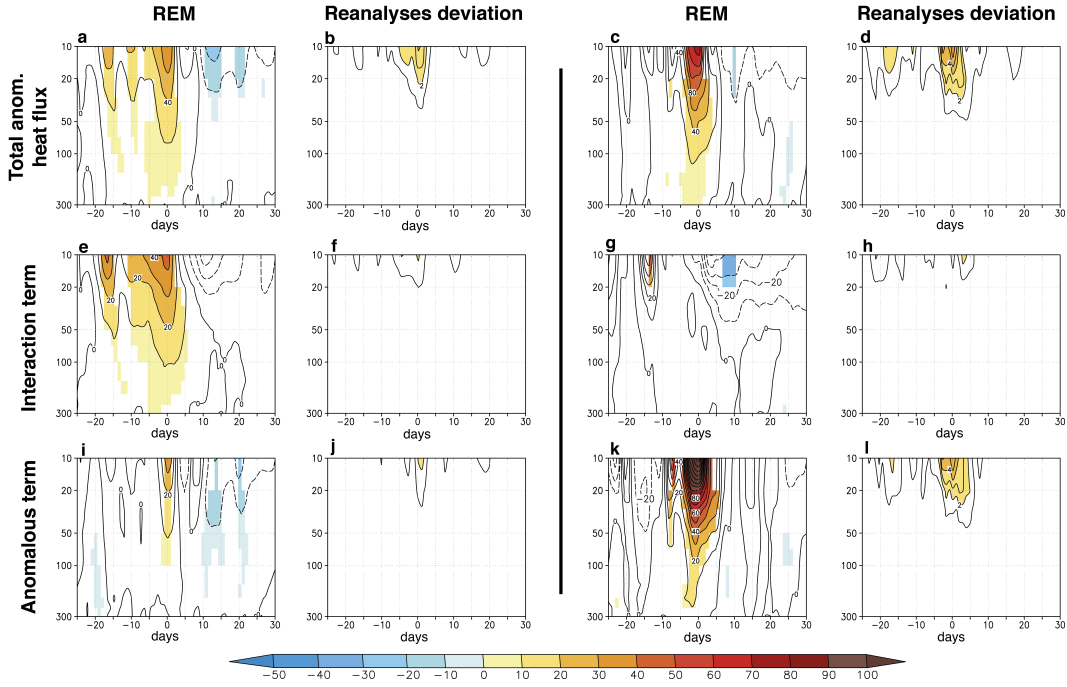


**Figure 6.3:** (a) REM compositing time evolution of the total anomalous eddy heat flux averaged over  $45^{\circ}\text{N}$ - $75^{\circ}\text{N}$  ( $\text{K m s}^{-1}$ ) at different levels from 29 days before to 30 days after the occurrence of WN1 SSWs in the comparison period. Contour interval:  $20 \text{ K m s}^{-1}$ . (b) Same as (a) but for the standard deviation of the reanalyses with respect to the REM. Contour interval:  $2 \text{ K m s}^{-1}$ . (e) and (f) Same as (a) and (b) but for the interaction between climatological and anomalous waves. Contour interval:  $10 \text{ K m s}^{-1}$ . (i) and (j) Same as (a) and (b) but for the contribution of the intrinsic wave activity associated with wave anomalies to the total anomalous heat flux. (c), (d), (g), (h), (k) and (l) Same as (a), (b), (e), (f), (i) and (j) respectively but for WN2 SSWs. Shading in (a), (e), (i), (c), (g) and (k) denotes statistically significantly anomalies at a 95% confidence level (Monte-Carlo test).

525 WN1 events are mainly triggered by the interaction between climatological and anomalous  
 526 waves (Figs. 6.3a, e and i) during persistent and moderately intense peaks of HF anomalies. Con-  
 527 versely, WN2 events are related to intense but short pulses of HF arising from anomalous wave  
 528 packets (Figs. 6.3c, g and k). The comparison among reanalyses results reveals that all datasets  
 529 can reproduce the different mechanisms involved in WN2 and WN1 SSWs. The spread is higher  
 530 for WN2 SSWs than for WN1 SSWs particularly during the days immediately before the occur-  
 531 rence of SSWs (Figs. 6.3b, d, f, h, j, and l). This is probably due to the smaller sample of WN2  
 532 SSWs.

533 The tropospheric circulation associated with the occurrence of WN1 and WN2 SSWs in the  
 534 satellite period has also been explored (Fig. 6.4). The tropospheric patterns preceding the SSWs  
 535 have been computed by analyzing the averaged geopotential height anomalies at 500hPa in the  
 536 [-10,0]-days prior to the central date of each type of SSW, while the surface signal after the oc-  
 537 currence of WN1 and WN2 SSWs has been analyzed by compositing the mean sea-level pressure  
 538 (MSLP) anomalies in the [5,35]-days after these dates. The precursor signals for WN1 SSWs and  
 539 WN2 SSWs show predominant WN1-like and WN2-like structures, respectively, that are similar to

540 the precursors of the most intense events of stratospheric vortex deceleration (Martineau and Son,  
 541 2015). We refer the reader to Cohen and Jones (2011) for earlier precursors. The SSW impact  
 542 shows a negative Northern Annular Mode (NAM) pattern with positive MSLP anomalies over the  
 543 polar cap in both cases, but some differences are found in lower latitudes of the Northeastern Pacific  
 544 and Atlantic basins. The Pacific responses resemble the tropospheric precursor patterns therein,  
 545 suggesting a possible remainder signal. In both cases (precursors and responses), the agreement  
 546 among reanalyses is very good and almost no differences have been detected.

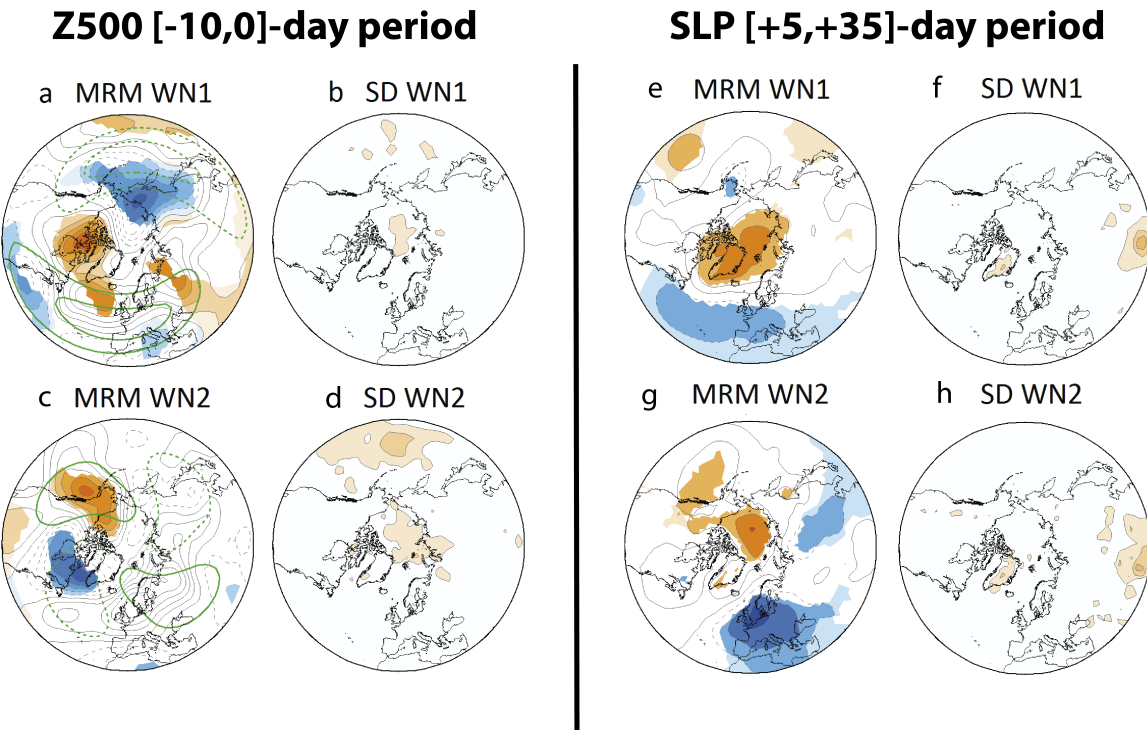


**Figure 6.4:** (a) Multi reanalysis mean (MRM) of WN1 SSW-based composites of 500 hPa geopotential height anomalies (contour interval 20 m) over the [-10, 0] day period before events for the comparison period (1979-2012). Only statistically significant anomalies at the 95% confidence level of the same sign (Monte Carlo test) in at least 66.7% of all reanalyses are shaded. (b) Standard deviation of the reanalyses with respect to the MRM divided by the square root of the number of reanalyses for WN1 SSWs (contour interval is 1 gpm). (c, d) Same as (a) and (b) but for WN2 SSWs, respectively. Green contours in (a) and (c) show the MRM climatological WN1 and WN2 of 500 hPa geopotential height from November to March, respectively (contours:  $\pm 40$  and  $\pm 80$  gpm). To the right, the MSLP is composited over the [5, 35] day period after SSWs. The panels follow the same order as the Z500 precursors. Contour interval is 2 hPa for MRM composites and differences and 0.1 hPa for the standard deviation of the reanalyses.

547 This analysis shows overall very good agreement among reanalyses in the representation of  
 548 the main features, triggering mechanisms and surface fingerprint of SSWs. Despite this, some  
 549 differences are found among reanalyses, particularly in the historical period and concerning the  
 550 NCEP-R1 reanalysis. Before 1979, SSWs in NCEP-R1 show a lower mean frequency and a dif-  
 551 ferent seasonal distribution with respect to JRA-55 and ERA-40 (Fig. 6.1). This disagreement  
 552 also extends to climatological fields and their variability in upper levels. A plausible cause of

553 this discrepancy is the strong artificial temperature trend affecting the early record of NCEP-R1  
 554 (Badin and Domeisen, 2014). Arguably, the characteristics of the reanalysis models play an im-  
 555 portant role in this period, since the number of available data to be assimilated at upper levels is  
 556 limited. Thus, we do not recommend the use of this reanalysis in the historical period for model  
 557 evaluation initiatives.

### 558 6.4.3 Sampling Uncertainty vs. Reanalysis Uncertainty

559 Studies of stratosphere-troposphere coupling are limited by the considerable dynamical variability  
 560 present in both the stratosphere and the troposphere below. This variability introduces considerable  
 561 sampling uncertainty into composite analyses, for example, and it is thus of interest to use all the  
 562 data that is available. The amount of observational data increased considerably after 1979 when  
 563 global satellite observations became broadly available. However, the basic theory underlying the  
 564 occurrence of SSWs was formulated by Matsuno (1971), and several well-known reviews of the  
 565 dynamics of these events were published well before a significant time series of satellite obser-  
 566 vations was available (Labitzke, 1977; McIntyre, 1982), indicating that the observational record  
 567 largely based on radiosondes is of considerable value. This can be expected to be even more the  
 568 case within the troposphere which is more easily observed with radiosondes.

569 Indeed, the uncertainty arising from dynamical variability that is intrinsic to the global circu-  
 570 lation is far larger than the uncertainty arising from observational uncertainty and the process of  
 571 assimilating this data into reanalysis products (Hitchcock, 2019). This is demonstrated in Figure  
 572 6.5. Figure 6.5a shows the time-series of zonal mean zonal wind at 10 hPa, 60 N, around 36 major  
 573 sudden stratospheric warmings from a single reanalysis, JRA-55. Events post 1979 are in solid  
 574 lines, while those prior to 1979 are in dashed lines. The broad spread across events at all lags from  
 575 the central date is evident, and the character of the variability in the two periods is not obviously  
 576 different. This inter-event variability can be compared with the differences for individual events  
 577 across reanalysis products.

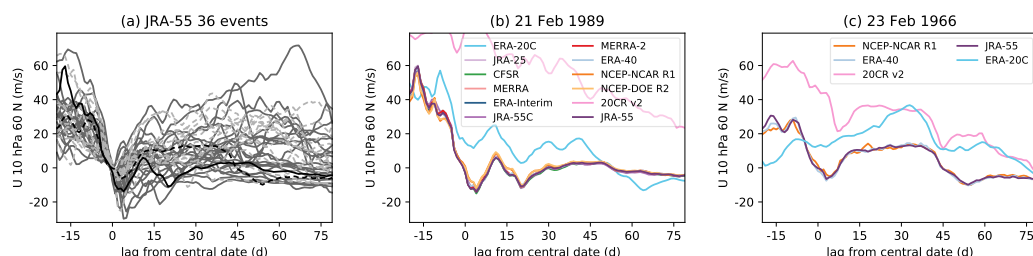


**Figure 6.5:** (a) Zonal winds at 10 hPa and 60N from JRA-55 for 36 sudden warmings. Events from the satellite period are in dark grey, those from the radiosonde period are in light grey and are dashed. (b) Winds for a single satellite-period event for all reanalyses; this event is shown by the black line in (a). (c) Zonal winds at 10 hPa and 60N for a single radiosonde-period event for all reanalyses covering this period; this event is shown by the dashed black line in (a).

578 Figure 6.5b shows the corresponding time series for one event (21 Feb 1989) during the post-  
 579 1979 period, for each of the 12 reanalyses. With the exception of the two reanalyses that ingest only  
 580 surface observations (ERA-20C, 20CR v2), the time-series are nearly indistinguishable relative to  
 581 the inter-event variability highlighted in Figure 6.5a. This is even more the case if one omits NCEP-  
 582 NCAR R1 and NCEP-DOE R2 whose forecast model top lies at 10 hPa. Although relatively few

583 reanalyses extend prior to 1979 (and only one of the more modern products), this close agreement  
 584 holds nearly as well for the pre-1979 period (Figure 6.5c).

585 Including the 21 years from 1958 to 1979, in addition to the 32 years from 1979 through  
 586 2010, can be expected to shrink confidence intervals by a factor of  $\sqrt{32/53} = 0.78$ ; about a 20%  
 587 reduction. For instance, Figure 6.6 shows the impact of including this period on the estimated  
 588 frequency of SSWs. Here the Lehtonen and Karpechko (2016) classification method is used to  
 589 define SSWs. Although not shown, similar results are found for the other classification methods.  
 590 The confidence intervals are generated by a bootstrapping procedure. For instance, for the post-  
 591 1979 period, sets of 32 years chosen at random (with replacement) from the period from 1958  
 592 through 2010; events that happen during these years are then used to generate an overall frequency.  
 593 If a year is chosen multiple times, the events that occurred during these years are also included  
 594 multiple times. This is carried out 10000 times; the 2.5th and 97.5th percentiles then define the  
 595 confidence interval. A similar procedure is used for the confidence intervals on the whole 1958-  
 596 2010 period but using sets of 53 years.

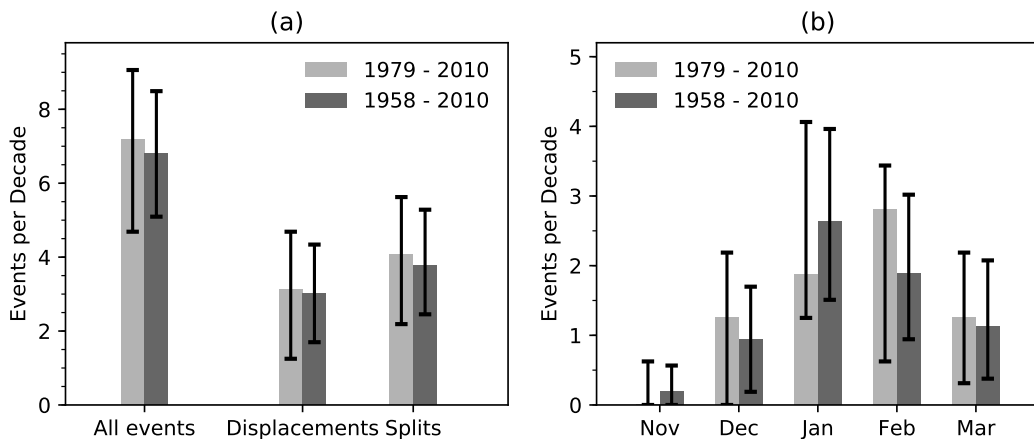


**Figure 6.6:** (a) Frequency of all SSW events, and of events classified as splits or displacements for the satellite period versus the entire period where quality reanalyses are available. (b) Same as (a) but for each month of extended winter. Error bars indicate 95% confidence intervals, see text for details.

597 The resulting confidence intervals are indeed reduced by a factor close to the 20% estimate  
 598 given above. The overall event frequency and the frequency of splits and displacements are some-  
 599 what reduced. The seasonal distribution of events is more substantially affected; within the broader  
 600 record more events occur in January than in any other month; the period from 1979-2010 had  
 601 relatively few January events and relatively many February events resulting in a rather different  
 602 seasonal distribution as shown in Figure 6.1 (though one well within sampling uncertainty).

603 Similar reductions in confidence intervals can be found for more dynamical quantities. Figure  
 604 6.7 shows three such examples. Figure 6.7a shows the anomalous zonal wind, integrated from 1000  
 605 hPa to 100 hPa, from days 5 to 60 following the central date. Figure 6.7b shows the anomalous  
 606 meridional momentum flux, also integrated from 1000 hPa to 100 hPa and averaged from days 5  
 607 to 60 following the central date. Finally Figure 6.7c shows the meridional heat flux at 100 hPa,  
 608 averaged from days -15 to 0, prior to the central date (in red), and averaged from days 5 to 60  
 609 following the central date (in blue). In all cases confidence intervals are generated by a similar  
 610 bootstrapping procedure; however in this case the events themselves are sub-selected, rather than

611 the years.

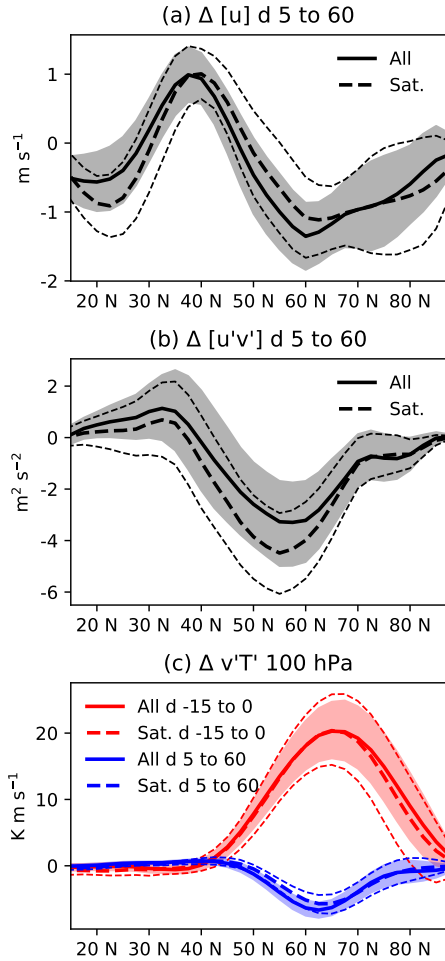


**Figure 6.7:** (a) Composite mean of vertically averaged (100 to 1000 hPa) zonal wind anomalies, averaged over lags 5 to 60 days following major warmings. The solid line shows the composite for all events while the dashed line shows the composite for the satellite era alone. Confidence intervals for the whole period are shaded while those for the satellite era are indicated by thin dashed lines. (b) Similar but for vertically integrated momentum fluxes. (c) Similar but for meridional heat fluxes at 100 hPa, averaged over lags -15 to 0 (in red), and over lags 5 to 60 (in blue).

612 Again, in all cases, including the whole period results in a slightly different meridional struc-  
 613 ture. The low-latitude easterly response is somewhat weaker in Figure 6.7a, the momentum flux  
 614 response is somewhat more positive at all latitudes (Figure 6.7b), and the heat fluxes in the recovery  
 615 period are somewhat more reduced (Figure 6.7c). More importantly, the reduction in confidence  
 616 intervals provides a stronger constraint for dynamical understanding and for model evaluation.

#### 617 6.4.4 Assessing the Internal Consistency of SSW Events in Reanalyses

618 Given that the sampling error tends to overwhelm differences in the representation of SSWs in  
 619 different reanalysis products, we consider an alternative approach to evaluating their fitness: an  
 620 assessment of their internal consistency. Many studies have investigated the evolution of zonal

mean zonal wind using zonal-mean momentum budgets applied to reanalysis data (e.g., Limpasuvan et al., 2004; Martineau and Son, 2015). Reanalysis data sets, however, are known to present biases with respect to observations and with respect to each other. For instance, recent studies by Lu et al. (2015) and Martineau et al. (2016) have highlighted discrepancies among data sets concerning the momentum budget. Here we summarize and show key figures from the analysis of Martineau et al. (2018b), which quantified uncertainties in the zonal momentum budget among the reanalysis data sets.

The comparison is performed among all conventional reanalysis data sets except for ERA-40 whose deficiencies are well documented in the literature (e.g., Martineau et al., 2016) and which terminates in 2002, limiting the sample of SSW events. The common dates identified in Table 6.2, beginning with the 29-Feb-80 event and ending with the 24-Mar-10 event, are used to perform composites of the momentum budget for SSW events. The zonal-mean momentum budget can be written as follows:

$$\frac{\partial \bar{u}}{\partial t} = \underbrace{f\bar{v}}_{f_v} - \underbrace{\frac{1}{a \cos^2 \phi} \frac{\partial (\cos^2 \phi \bar{u}' v')}{\partial \phi}}_{du' v' / dy} - \bar{v} \underbrace{\frac{1}{a \cos \phi} \frac{\partial (\bar{u} \cos \phi)}{\partial \phi}}_{Adv_\phi} - \bar{\omega} \underbrace{\frac{\partial \bar{u}}{\partial p}}_{Adv_p} - \underbrace{\frac{\partial (\bar{u}' \omega')}{\partial p}}_{du' \omega' / dp} + R \quad (6.1)$$

where  $f$  is the Coriolis parameter,  $u$ ,  $v$ ,  $\omega$  are the zonal, meridional, and vertical components of wind,  $\phi$  is the latitude,  $p$  is the pressure, and  $a$  is the mean radius of the Earth (6371 km). Overbars and primes denote zonal mean and anomalies with respect to the zonal mean, respectively. While the left-hand side term expresses the zonal-mean zonal wind tendency, terms of the right-hand side represent forcing terms. They are, in order, the acceleration due to the Coriolis torque, the meridional convergence of momentum fluxes, the advection of zonal momentum by the meridional wind, the vertical advection of zonal momentum by the vertical wind, and the vertical convergence of vertical momentum fluxes. The last term,  $R$ , is referred to as the residual and represents sub-grid scale processes such as gravity wave drag and numerical diffusion. It also includes imbalances in the momentum equation introduced by the data assimilation process (analysis increment), errors due to the interpolation from model levels to pressure levels, and errors related to the numerical methods employed to evaluate each term of the equation. All calculations are based on the zonal-mean data set of global atmospheric reanalyses on pressure levels (Martineau, 2017; Martineau et al., 2018c) which provides dynamical variables on a common  $2.5^\circ$  by  $2.5^\circ$  latitude-longitude grid for all reanalysis datasets at six-hour intervals. The diagnostics presented here are markedly more sensitive to the choice of data set than horizontal resolution (Martineau et al., 2018c).

Figure 6.8 shows the composite evolution of all terms of the zonal-mean momentum equation during SSW events. In addition to the terms evaluated and shown for each individual data set, the standard deviation among an ensemble of the latest reanalysis data (CFSR, ERA-Interim, JRA-55 and MERRA-2) is displayed. SSW events are characterized by an intense deceleration (up to  $-7 \text{ m s}^{-1} \text{ day}^{-1}$  at 3 hPa) of the zonal-mean zonal wind in the mid-stratosphere. Uncertainties in the zonal wind tendency are typically small in comparison to other terms of the momentum equation and are largest several days before the onset date (day 0). The dominant forcing terms are those that are typically included in the quasigeostrophic version of the momentum equation - i.e., the acceleration due to the Coriolis torque and the convergence of meridional fluxes of momentum. These two forcings are strongly opposed, but not completely. Their sum results in a net deceleration before the onset of SSW events. Uncertainties in these forcing terms due to inter-reanalysis discrepancies typically peak several days before the onset of SSW events. Other forcing terms that

are left out of the QG approximation have smaller magnitudes and show better agreement among the reanalyses. Finally, the residual is typically negative before the onset of SSW events, in part due to the exclusion of gravity wave drag from our analysis (Martineau et al., 2016). It becomes more neutral after the onset, suggesting a more dynamically quiet period.

It is worth noting that preceding lag 0, JRA-25 shows a markedly larger residual in comparison to other reanalyses both in the mid and upper stratosphere. This large negative residual may be attributed to an underestimation of deceleration by the Coriolis torque in the mid stratosphere and an overly strong momentum flux convergence in the upper stratosphere in comparison to other reanalyses (not shown, see Martineau et al. (2016) for more details). Note that NCEP-NCAR (R1) and NCEP-DOE (R2) are also clear outliers for these two forcings in the mid-stratosphere. Their residual is however not shown here since vertical motion is not provided in the stratosphere.

The vertical profiles of the forcing terms and their uncertainties are shown in Figure 6.9. Here, the inter-reanalysis standard deviation is shown separately for the ensemble of latest reanalyses and an ensemble of all reanalyses (listed in legend). Overall, all forcing terms display an exponential increase of uncertainties with height in the stratosphere. Again, the Coriolis torque and the convergence of meridional momentum fluxes dominate in terms of uncertainty. It is also noteworthy that uncertainties of the latest reanalysis ensemble are always smaller than the all reanalysis ensemble in the stratosphere which suggests an enhanced consistency in the representation of the atmospheric circulation in the modern reanalysis products.

Martineau et al. (2018a) have noted that not only the mean forcings between the Coriolis torque and momentum flux convergence are strongly opposed, but also the inter-reanalysis discrepancies in the Coriolis torque are often compensated for by inter-reanalysis discrepancies in the momentum fluxes. This results in a seemingly better self-consistency of the momentum equation (small residual) although the disagreement between data sets about the dominant momentum forcing terms can be large. This compensation could be the result of an induced meridional overturning circulation in response to biases in wave drag from planetary waves or gravity waves among the data sets. The meridional overturning circulation is an ageostrophic circulation and is thus not constrained by the thermal structure of the atmosphere like the zonal mean zonal winds which largely obey geostrophic and hydrostatic balance in the extratropics.

The aforementioned results characterized uncertainties of the momentum budget in reanalysis data sets by considering all SSW events but the study of Martineau et al. (2018a) provides a more thorough analysis by investigating differences between SSW events characterized by a split or displacement of the stratospheric polar vortex. The classification is done by both using vortex moment diagnostics (see Section 6.4.2) and by identifying the dominant fluxes of wave activity from the troposphere to the stratosphere (whether dominated by wavenumber 1 or 2) prior to the events. Overall, there is no striking difference in the uncertainties of the momentum budget between these different types of events. It is rather found that the intensity of the event, evaluated by the magnitude of the deceleration of zonal-mean zonal wind prior to the reversal, is more relevant for the agreement between reanalysis data sets. As is somewhat intuitive, the events that showed the strongest deceleration and largest forcing terms were shown to suffer from larger inter-reanalysis uncertainties.

In summary, there is generally a good agreement between the various terms of the zonal-mean momentum budget among reanalysis data sets. The discrepancies are small enough as to not introduce important uncertainties in our understanding of the dynamical evolution of SSW events. Inter-reanalysis uncertainty typically increases exponentially with height as the forcing terms also

707 grow in magnitude. The dominant forcing terms, i.e., momentum flux convergence and the Corio-  
708 lis force, dominate the budget and have the largest uncertainties. The residual also increases with  
709 height, indicative of the greater role played by gravity waves in the momentum budget in the mid-  
710 to-upper stratosphere. Differences in the contribution of gravity waves to the momentum budget  
711 among reanalyses are hard to evaluate since gravity wave drag is not commonly provided for the  
712 reanalysis data sets; we therefore recommend that future data sets provide daily parameterized  
713 gravity wave drag on the standard pressure levels.

## 714 **6.5 Annular Modes**

715 The annular modes have been used to quantify the coupling between the stratosphere and tropo-  
716 sphere, particularly that associated with SSW events (e.g., Thompson and Wallace, 2000; Baldwin  
717 and Dunkerton, 2001; Kushner, 2010). In the troposphere, the annular modes characterize merid-  
718 ional shifts in the extratropical jet streams; a positive index indicates the jet is located poleward  
719 of its climatological position. The jet streams are associated with the extratropical storm tracks,  
720 so that the annular modes are linked with shifts in storm activity, particularly in Northern Europe  
721 and eastern North America (e.g., Thompson and Wallace, 1998). In the stratosphere, the annular  
722 modes chiefly characterize variations in the strength of the polar vortex. A positive index indicates  
723 a stronger than average vortex, so that the breakdown of the vortex in an SSW is associated with  
724 an abrupt shift to a very negative annular mode index in the stratosphere.

725 The negative shift in the stratospheric annular mode index associated with an SSW typically  
726 precedes a similar (albeit weaker) shift towards a negative annular mode index in the troposphere  
727 by a few days (Baldwin and Dunkerton, 2001; Karpechko et al., 2017). The equatorward shift in  
728 the tropospheric jet stream persists on the order of 30 to 60 days, associated with the slow recovery  
729 time scale of the lower stratospheric vortex (e.g., Gerber et al., 2010) and potential feedback with  
730 baroclinic eddies in the troposphere (e.g., Song and Robinson, 2004). SSWs are therefore impor-  
731 tant for seasonal to subseasonal forecasts (e.g., Sigmond et al., 2013; Butler et al., 2019; Domeisen  
732 et al., 2019b).

733 In addition, the annular modes have been used to investigate cases where the polar vortex is  
734 stronger than average (Baldwin and Dunkerton, 2001; McDaniel and Black, 2005). These “Polar  
735 Vortex Intensification” events (hereafter strong vortex events) are somewhat of an opposite  
736 analogue to a SSW, but lack a clear, abrupt onset. A stronger than average polar vortex (i.e., a  
737 positive annular mode state in the stratosphere) is typically associated with a poleward shift in the  
738 tropospheric jet (i.e., a positive annular mode in the troposphere).

### 739 **6.5.1 Consistency of the annular mode index across reanalyses in the post and 740 pre-satellite periods**

741 As detailed by Gerber and Martineau (2018), we use a simplified procedure to compute the annular  
742 mode indices from the reanalyses. As proposed by Baldwin and Thompson (2009), the annular  
743 mode index is defined by the polar cap averaged geopotential height (all latitudes poleward of  
744 65°), normalized to have zero mean and unit variance. To ensure that the annular mode indices  
745 characterize meridional shifts in geopotential height at all levels, the global mean geopotential  
746 height on each pressure level is first removed at each time step before computing the polar cap  
747 averages (Gerber et al., 2010). In keeping with the sign convention of Thompson and Wallace  
748 (2000), we also reverse the sign, so that a high index state is associated with a lower than average  
749 polar cap geopotential height.

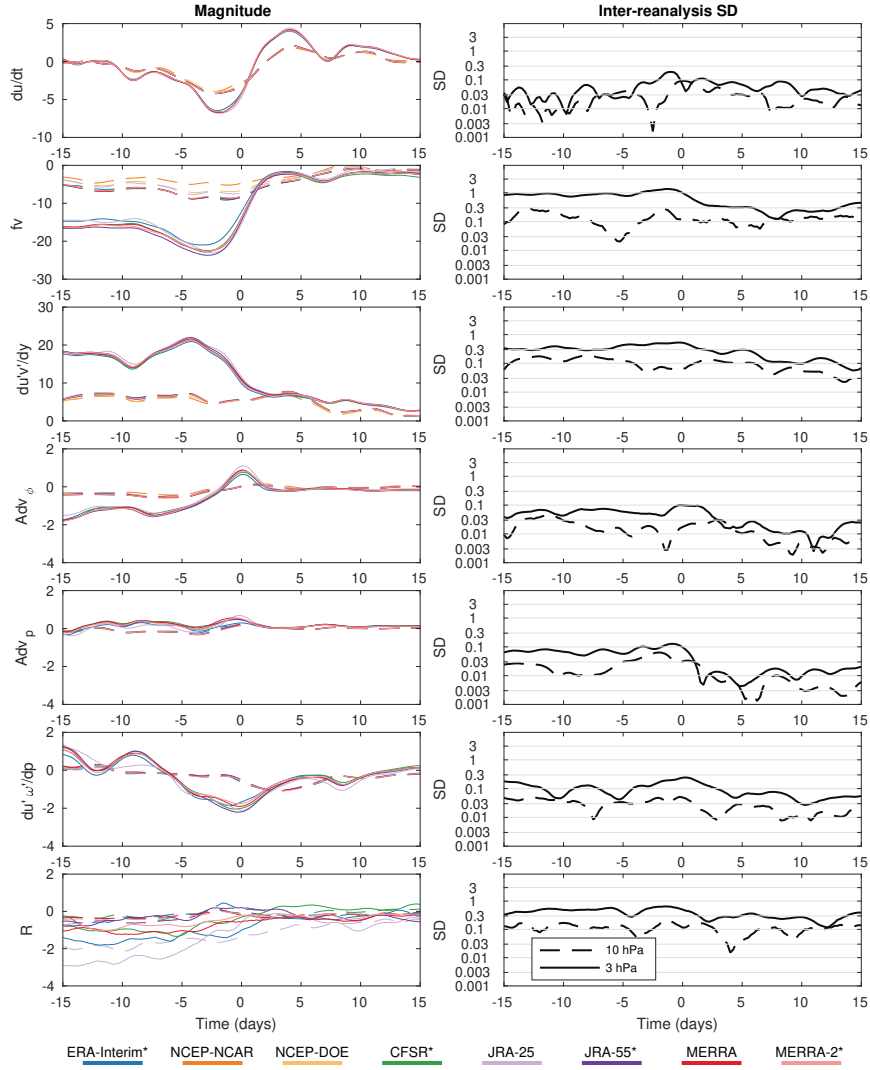


**Figure 6.8:** (a) Evolution of forcing terms of the zonal-mean momentum equation at 10 hPa (dashed lines) and 3 hPa (solid lines) in the course of SSW events. All variables are averaged from 45 to 85°N. Note that the range of the y axis in each panel is different. (b) The inter-reanalysis spread (standard deviation) of the corresponding terms are shown for the latest reanalysis ensemble members (indicated with a \* in the legend). The standard deviation is shown on a logarithmic scale: the spacing between tick marks represents a decrease or increase of the standard deviation by a factor of about 3. All quantities are expressed in  $\text{ms}^{-1}\text{day}^{-1}$ .

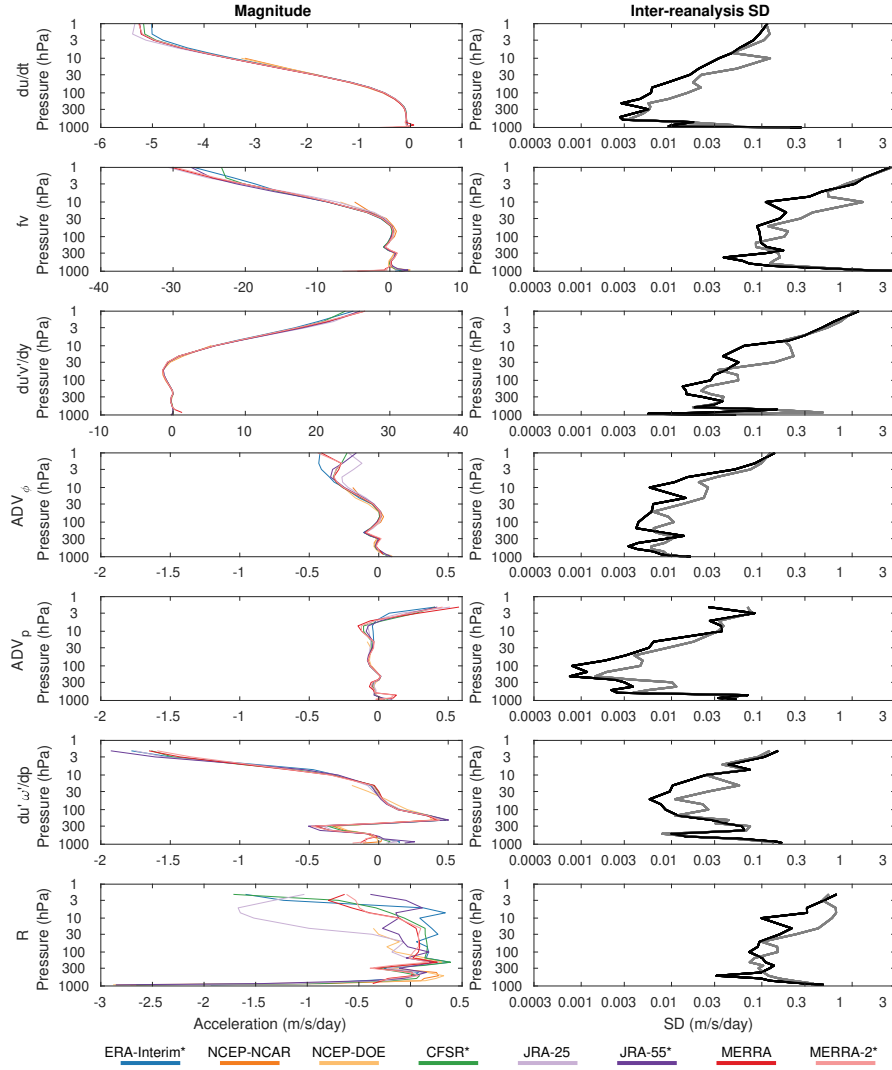


**Figure 6.9:** Vertical profiles of each term in the momentum equation averaged from lags 5 to 0 days before SSW events. All variables are averaged between 45 and 85°N. Individual reanalyses are shown to the left and the inter-reanalysis standard deviation is shown to the right on a logarithmic scale. The latter is shown for all reanalyses (grey) and for just the modern reanalyses (black; indicated with a \* in the legend). All quantities are expressed in units of  $\text{ms}^{-1}\text{day}^{-1}$ .

This definition of the annular mode requires extrapolation of data to pressure levels below the surface in regions of high topography, which was done by the reanalysis centers with the exception of the MERRA products. To avoid introducing extrapolation errors, we omit MERRA and MERRA2 from comparisons below 700 hPa. We focus on a subset of the pressure levels between 1000 and 1 hPa that were shared by all reanalyses. Levels above 10 hPa, however, are unavailable for NCEP-R1/R2 and NOAA 20CR v2/v2c reanalyses.

For the satellite era, 1979 onward, Gerber and Martineau (2018) found that a reanalysis ensemble mean (REM) constructed from the most recent reanalyses (ERA-Interim, JRA-55, and NCEP-CFSR) provided a reliable benchmark for comparison. MERRA2 was not included in the REM due to missing data below 700 hPa, but the results are nearly identical if it is included. The annular mode indices in the modern reanalyses are correlated  $R^2 > 0.96$  with each other at all levels in the Northern Hemisphere and up to 3 hPa in the Southern Hemisphere; NCEP-CFSR's correlation with the others drops to  $R^2 = 0.9$  at 1 hPa in the Southern Hemisphere. For the pre-satellite period, it was unclear if a REM was meaningful, particularly in the austral hemisphere. In the analysis shown in Figure 6.10, JRA-55 is chosen among modern full-input reanalyses as an arbitrary point of comparison.

Figure 6.10 contrasts consistency between the reanalyses in the post- and pre-satellite periods. To assess performance during the satellite era, Figs. 6.10a and c correlate the annular modes computed from each individual reanalysis with the REM index over the standard WMO climatological period, 1981-2010. Essentially the same results would be found for any period after 1979, with some evidence of greater agreement in the last decades at upper levels (not shown). In the Northern Hemisphere, the annular mode indices computed from all of the full-input reanalyses are almost indistinguishable (the squared correlations are near one). In the Southern Hemisphere, there is reasonable agreement between all the full-input reanalyses ( $R^2 > 0.95$  up to 10 hPa), but with evidence of tighter agreement amongst the more recent reanalyses ( $R^2 \approx 0.99$  up to 3 hPa). While not shown here, an early output of ERA5 (2008-2016) was compared with the other modern reanalyses by Gerber and Martineau (2018) and shown to be as good as the other modern reanalyses.

In the Northern Hemisphere, the conventional-input JRA-55C reanalysis provides a very good estimate of the state of the annular mode up to 10 hPa. JRA-55C's annular mode index, however, is noticeably less correlated with the REM in the Southern Hemisphere, suggesting the satellite observations are critical for quantifying the large scale circulation of the austral hemisphere. At the surface, and throughout most of the troposphere, the surface-input reanalyses 20CRv2/v2c and ERA-20C are also well correlated with the REM. The annular mode indices in the 20CR reanalyses, however, quickly decorrelate with the REM above the tropopause, suggesting that these reanalyses cannot effectively capture stratospheric variability. ERA-20C also loses skill in the stratosphere, but much more slowly, particularly in the Northern Hemisphere. The  $R^2$  of approximately 0.6 at 10 hPa indicates that ERA-20C captures 60% of the variance in the annular mode at this height in the stratosphere. As discussed in greater detail by Gerber and Martineau (2018), ERA-20C appears to capture approximately half of the observed SSWs, and simulates the same frequency of events overall.

We note that the JRA-55AMIP integration does not meaningfully capture any of the annular mode variability. This was an expected result; this integration is not a reanalysis, but rather the JRA-55 model forced with observed SSTs, as in a standard Atmospheric Model Intercomparison Project (AMIP) simulation. Knowledge of the sea surface temperature is not sufficient to constrain the large-scale circulation of either hemisphere.

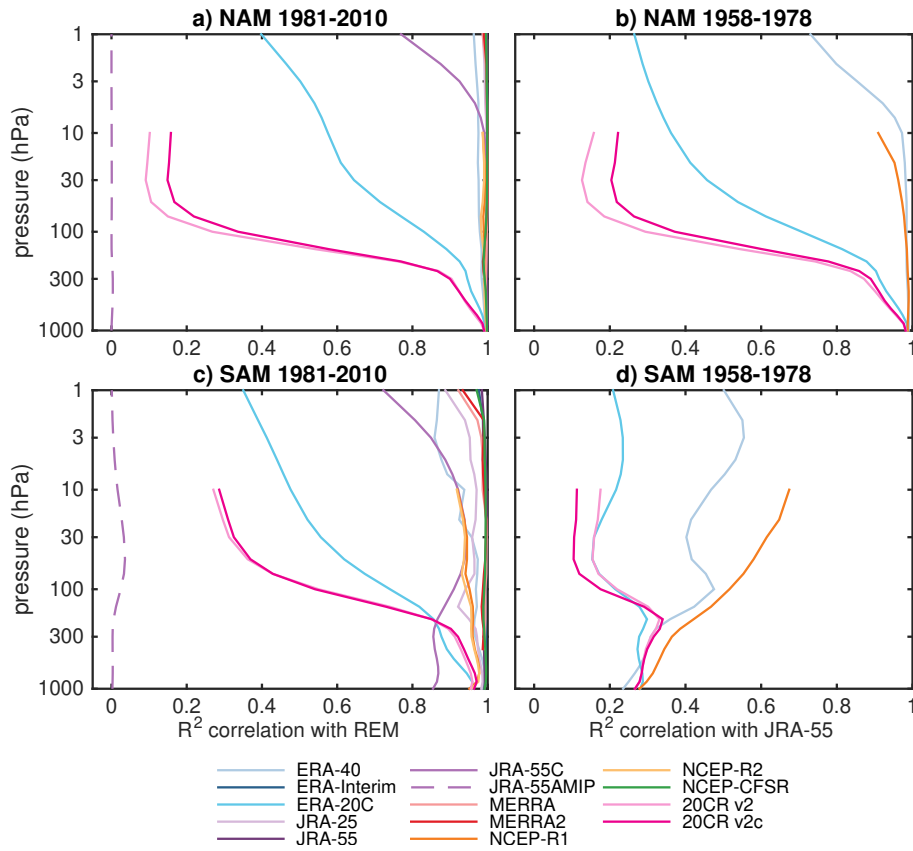


**Figure 6.10:** The squared correlation between the (a, b) Northern and (c, d) Southern Annular Mode indices computed from each individual reanalysis with (a, c) a Reanalysis Ensemble Mean (REM) for the period 1981-2010, and (b, d) with the Annular Mode index of JRA-55 for the pre-satellite period, 1958-1978. As detailed in the text, the REM for the more recent period is constructed from three of the most recent reanalyses (ERA-Interim, JRA-55, and NCEP-CFSR). In the pre-satellite period, a REM proved less meaningful. Comparable plots are obtained if NCEP-R1 or ERA-40 are used instead of JRA-55.

Only six reanalyses provide coverage in the pre-satellite era. Here we restrict ourselves to the period 1958-1979, as only NCEP-R1 and the surface-input reanalyses extend further back in time, but Gerber and Martineau (2018) consider earlier periods. We have arbitrarily chosen JRA-55 as the reference time series among the modern full-input reanalyses for Figs. 6.10b and d, but a qualitatively similar structure is found if ERA-40 or NCEP-R1 is used instead. In the Northern Hemisphere, we find that the annular mode is consistently represented in the full-input reanalyses, with growing uncertainty above 10 hPa (where NCEP-R1 is not available). This result is consistent with the ability of the conventional input reanalysis JRA-55C to capture Northern Annular Mode variability in the satellite period.

While ERA-20C still captures more of the variability in the stratosphere in comparison to the 20CR reanalyses, the  $R^2$  correlation is weaker in the pre-satellite period. At 10 hPa, ERA-20C captures only 40% of the variability in the full-input reanalysis JRA-55 (or equivalently, ERA-40 and NCEP-R1), compared to 60% in the satellite era. This could be due to fewer surface observations during this earlier period.

809 In the Southern Hemisphere, the situation is different. There is little agreement between JRA-  
810 55 and the other reanalyses. Similarly poor agreement is found if NCEP-R1 or ERA-40 is chosen  
811 as the reference time series (not shown), though we do find the NCEP-R1 is somewhat better  
812 correlated with the surface-input reanalyses in the troposphere than either JRA-55 or ERA-40.  
813 The poor consistency between the reanalyses in the pre-satellite period was somewhat expected,  
814 given the inability of JRA-55C to capture the Southern Annular Mode in recent years. But the fact  
815 that JRA-55C still captures 85% or more of the variance in the REM at nearly all levels suggests  
816 that a scarcity of conventional observations before 1979 is a larger part of the problem.

817 As discussed in Gerber and Martineau (2018), it is difficult to assess the synoptic variability  
818 of the Southern Annular Mode from direct measurements. On monthly time scales, Marshall  
819 (2003) has constructed a station based index that is correlated at approximately  $R=0.85$  with the  
820 850 hPa Southern Annular Mode index in all reanalyses over the period 1979-2001. (This period  
821 was chosen to allow comparison with ERA-40.) For JRA-55 and ERA-40, this correlation drops  
822 markedly (to approximately 0.5) in the pre-satellite period 1958-1978. NCEP-R1's correlation also  
823 weakens, but only drops to approximately 0.7. In contrast, the surface based reanalyses ERA-20C  
824 and 20CR maintain their correlation with the Marshall (2003) index.

825 The 20CR products, however, have been shown to miss most of stratospheric variability in  
826 earlier periods. Thus, for probing the large scale circulation of the stratosphere-troposphere in the  
827 pre-satellite Southern Hemisphere atmosphere, ERA-20C might actually provide a more reliable  
828 estimate, even though NCEP-R1, ERA-40, and JRA-55 assimilate radiosonde data and other free  
829 atmosphere observations.

### 830 **6.5.2 Sampling Uncertainty vs. Reanalysis Uncertainty**

831 As found with the evolution of the stratosphere during an SSW event in Section 6.4.3, our ability  
832 to quantify the large-scale tropospheric response to SSWs and strong vortex events is primarily  
833 limited by the finite length of the reanalysis records, not differences between the reanalyses. Figure  
834 6.11 compares the sampling uncertainty in the “dripping paint” plots of Baldwin and Dunkerton  
835 (2001) to uncertainty associated with differences in the reanalyses. Panels (a) and (b) provide an  
836 update on the evolution of the annular mode index about weak and strong vortex events, now based  
837 on almost 6 decades of JRA-55 reanalysis. Following Baldwin and Dunkerton (2001), composites  
838 are centered about the date the 10 hPa index drops below -3 (rises above 1.5) standard deviations.  
839 The asymmetry in event criteria was based in part on the fact that the annular mode index at  
840 this level is skewed negative on account of SSWs, but 1.5 standard deviations is a much weaker  
841 threshold, such that more strong events are identified.

842 Gerber and Martineau (2018) show that using a consistent set of event dates is important for  
843 this comparison. The threshold nature of the event detection implies that very small differences  
844 between reanalyses can lead to the detection of different events (or more frequently, a shift in  
845 the timing of a given event). This effectively aliases sampling uncertainty in a comparison of  
846 reanalyses: the key is that the annular mode indices vary very little between reanalyses (differences  
847 are on the order of 1%), but the inter-event variance is of order unity.

848 The weak vortex composite (Figure 6.11a) shows a rapid breakdown of the stratospheric polar  
849 vortex in the week preceding an event, evident first at upper levels, but become nearly synchronous  
850 in height by the time of onset. The stratospheric vortex then slowly recovers, from top to bottom,  
851 taking nearly three months in the lower stratosphere. During this long period of recovery, the

852 tropospheric annular mode tends to be weakly negative, indicating an equatorward shift in the jet  
 853 stream.

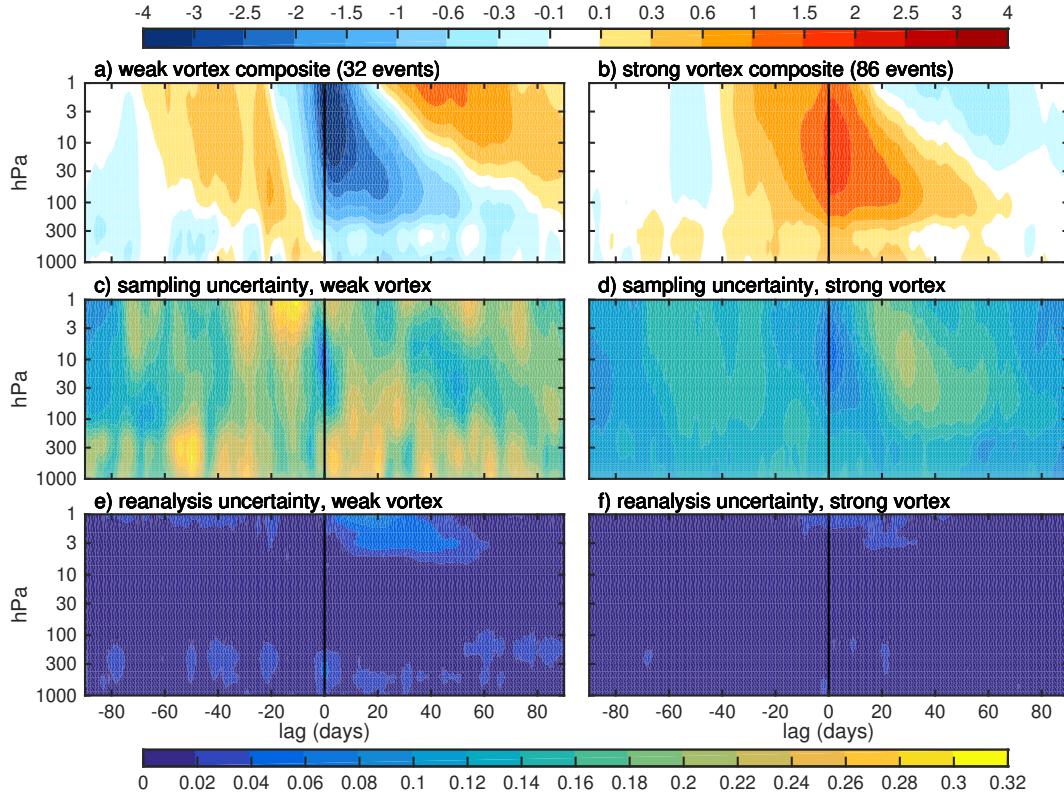


**Figure 6.11:** Composites of the Northern Annular Mode indices as a function of lag and pressure for (a) weak and (b) strong vortex events, based on JRA-55 reanalyses over the period 1958-2016. Following Baldwin and Dunkerton (2001), weak (strong) events are identified when the NAM index at 10 hPa drops below -3 (rises above 1.5), and must be separated by a minimum of 30 days. The remaining panels quantify the uncertainty in the NAM index evolution as a function of lag and pressure. (c) and (d) show the *sampling uncertainty* in the mean weak/strong composites shown in Figs. 6.11a,b, expressed as a one standard deviation error bound. Panels (e) and (f) show the *reanalysis uncertainty*: the standard deviation between composites of weak/strong vortex events based on the 4 most recent reanalysis products (ERA-Interim, JRA-55, MERRA2, and CFSR/CFSv2) separately, for the period 1980-2016. As discussed in the text, a standardized set of event dates are used to prevent the aliasing of sampling error.

854 The strong vortex events (Figure 6.11b) exhibit a similar structure, but shifted earlier in time  
 855 relative to date of event onset. The stratospheric vortex exhibits a positive annular mode (i.e., is  
 856 stronger than average) for over a month in advance, associated with a positive tropospheric annular  
 857 mode (poleward shift in the tropospheric jet) that is already fully developed by the onset. This shift  
 858 is partly due to the fact that strong vortex events tend to build slowly, on the time scale of radiative  
 859 forcing, and so are harder to align in time. With respect to the amplitude of these events, pay close  
 860 attention to the color scale. A weak vortex event is associated with a 3 standard deviation drop  
 861 in the annular mode index in approximately 1 week, corresponding to a 1.4 km rise in the 10 hPa  
 862 surface at the pole. In contrast, the strong vortex event is associated with a more gradual 0.7 km  
 863 drop in the 10 hPa surface over a month.

864 Figures 6.11c and d show the 1 standard deviation error bound on the weak and strong vortex  
865 composites, respectively. As shown by Gerber and Martineau (2018), inter-event variance of the  
866 annular mode indices is on the order of unity at all times except in the stratosphere at event onset  
867 (which occurs by construction: the 10 hPa index annular mode is always approximately -3 or 1.5 at  
868 lag 0). The sampling uncertainty of the composite is thus approximately 1 over the square root of  
869 the number of events. For weak vortex cases, where we have only 32 events, this is approximately  
870 0.2, of the same order as the signal at any given time! As argued by Baldwin and Dunkerton (2001),  
871 the tropospheric response is only significant if one averages over an extended period. This takes  
872 advantage of the fact that the tropospheric annular mode tends to exhibit memory on the order of  
873 10 days (e.g., Gerber et al., 2010). If we ask for a 95% confidence interval at any given time, we  
874 need the signal to be about equal to two standard deviations, requiring on the order of 100 events,  
875 a point we just approach in the case for strong vortex events.

876 Differences between the reanalyses are an order of magnitude smaller than the sampling error,  
877 as shown in Figs. 6.11e and f. This measure of the “reanalysis uncertainty” was constructed  
878 by comparing weak and strong vortex composites based on the most recent reanalyses (ERA-  
879 Interim, JRA-55, MERRA2, and CFSR/CFSv2) separately. We find that composites based on  
880 one reanalysis versus another are almost indistinguishable, provided one uses a standardized set  
881 of event dates. As the uncertainty is more than 10 times smaller than the sampling uncertainty,  
882 we’d need a record 100 times as long (i.e., 6000 years!) for the choice of reanalysis to become as  
883 important as sampling uncertainty.

884 A similar conclusion applies to other measures of the coupling between the stratosphere and  
885 troposphere through the polar vortex, such as the variance and persistence of the annular mode  
886 indices as a function of season explored by Baldwin et al. (2003) and Gerber et al. (2010): results  
887 based on one reanalysis are not significantly different from those based on another with respect  
888 to the sampling uncertainty. This suggests that lengthening the reanalysis record has a substantial  
889 effect on our ability to quantify the coupling between the troposphere and stratosphere.

890 The sampling uncertainty shown in Figs. 6.11c and d was based on JRA-55, which provides  
891 two additional decades (30% more years) than the other most recent reanalyses which are restricted  
892 to the satellite era. As the sampling error decays with the square root of the number of events,  
893 these error bounds are 20% smaller than could be obtained from the other modern reanalyses. This  
894 reduction depends on the assumption that JRA-55’s reanalysis from 1958-1978 is of sufficiently  
895 high quality, supported by our comparison of the pre-satellite era reanalyses in Figure 6.10, and  
896 the fact that JRA-55C does a good job of capturing annular variability since 1979 without the aid  
897 of satellite observations. We look forward to assessing the ERA5 reanalysis, which is planned to  
898 extend back to 1950.

## 899 **6.6 Stratospheric Final Warming Events**

900 The extratropical stratosphere exhibits a pronounced seasonal cycle with westerly winds in the winter  
901 hemisphere (with the exception of SSW events) and easterly winds in the summer hemisphere.  
902 The final transition from the westerlies to the easterlies, which occurs every year, is referred to as  
903 a Stratospheric Final Warming (SFW) event. Similar to SSW events, SFW events show a signature  
904 of zonal-mean zonal wind deceleration in the troposphere, indicative of a downward coupling,  
905 and a signature of enhanced upward Eliassen-Palm (EP) flux propagation to the stratosphere prior  
906 to the events (Black and McDaniel, 2007; Sun and Robinson, 2009). As such, they allow us to  
907 evaluate the representation of stratosphere-troposphere dynamical coupling in both hemispheres.

908 There is greater variability of final warmings in the Northern Hemisphere compared to the South-  
909 ern Hemisphere, but stratospheric ozone loss has influenced their statistics in the Southern Hemis-  
910 phere. Given their influence on the troposphere, the timing of the final warming has implications  
911 for seasonal forecasting (e.g., Ayarzagüena and Serrano, 2009; Hardiman et al., 2011; Byrne and  
912 Shepherd, 2018; Lim et al., 2018; Butler et al., 2019).

913 The final warming of the polar vortex is of key importance in chemistry-climate models. Once  
914 the polar vortex has broken down, ozone rich air can be transported to polar latitudes again. In  
915 the Southern Hemisphere, a late final warming in models will mean that the simulated Antarctic  
916 ozone hole persists longer through the year than is observed. A bias in the final warming time  
917 is also an indication of polar temperature biases, which will adversely affect the modelling of  
918 heterogeneous ozone destruction there (Eyring et al., 2006). Adequate representation of the timing  
919 of the final warming in reanalysis data sets therefore has important implications for the evaluation  
920 of chemistry-climate models.

921 The final warming date is defined here as the day on which the zonal mean zonal wind at  
922 60° becomes easterly for the final time during winter/spring. This can be sufficiently diagnosed  
923 using monthly mean data (calculating the day of the final warming using linear interpolation and  
924 assuming the monthly mean value represents the value on day 15 of the month) and occurs first in  
925 the mesosphere in the Southern Hemisphere (Fig. 6.12; shown only up to 1 hPa) but first in the  
926 mid-stratosphere in the Northern Hemisphere. With the exception of 20CR, all reanalysis products  
927 agree on the mean final warming date to within 6 days.

928 A closer study of the final warming in the Northern Hemisphere reveals that in some years  
929 the final warming occurs first in the mid-stratosphere ("10hPa-first years"), but in some years  
930 occurs first in the mesosphere ("1hPa-first years") (Figure 6.13). In 27 of the 32 years used,  
931 the reanalysis products all agree on the final warming type. Although there is generally a good  
932 agreement among full-input reanalyses, ERA-40 shows larger discrepancies in the mid- to lower-  
933 stratosphere transition date with respect to other data sets.

934 Correctly simulating the proportion of 10 hPa-first years and 1 hPa-first years is an area in  
935 which climate models do not currently perform well. In the reanalyses 68—79% of years are  
936 10 hPa-first years, whereas only 36% of all modeled years, using the chemistry-climate models  
937 participating in phase 2 of the Chemistry-Climate model Validation activity (CCMVal-2) are 10  
938 hPa-first years (Hardiman et al., 2011). Thiéblemont et al. (2019) note a similar underestimation  
939 of 10 hPa-first years in the CESM and EMAC climate models.

## 940 6.7 Modulation of Stratosphere-Troposphere Coupling by ENSO and 941 QBO

942 The Northern-Hemisphere winter stratospheric polar vortex varies in strength from year to year  
943 with several external factors (Yoden et al., 2002). One prominent source for this interannual vari-  
944 ability is ENSO, the main mode of interannual variability in the tropical troposphere. During its  
945 warm phase (El Niño), Rossby wave trains propagate towards mid-latitudes in the Northern Hemis-  
946 phere (NH) in boreal winter, strengthening the Aleutian low (e.g., Horel and Wallace, 1981).  
947 As a consequence, upward propagation of planetary waves into the stratosphere is enhanced,  
948 which results in a weaker and a warmer polar stratosphere (e.g., Brönnimann, 2007; Cagnazzo  
949 and Manzini, 2009). Although its teleconnectivity to the stratosphere is weaker than El Niño, the  
950 cold ENSO phase, La Niña, weakens the Aleutian low leading to reduced upward-propagating

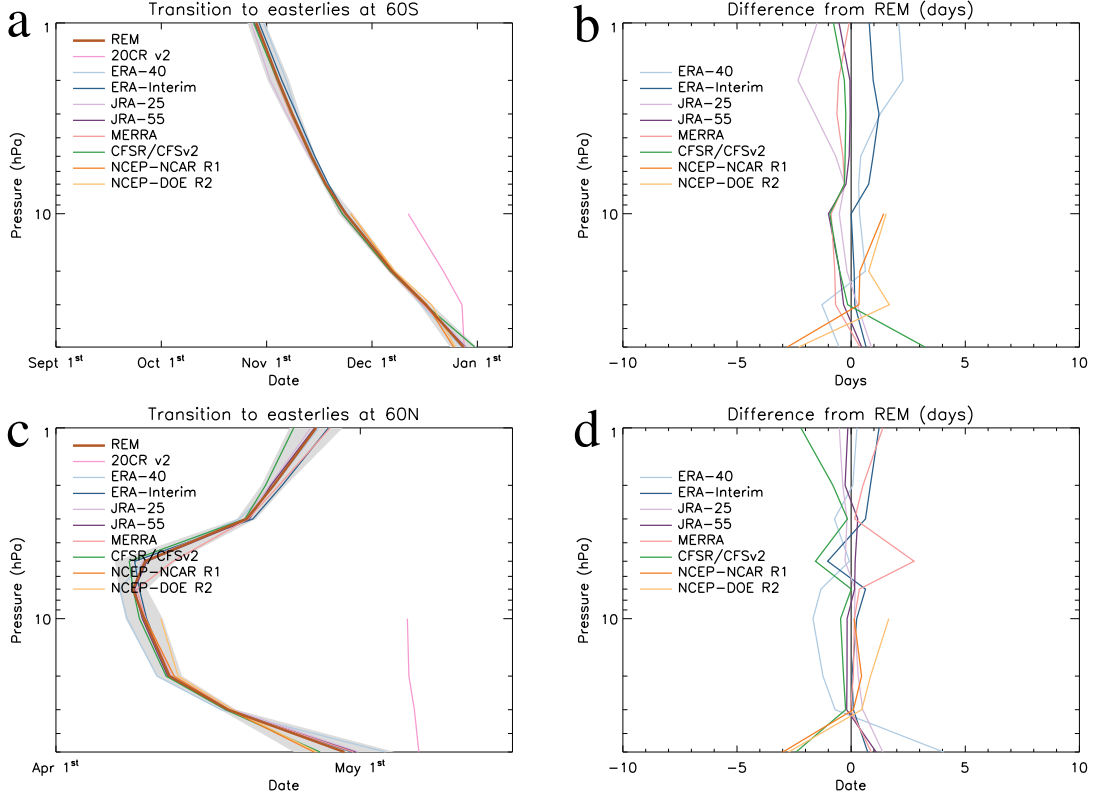


**Figure 6.12:** The final transition of zonal mean zonal wind from westerly to easterly at (a)  $60^{\circ}\text{S}$  and (c)  $60^{\circ}\text{N}$  is shown for the period 1979–2010 for all reanalysis data products except 20CR v2 (which uses 1979–2009) and ERA-40 (which uses 1979–2002). The multi-reanalysis mean (REM) is shown as a thick brown line, and uses data from all products except 20CR v2. The dark gray shading indicates the inter-reanalysis standard error (again excluding 20CR v2), scaled to represent a 95% confidence interval. The difference, in the final warming times shown in panels a and c, of each reanalysis from the multi-reanalysis mean is shown in (b,d). 20CR v2 is excluded from the REM since final warming times, especially in the Northern Hemisphere, are significantly later in this reanalysis and, given the remarkable agreement in final warming times across all other reanalysis datasets, the final warmings in 20CR v2 are very likely to be biased late.

wave activity into the stratosphere and a strengthening of the polar vortex (Butler and Polvani, 2011; Iza et al., 2016). For a comprehensive review of ENSO-stratosphere teleconnections, see Domeisen et al. (2019a).

ENSO's influence on the extratropical circulation is not limited to the time-mean flow. Barriopedro and Calvo (2014) found an ENSO modulation of the blocking precursors of SSWs, leading to distinctive wave signatures of SSWs during opposite ENSO phases: during El Niño, SSWs are predominantly associated with wavenumber-1 amplification in the lower stratosphere, whereas La Niña SSWs tend to occur after wavenumber-2 amplification (see also Song and Son (2018)). The way blocking events interfere with stationary waves and either amplify or damp the total injection of wave activity into the stratosphere depends critically on their location (e.g., Woollings et al., 2010; Nishii et al., 2011; Martius et al., 2009; Castanheira and Barriopedro, 2010).

Another source of interannual variability of the strength of the stratospheric polar vortex is

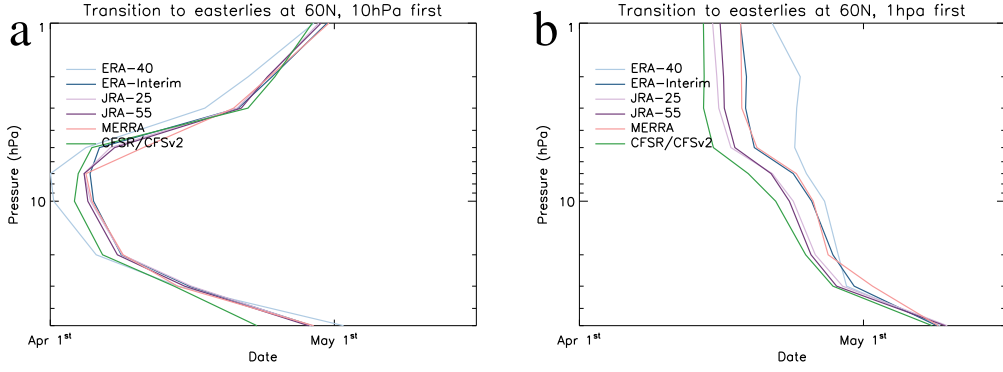


**Figure 6.13:** Mean final warming date at 60°N (as in Figure 6.12) composited over (a) 10 hPa-first years and (b) 1 hPa-first years (defined in text). The percentage of 10 hPa-first years is: 73.9 in ERA-40, 78.1 in ERA-Interim, 75.0 in JRA-25, 75.0 in JRA-55, 78.1 in MERRA, and 68.8 in NCEP-CFSR. Data from the reanalyses 20CR, NCEP-R1, and NCEP-R2 does not extend above 10 hPa, so these products cannot be used for this diagnostic.

963 the QBO which can modulate the nature and propagation of extratropical planetary-scale waves  
 964 (Holton and Tan, 1980; Garfinkel et al., 2012b). Several studies (Garfinkel and Hartmann, 2007;  
 965 Calvo et al., 2009; Richter et al., 2011; Taguchi, 2015) further suggested some nonlinear influence  
 966 of QBO and ENSO onto the stratospheric polar vortex such that when the QBO is in a westerly  
 967 phase in the lower stratosphere, the polar night jet weakens and SSW probability increases for the  
 968 warm ENSO phase (El Niño), whereas the changes are opposite for the QBO easterly winters.

969 Alternative criteria have been used in the literature to define cold and warm ENSO phases. In  
 970 the following analyses, we have focused on the most commonly used Niño 3.4 index based on  
 971 monthly mean SST anomalies in the region from 5°S-5°N and 170°E-120°W with reference to  
 972 1981-2010 climatology. Standard El Niño and La Niña phases are defined by plus or minus 0.5  
 973 K anomalies in this region, as done in Section 6.7.2. In Sections 6.7.1 and 6.7.3, more restrictive  
 974 criteria (1 standard deviation anomalies) were applied to focus on more extreme events. The period  
 975 of averaging, DJF vs. a more extended winter season, was also varied depending on the scientific  
 976 focus. The criteria for selecting warm and cold phases and the resulting years are therefore listed  
 977 in each section; winters are identified by the year in January, e.g., 1983 refers to the 1982-1983  
 978 winter.

### 979 6.7.1 Troposphere-stratosphere coupling through ENSO

980 The wintertime-mean stratospheric response to El Niño and La Niña conditions is first compared  
 981 among reanalysis datasets. Monthly mean data from ERA-Interim, JRA-55, NCEP-CFSR, and  
 982 MERRA reanalyses are used. First, for each field, time series from 1979 to 2013 are detrended and  
 983 anomalies are computed with respect to the 1981-2010 climatology. El Niño and La Niña events  
 984 are defined using the standardized NDJF sea surface temperature anomaly of the Niño 3.4 index  
 985 from the NCEP-CPC. El Niño (La Niña) winters are selected above (below) 1 SD (-1SD). The  
 986 composites include 7 El Niño winters (1983, 1987, 1992, 1995, 1998, 2003, 2010) and 5 La Niña  
 987 winters (1989, 1999, 2000, 2008, 2011). The statistical significance of the composites is assessed  
 988 with a Monte Carlo test at the 95% confidence level.

989 Figure 6.14 shows the latitude-pressure December-January-February (DJF) average of the zonal

mean zonal wind anomalies composited for El Niño (up) and La Niña (bottom) events. In the polar stratosphere the El Niño (La Niña) signal is characterized by a robust weakening (strengthening) of the zonal mean zonal wind in all reanalyses. All reanalyses agree on the significant area and the sign of the anomalies, with the largest polar stratospheric signal peaking at  $-7 \text{ ms}^{-1}$  for El Niño and  $8 \text{ ms}^{-1}$  for La Niña. Therefore, a good agreement across reanalyses is found for El Niño and La Niña polar stratospheric responses.

To quantify the relationship between the strength of the Aleutian low, modulated by ENSO, and the response of the stratospheric polar vortex, Figure 6.15 shows the scatter plot of the Z index at 500 hPa (average of geopotential height anomalies between  $40^\circ\text{N}$ - $60^\circ\text{N}$  and  $180^\circ\text{E}$ - $210^\circ\text{E}$ ) versus the U index (zonal mean zonal wind averaged at  $60^\circ\text{N}$  between 10 and 30 hPa), similar to Cagnazzo et al. (2009). It is important to note that these Z and U index values for each event are very similar among reanalyses. El Niño winters (squares) are associated with negative values of the Z and U indices. This corroborates that the deepened Aleutian low related to the negative Z index increases the upward wave propagation into the stratosphere leading to a weaker polar vortex. In contrast, La Niña winters (triangles) are mainly related to positive Z and U indices, due to an anomalously weak Aleutian low and in agreement with the observed positive wind anomalies respectively, since a weakened Aleutian low inhibits the upward wave propagation leading to a stronger polar vortex.

Results show an excellent agreement among reanalyses. Therefore, we conclude that for the purpose of studying the coupling between the stratosphere and the troposphere during El Niño and La Niña events, any of the compared reanalyses is equally suitable, as Iza et al. (2016) noted for La Niña events.

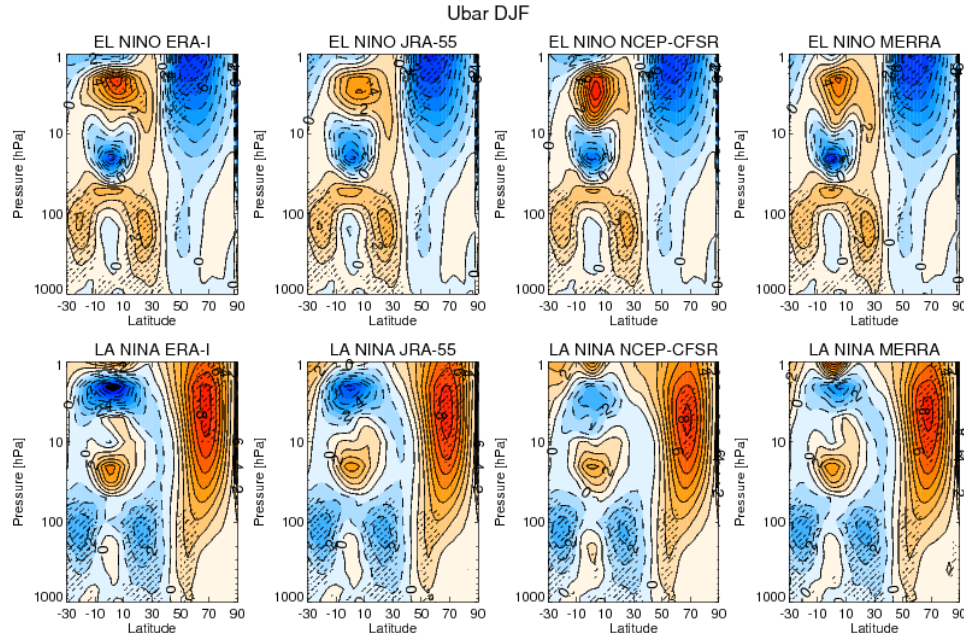


**Figure 6.14:** Latitude-pressure cross sections of the composite DJF average of monthly zonal mean wind anomalies for (top) El Niño and (bottom) La Niña events, from left to right for ERA-Interim, JRA-55, NCEP-CFSR, and MERRA reanalyses. Contour intervals are  $\pm 1 \text{ m s}^{-1}$ . Solid (dashed) contours denote positive (negative) anomalies. Stippling indicates significance at the 95% level.

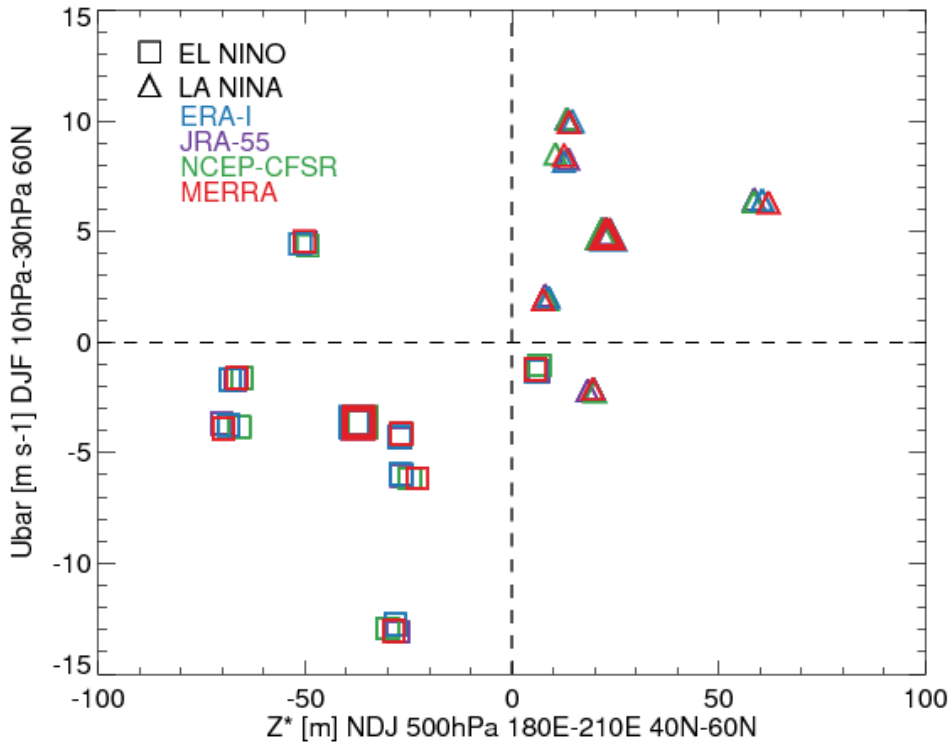


**Figure 6.15:** Scatter plot of the NDJ mean Z index, versus DJF U index. Squares (triangles) represent each El Niño (La Niña) event and the corresponding larger symbols represent El Niño and La Niña events composite.

### 6.7.2 Blocking patterns associated to SSWs and the modulation of ENSO

The intercomparison of ENSO's influence on the stratosphere among reanalyses is then extended to ENSO's influence on SSW events and their blocking precursors. The analysis contrasts interdataset uncertainties with the uncertainties associated with the definition of blocking events by using three different blocking definitions.

Daily mean geopotential height at 500 (Z500) and 100 (Z100) hPa is used for this analysis which is performed for the full 1958-2012 period and the 1979-2012 satellite period. For the latter period, the REM is computed from the NCEP-CFSR, ERA-Interim, JRA-55 and MERRA reanalyses. The REM of the full period is based on the NCEP-NCAR, ERA-40 (completed with ERA-Interim from 2002 to 2012 since the two agree well over their overlapping period from 1979 to 2002) and JRA-55 reanalyses. Fields were interpolated (if required) to the same common  $2.5^\circ \times 2.5^\circ$  grid before any further analysis is carried out. Anomalies are defined with respect to the daily climatology of 1981-2010.

SSW central dates are chosen from the common dates identified in Table 6.2. ENSO winters were characterized by the NDJFM average of the monthly Niño 3.4 index (<http://www.cpc.ncep.noaa.gov/>). EN and LN winters were identified when Niño 3.4  $\geq 0.50^\circ\text{C}$  and Niño 3.4  $\leq -0.50^\circ\text{C}$ , respectively. The resulting warm phase years are 1958, 1966, 1969, 1973, 1983, 1987, 1988, 1992, 1995, 1998, 2003, 2005, 2007, and 2010. Cold phases were identified in 1962, 1963, 1965, 1967, 1968, 1971, 1972, 1974, 1975, 1976, 1984, 1985, 1989, 1996, 1999, 2000, 2001, 2006,

1030 2008, 2009, 2011, and 2012.

1031 We employed three blocking detection methods, which cover most approaches to blocking  
1032 definition: 1) the absolute method (ABS), based on the detection of reversals in the meridional  
1033 Z500 gradient; 2) the anomaly method (ANO), using Z500 anomalies above a given threshold; 3)  
1034 the mixed method (MIX), a hybrid definition of the two previous approaches. These definitions  
1035 are described in more details in Woollings et al. (2018). All methods give two preferred regions  
1036 for blocking occurrence: one over the Atlantic and one over the Pacific basins, with maximum  
1037 blocking frequencies of about 15% of days in NDJFM. However, there are substantial differences  
1038 among definitions in the blocking location within each basin as well as in the relative frequencies  
1039 of Atlantic vs Pacific blocking (Woollings et al., 2018).

1040 Blocking precursors of SSWs were identified for each reanalysis by performing 2-D composites  
1041 of blocking frequency for the [-10,0]-day period before the central dates of SSWs. This was carried  
1042 out separately for SSWs occurring during El Niño and La Niña winters. The REM for the full  
1043 period is shown in Figure 6.16. There is a spatial preference for different blocking precursors of  
1044 SSWs depending on the ENSO phase, with enhanced (reduced) blocking frequencies over eastern  
1045 North America and the North Alantic (eastern Pacific) during El Niño, and nearly opposite patterns  
1046 for La Niña winters. Thus, SSWs are often preceded by North Atlantic sector blocking during El  
1047 Niño, while eastern Pacific blocks are the preferred precursors of SSWs in La Niña winters. The  
1048 comparison across reanalyses reveals a good agreement, with differences that are much smaller  
1049 than among blocking definitions (everywhere except the blue dots in Figure 6.16). The intensity,  
1050 significance and spatial extension of the signal weaken for the satellite period (1979-2012, not  
1051 shown).

1052 The composites of blocking precursors of SSWs for El Niño and La Niña winters are similar  
1053 to those obtained for wavenumber-1 and wavenumber-2 SSWs, respectively (Song and Son, 2018;  
1054 Ayarzagüena et al., 2019), which hints at a modulation of the characteristics of SSW events. .  
1055 To further illustrate the association between ENSO and the dominant wave signatures of SSWs,  
1056 the temporal evolution of Z100 wavenumber components are evaluated for the [-30, 30]-day period  
1057 surrounding the central date of SSWs (Figure 6.17). The results confirm that SSWs are significantly  
1058 preceded by wavenumber-1 amplification during El Niño, whereas SSWs preferably occur after  
1059 wavenumber-2 amplification in La Niña winters (Taguchi and Hartmann, 2006). During La Niña,  
1060 the wavenumber-2 signal is accompanied by significant anomalies in wavenumber-1, albeit they  
1061 are smaller and/or shorter-lasting. This difference in wave driving does not, however, necessarily  
1062 affect the ratio of vortex splits to displacement (Garfinkel et al., 2012a). This modulation of  
1063 SSW characteristics by ENSO is achieved through a change in the preferred blocking location,  
1064 which injects different scales of wave activity into the stratosphere, and thus forces different types  
1065 of SSWs (e.g., Barriopedro and Calvo, 2014). We note that the sensitivity of these results to the  
1066 choice of reanalysis is very weak.

1067 The modulation of SSW properties by ENSO is robustly observed across reanalyses when the  
1068 1958-2012 period is used, but less evident in the 1979-2012 period. This suggests decadal vari-  
1069 ability in the ENSO-blocking-SSW relationship (e.g., Rao et al., 2019), biases in the pre-satellite  
1070 period or sampling issues affecting the shorter satellite period. The differences among blocking  
1071 definitions are much larger than differences among reanalyses, likely contributing to the discrep-  
1072 ancies in the blocking-SSW relationship reported in the literature.

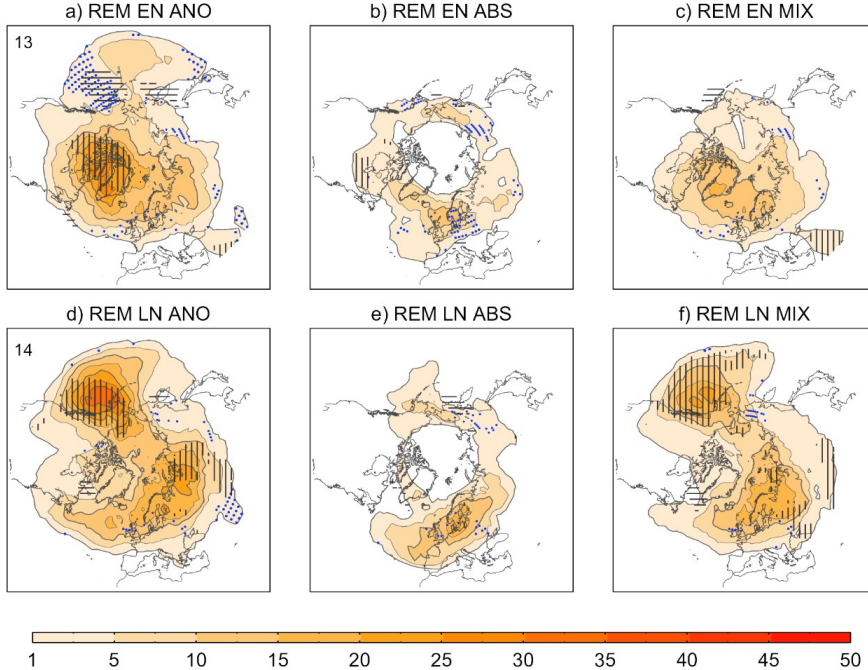


**Figure 6.16:** Reanalysis ensemble mean composites of blocking frequency for the [-10,0]-day period before the central dates of SSWs occurring during El Niño (top) and La Niña (bottom) winters of the 1958-2012 period for three different blocking definitions (columns). The blocking frequency is expressed as the percentage of time (over the 11-day period) during which a blocking was detected at each grid point. Vertical (horizontal) black lines indicate regions with blocking activity significantly higher (lower) than the climatology at the 90% confidence level in at least 66% of the reanalyses. The significance is derived from a bootstrap of 1000 members, each one containing the same number of cases and dates as the SSWs of each composite but with random years of occurrence. Blue dots highlight grid points where the inter-reanalysis spread for a given blocking definition is larger than the spread across the reanalysis ensemble mean of blocking definitions. The numbers in the upper left corner of panels a), d) indicate the sample size of SSWs during El Niño and La Niña winters, respectively.

### 6.7.3 Nonlinear modulation of the extratropical stratosphere by ENSO and QBO

Finally, we evaluate the representation of nonlinearities in the modulation of DJF-mean polar vortex strength and SSW occurrence with ENSO and QBO among reanalyses. SSW onset dates are defined by the common dates established in Section 6.4.1 and the DJF zonal mean zonal wind at 60°N and 10 hPa is used as a proxy for strength of the polar night jet. The analysis period ranges from 1979 to 2011, except for 20CR v2 (1979-2010). The DJF climatology for each reanalysis is based on the 1981-2010 period.

In order to define ENSO phases, the monthly Niño 3.4 index (provided by NOAA/CPC) is averaged over DJF. The DJF mean of the zonal mean zonal wind at the equator and 50 hPa in the respective reanalyses is used to define QBO phases. All DJF seasons are classified into six groups defined by three ENSO and two QBO conditions. Two of the three ENSO conditions are El Niño and La Niña, when the DJF mean Niño 3.4 index exceeds  $\pm 1$  standard deviation (both inclusive); warm phase years (EN) were identified in 1983, 1987, 1992, 1998, and 2010, and cold phases (LN) in 1989, 1999, 2000, 2008, and 2011. The third ENSO condition is neutral (NT)

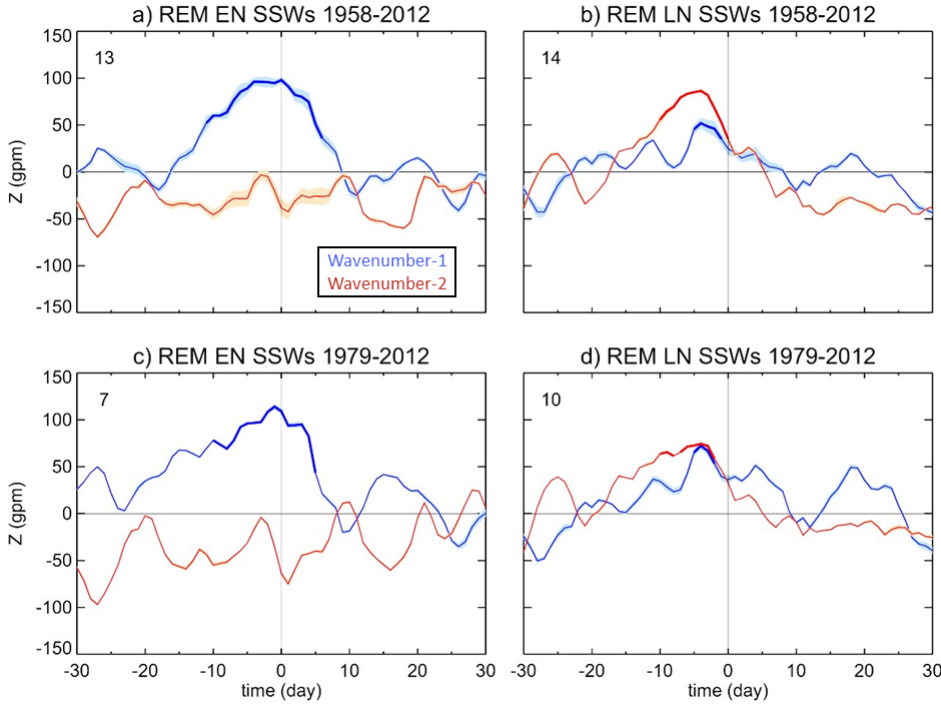


**Figure 6.17:** Reanalysis ensemble mean composites of the temporal evolution of 100 hPa geopotential height wavenumber-1 (blue) and wavenumber-2 (red) amplitude anomalies at 60°N (gpm) for the [-30,30]-day period around the central dates of SSWs occurring during El Niño (left) and La Niña (right) winters of the full (1958-2012, top) and satellite (1979-2012, bottom) period. Shading denotes the  $\pm 2$  sigma level across reanalyses. The time intervals highlighted with thick lines indicate significant differences with respect to climatology at the 95% confidence level in at least 66% of the reanalyses. The significance is assessed with a bootstrap test of 1000 samples with the same number of cases and calendar days as the SSWs of each composite but with random years of occurrence. The numbers in the upper left corner of each panel indicate the sample size of the composite.

for remaining years. The mean and standard deviation of the ENSO index are calculated for the 1981-2010 period.

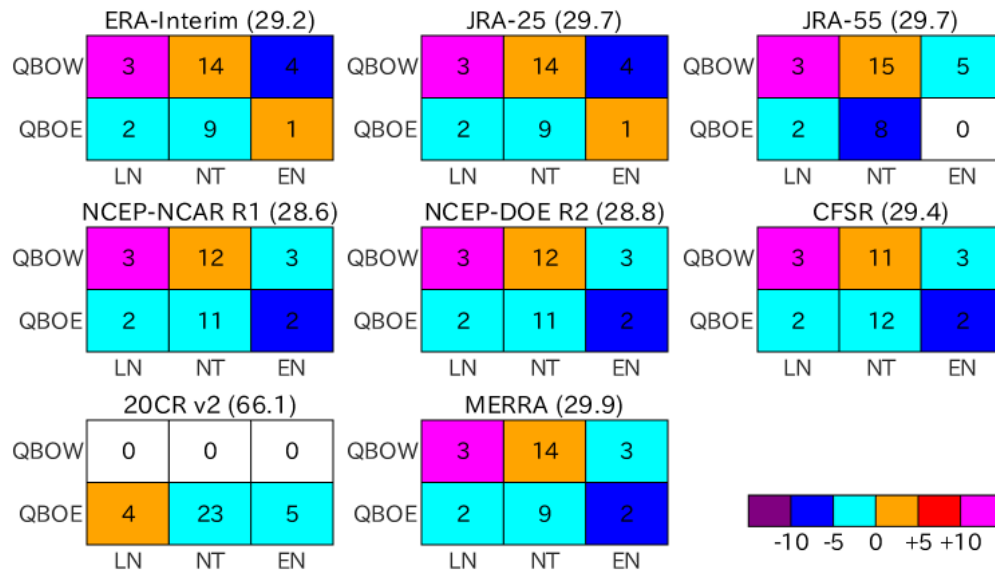
The two QBO conditions are easterly (ELY) and westerly (WLY), when the DJF mean zonal wind in the equatorial lower stratosphere is negative or positive (the latter includes zero). The resultant grouping is slightly different among the reanalyses, as the equatorial zonal wind is different. Alternatively, we also use 50 hPa equatorial zonal wind data archived at Free University Berlin to standardize the QBO classification for all reanalyses, which yields similar results (not shown). It is noted that the classification of about 30 years into the six groups implies that in some cases the sample size is small and therefore it is difficult to obtain statistically significant results. Before focusing on changes with ENSO and QBO, it will be useful to mention that except for 20CR v2, the interannual variability of the DJF mean vortex strength is highly correlated between the reanalyses, with correlation coefficients over +0.99.

Figure 6.18 shows heat maps based on composite zonal wind anomalies of each reanalysis for the six groups. As expected from the high correlations of the interannual variability of the zonal wind, the plots show that the changes in the vortex strength with ENSO and QBO are more or

less similar among the reanalyses, except for 20CR v2 whose climatological vortex strength is notably more than twice that of other reanalyses. Specifically, the zonal wind anomalies tend to be slightly negative for ELY winters regardless of the ENSO conditions. For WLY conditions, the zonal wind anomalies exhibit a clear decreasing tendency with the ENSO SST conditions, from La Niña (positive wind anomalies) through neutral to El Niño (negative anomalies).

It is noted that the sample sizes of the six groups are not the same among all reanalyses, implying that the equatorial zonal wind and hence QBO classification are different in some cases. This may matter when one extracts changes with QBO conditions that are defined using an equatorial zonal wind index in the respective reanalyses, but this effect seems limited here since most reanalyses show similar results.

Figure 6.19 similarly shows heat maps of SSW probabilities for the six groups. Here, for each group, the SSW probability is a ratio (times 100) of the number of SSWs to the number of years. The charts show that although the classification of QBO years is slightly different among the reanalyses, the changes in the SSW probabilities are similar among the data sets, except for 20CR v2 which has no SSWs. For ELY, the probabilities tend to decrease from La Niña, through neutral, to El Niño. A characteristic feature is the highest SSW probability for La Niña and ELY (group 1). On the other hand, for WLY, the probabilities slightly increase in the opposite way, from La Niña, through neutral, to El Niño, consistent with the changes in the zonal wind anomalies (Figure 6.18). These changes in the SSW probabilities do not necessarily match changes in DJF zonal wind anomalies (Figure 6.18), since the occurrence or absence of a SSW during each winter depends not only on the DJF mean vortex strength but also on its variance.



**Figure 6.18:** Heat maps showing composite anomalies of the DJF-mean zonal wind at 60°N, 10 hPa for the six groups in the eight reanalyses as indicated above each panel. The number indicated in each cell denotes the sample size. Each panel also includes the DJF climatological wind value in  $\text{ms}^{-1}$  in parentheses.

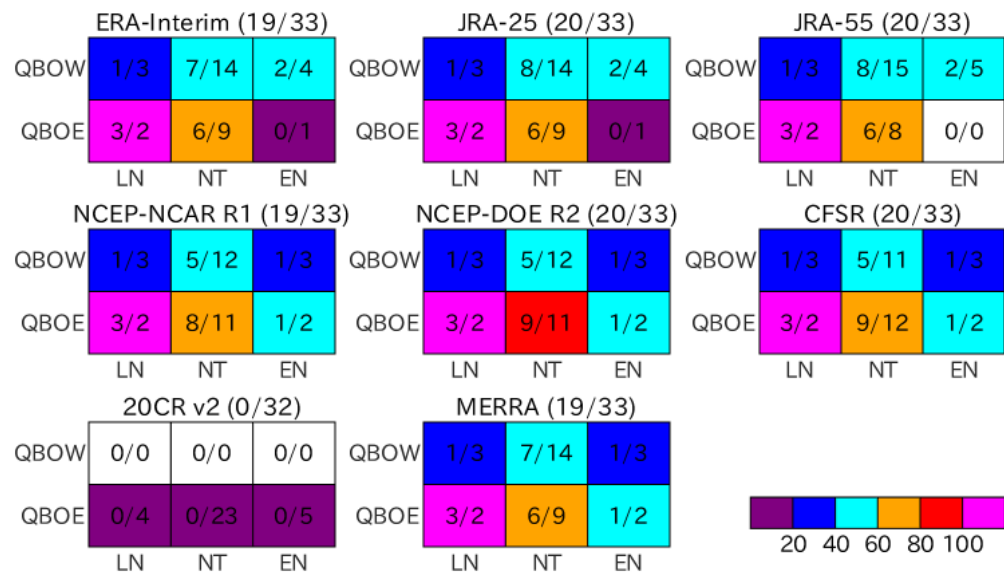


**Figure 6.19:** Same as Figure 6.18, but for SSW probabilities (in %) computed as the ratio of the number of SSWs to the number of years for each group (indicated in each cell). The numbers in the title indicate total number of SSW / total number of years.

1123 **6.8 Stratosphere-Troposphere Coupling through the Antarctic Ozone  
1124 Hole**

1125 In recent decades, severe stratospheric ozone depletion has led to the Antarctic ozone hole in  
1126 austral spring (Thompson and Solomon, 2002). This has resulted in substantial cooling in the  
1127 lower stratosphere, leading to an increase in the latitudinal temperature gradient and a consequent  
1128 strengthening of the stratospheric polar vortex. Through mid-to-late spring, this mid-to-high lat-  
1129 itude circulation anomaly descends from the lower stratosphere to reach the troposphere during  
1130 austral summer (e.g., Son et al., 2018). The anomalous tropospheric circulation is associated with  
1131 a noticeable increase in zonal mean sea level pressure difference between the mid and high lati-  
1132 tudes, commonly referred to as an increase in the positive phase of the Southern Annular Mode  
1133 (SAM). The positive SAM is generally marked by a poleward displacement and intensification of  
1134 the tropospheric mid-latitude jet. Although ozone loss has a direct impact on stratospheric temper-  
1135 atures by reducing the absorption of incoming solar radiation, a number of studies show that the  
1136 anomalous circulation is strongly influenced by changes to wave forcing and wave mean-flow in-  
1137 teraction (Orr et al., 2012). Here, the impacts of the ozone hole on the dynamical coupling between  
1138 the stratosphere and the troposphere in the spring and summer Southern Hemisphere are examined  
1139 in the ERA-Interim, JRA-55, MERRA, and CFSR reanalyses datasets.

1140 Figure 6.20 shows the trends in zonal mean temperature over the SH polar region between  
1141 1979 and 2001 for the four datasets. This period is chosen for two reasons. First, the size of the  
1142 ozone hole increased steadily during this period (Huck et al., 2007). Second, the trends in the four  
1143 reanalyses were largest for this period (not shown), which allows to identify important differences  
1144 between the datasets. In ERA-Interim, the cooling starts at 30 hPa in October and peaks at around  
1145 100 hPa between mid-November and early December (with trends reaching -4 K per decade),  
1146 which is in good agreement with radiosonde data from Antarctica (Thompson and Solomon, 2002).  
1147 The other three reanalyses all show broadly similar results with downward descent pattern from  
1148 30 hPa to 300 hPa. However, compared to ERA-Interim, CFSR shows considerably stronger and  
1149 longer-lasting cooling (by up to  $-1 \text{ K dec}^{-1}$ ) between 100 and 300 hPa, and enhanced warming  
1150 below 300 hPa (by around  $0.5 \text{ K dec}^{-1}$ ). This would lead to a comparative weakening of the  
1151 atmospheric stability near the tropopause. In both CFSR and MERRA, the cooling also starts  
1152 noticeably earlier than ERA-Interim.

1153 Figure 6.20 also shows the corresponding trends in zonal wind over the SH polar regions, with  
1154 all four reanalyses showing the expected strengthening of the SH circumpolar winds from the  
1155 lower stratosphere down to the surface. In ERA-Interim, the strengthening starts in mid-to-late  
1156 September at 30 hPa, peaks at around  $5 \text{ m s}^{-1} \text{ dec}^{-1}$  between late November and early December,  
1157 and reaches the lower troposphere in January. The results from ERA-Interim, JRA-55 and MERRA  
1158 are in relatively good agreement, with differences not exceeding  $\pm 0.3 \text{ m s}^{-1} \text{ dec}^{-1}$ . However,  
1159 in CFSR the initial strengthening of the winds in the lower stratosphere occurs earlier than in  
1160 ERA-Interim, while in the lower troposphere they are delayed, indicating a comparatively slower  
1161 downward descent rate in CFSR.

1162 Figure 6.21 shows the trends of the total Eliassen-Palm (EP) flux divergence from  $40\text{-}80^\circ\text{S}$   
1163 derived from the four datasets. We note that MERRA data is excluded from this analysis below  
1164 400 hPa because, unlike other reanalyses, data is not extrapolated below the surface and thus  
1165 zonal-mean diagnostics are not comparable. The EP flux is assessed from a common grid for all  
1166 data sets (Martineau, 2017; Martineau et al., 2018c). In ERA-Interim, there are positive EP flux

1167 divergence anomalies from September to November and negative EP flux divergence anomalies  
1168 from December to February in the lower stratosphere, which imply a strengthening of the polar  
1169 vortex in spring followed by a delayed breakup of the vortex in summer. This is consistent with the  
1170 circulation changes shown in Fig. 6.20. In the stratosphere, the anomalies of EP flux divergence  
1171 are dominated by planetary waves. In the troposphere, both planetary and synoptic waves are  
1172 affected. In late austral spring, a region of positive EP flux descends from the upper troposphere  
1173 down to the surface, which is dominated by planetary waves in the upper troposphere and synoptic  
1174 waves in the lower troposphere. These wave forcing anomalies are consistent with the downward  
1175 descent of strengthened circumpolar winds, shown in Figure 6.20. The other three reanalyses show  
1176 a broadly similar pattern in the stratosphere, particularly JRA-55, although the negative EP flux  
1177 divergence trend in summer is typically strongest in ERA-Interim (by around  $-0.2 \text{ m s}^{-1} \text{ d}^{-1} \text{ dec}^{-1}$ ).  
1178 Considerable differences are detected when compared to MERRA and particularly CFSR, which  
1179 take the form of alternating positive and negative horizontally-orientated bands in total (planetary  
1180 and synoptic) wave contributions. The disagreement is most profound in the troposphere, with  
1181 differences reaching  $\pm 0.8 \text{ m s}^{-1} \text{ d}^{-1} \text{ dec}^{-1}$ . In all four reanalyses the region of negative EP flux  
1182 divergence descends into the upper troposphere during summer, but is less pronounced in ERA-  
1183 Interim largely due to differences in the synoptic wave component.

1184 We also found that the corresponding trend in the vertical component of EP flux (Fig. 6.22) is  
1185 characterized by reduced planetary wave propagation from the troposphere into the stratosphere  
1186 in austral spring and enhanced planetary wave propagation in austral summer. All four re-  
1187 analyses demonstrate similar broad features. Nevertheless, it is apparent that ERA-Interim and  
1188 JRA-55 show stronger and longer lasting upward wave propagation in austral spring compared to  
1189 MERRA and CFSR. In the troposphere, the intensification of winds during summer is associated  
1190 with anomalies of both vertical and horizontal (not shown) synoptic EP flux divergence anom-  
1191 alies. The results for CFSR, in particular, show considerable differences when compared with the  
1192 other three reanalyses. The disagreement again takes the form of alternating positive and negative  
1193 horizontally-orientated bands.

1194 These banded features most likely originate from the stability parameter in the vertical com-  
1195 ponent of the EP flux, which is affected by the banded structure of zonally-averaged temperature  
1196 trend anomalies (Fig. 6.20). This may be due in part to model drift induced by radiative heating  
1197 imbalance during data assimilation, rather than observational errors (e.g., Lu et al., 2015). Simi-  
1198 lar banded structures are observed in temperature anomalies (Fig. 1 of Long et al., 2017, see also  
1199 Chapter 3) and may result from discontinuities in the assimilation of temperatures retrieved from  
1200 satellite sensors, which are known to show vertical oscillations when compared among sensors.

1201 The four modern reanalyses support the notion that ozone depletion leads to a strengthening of  
1202 the stratospheric polar vortex and consequent downward movement of zonal mean anomalies. They  
1203 broadly agree on characterising the dynamical evolution of circulation anomalies and associated  
1204 wave forcing in high southern latitudes during the period of formation of the ozone hole (Thompson  
1205 et al., 2011; Son et al., 2010, 2018). The wave driving characteristics associated with the circulation  
1206 changes are in general agreement with the hypothesis examined by Orr et al. (2012). Noticeably  
1207 large differences in EP fluxes and divergence are found in CFSR compared to the other three  
1208 reanalyses datasets, which appear to be related to the aforementioned vertically alternating positive  
1209 and negative anomalies in temperature.

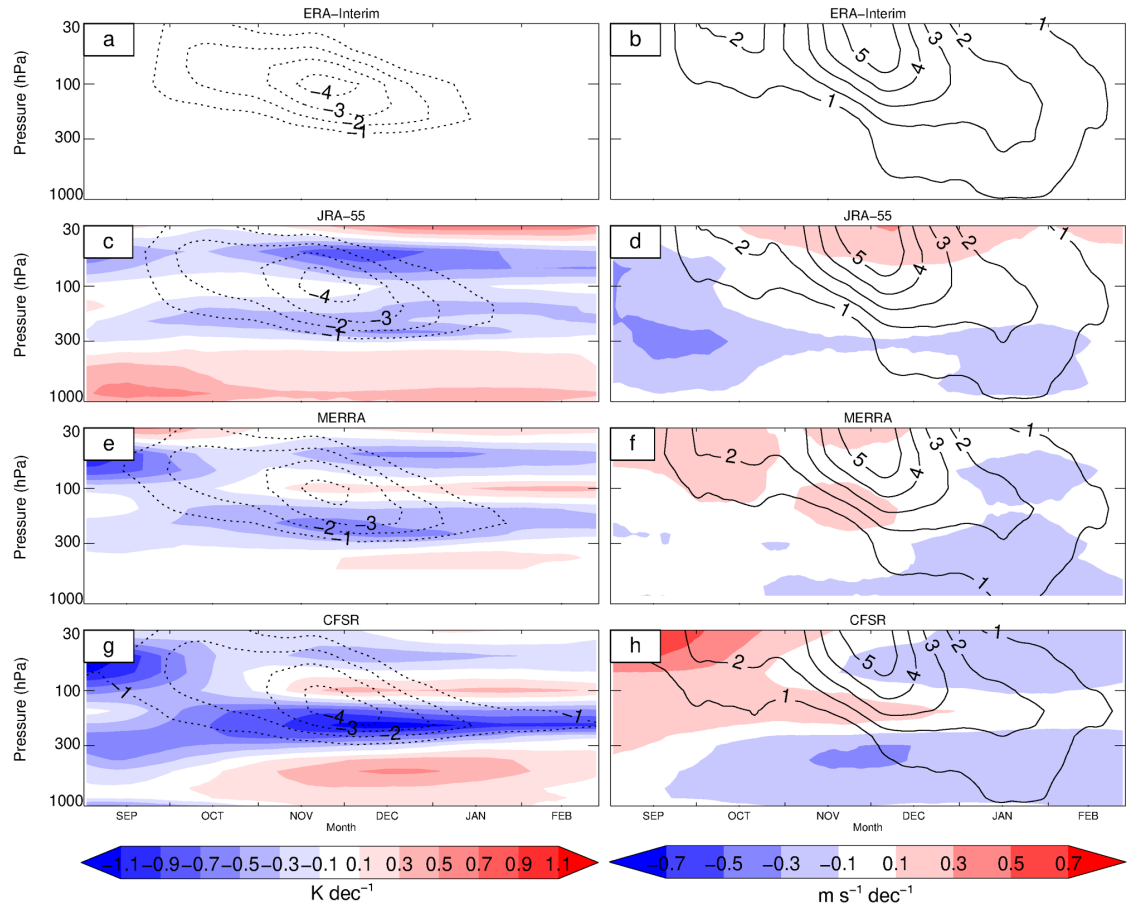


**Figure 6.20:** (left) The dashed contours show time-height cross sections of zonal-mean temperature trend (with contour intervals of  $1 \text{ K dec}^{-1}$ ) averaged over latitudes  $60\text{-}90^\circ\text{S}$  during 1979-2001 for a) ERA-Interim, c) JRA-55, e) MERRA, and g) CFSR. The shadings show the differences between the various reanalyses and ERA-Interim at intervals of  $\pm 0.1$ ,  $\pm 0.3$ ,  $\pm 0.5$ ,  $\pm 0.7$ ,  $\pm 0.9$  and  $\pm 1.1 \text{ K dec}^{-1}$ . (right) The contours show time-height cross sections of zonal-mean zonal wind trend (with contour intervals of  $1 \text{ m s}^{-1} \text{ dec}^{-1}$ ) averaged over latitudes  $50\text{-}70^\circ\text{S}$  during 1979-2001 for b) ERA-Interim, d) JRA-55, f) MERRA, and h) CFSR. The shadings show the differences between the various reanalyses and ERA-Interim at intervals of  $\pm 0.1$ ,  $\pm 0.3$ ,  $\pm 0.5$ , and  $\pm 0.7 \text{ m s}^{-1} \text{ dec}^{-1}$ .

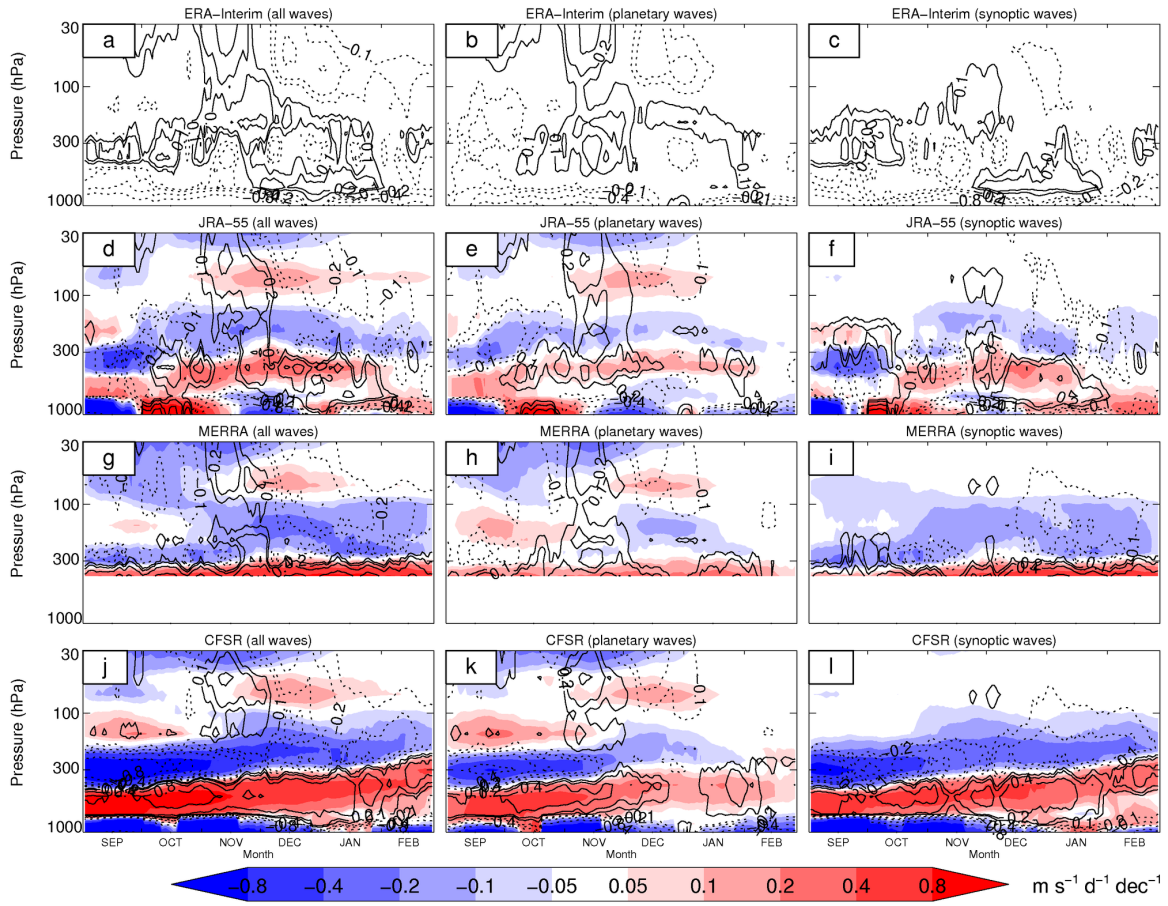


**Figure 6.21:** The contours show time-height cross sections of the trend in the EP flux divergence due to all waves (left), planetary-scale waves (middle) and synoptic-scale waves (right) averaged over the latitude band of 40-80°S during 1979-2001 for (a-c) ERA-Interim, (d-f) JRA-55, (g-i) MERRA, and (j-l) CFSR at intervals of  $\pm 0.1$ ,  $\pm 0.2$ ,  $\pm 0.4$  and  $\pm 0.8 \text{ m s}^{-1} \text{ d}^{-1} \text{ dec}^{-1}$ . Solid and dashed contours indicate positive and negative values, respectively. The shadings show the differences between the various reanalyses and ERA-Interim at intervals of  $\pm 0.05$ ,  $\pm 0.1$ ,  $\pm 0.2$ ,  $\pm 0.4$  and  $\pm 0.8 \text{ m s}^{-1} \text{ d}^{-1} \text{ dec}^{-1}$ . Note that MERRA data below 400 hPa is excluded.

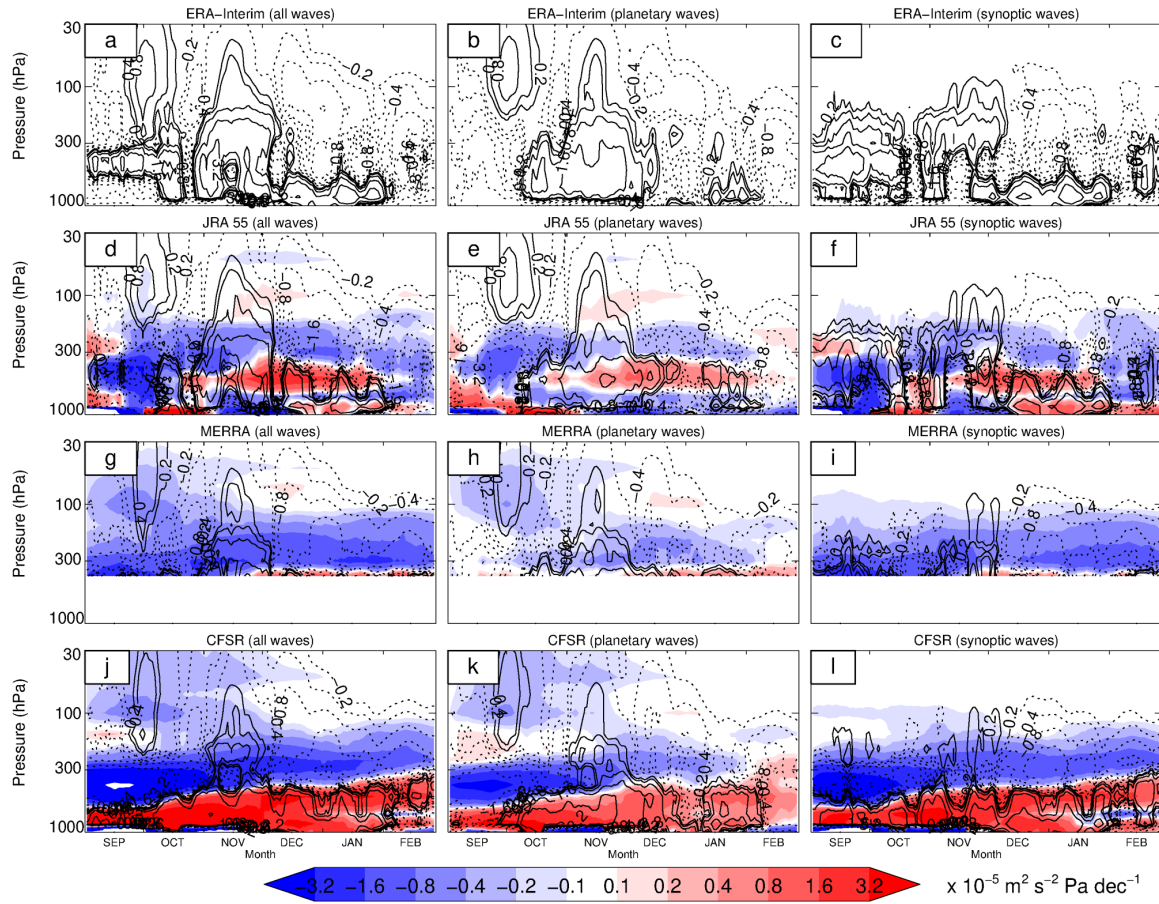


**Figure 6.22:** The contours show time-height cross sections of the trend in the vertical component of EP flux due to all waves (left), planetary-scale waves (middle) and synoptic-scale waves (right) averaged over the latitude band of 40-80°S during 1979-2001 for (a-c) ERA-Interim, (d-f) JRA-55, (g-i) MERRA, and (j-l) CFSR at intervals of  $\pm 0.2$ ,  $\pm 0.4$ ,  $\pm 0.8$ ,  $\pm 1.6$ ,  $\pm 3.2$  and  $\pm 10.0 \times 10^{-5} \text{ m}^2 \text{ s}^{-2} \text{ Pa dec}^{-1}$ . Solid and dashed contours indicate positive and negative values, respectively. The shadings show the differences between the various reanalyses and ERA-Interim at intervals of  $\pm 0.1$ ,  $\pm 0.2$ ,  $\pm 0.4$ ,  $\pm 0.8$ ,  $\pm 1.6$  and  $\pm 3.2 \times 10^{-5} \text{ m}^2 \text{ s}^{-2} \text{ Pa dec}^{-1}$ . Note that MERRA data below 400 hPa is excluded.

## 1210 6.9 Conclusions and Future Work

1211 We have assessed the reanalyses' representation of large scale coupling between the troposphere  
1212 and the stratospheric polar vortices, which are present during the extended winter season (or, polar  
1213 night) of each hemisphere. This coupling is chiefly effected through major Sudden Stratospheric  
1214 Warming (SSW) events, which are found almost exclusively in the Northern Hemisphere. Much  
1215 of our focus has thus been on the boreal extratropical atmosphere on synoptic to intraseasonal  
1216 time scales (Section 6.4). The influence of the tropics on the Northern Hemisphere polar vortex,  
1217 however, is felt through modulation of SSWs by the tropical ocean (ENSO) and stratosphere (QBO)  
1218 on lower frequencies (Section 6.7). Large scale coupling on synoptic to seasonal timescales in  
1219 both hemispheres was assessed by comparing the annular mode indices and final warming events  
1220 in Sections 6.5 and 6.6, respectively. Finally, anthropogenic induced ozone loss caused significant  
1221 trends in the polar vortex over Antarctica, as assessed in Section 6.8.

1222 Our assessment has largely focused on the self-consistency of a given reanalysis, and the con-  
1223 sistency between the different reanalyses, as opposed to a direct validation against measurements.  
1224 The large scale circulation cannot be easily assessed from measurements directly. Surface based  
1225 observations (e.g., radiosondes) generally provide a very localized (point) measurement, while  
1226 satellite irradiance measurements provide indirect information about composition and tempera-  
1227 ture<sup>2</sup>. These measurements can of course be directly linked to the large scale circulation, but the  
1228 best way of doing so is through a reanalysis, which allows one to interpolate between localized  
1229 measurements and incorporate retrieval information to infer temperature, and hence the balanced  
1230 circulation.

1231 Figs. 6.23 and 6.24 provide an overview of reanalyses performance for the satellite (1979-)  
1232 and pre-satellite (1958-78) periods respectively, based on metrics discussed in Sections 6.4 to 6.8.  
1233 We have used the 4 point scale used by all chapters in this report. In some cases, we struggled to  
1234 find entirely objective measures to provide these scores, and therefore urge the reader to consult  
1235 the relevant sections of the report for a more careful analysis. *Demonstrated suitable* indicates  
1236 that a reanalysis provides a self-consistent representation of the large scale circulation that is very  
1237 similar to other reanalyses at the same level. For the very large scale structures (e.g., planetary wave  
1238 structure preceding an SSW), nearly all full-input reanalyses provide a comparable representation.  
1239 As detailed in previous sections, on finer scales, and particularly at higher elevations, the more  
1240 recent reanalyses become more clearly superior.

1241 *Suitable with Limitations* indicates that a reanalysis provides a fairly consistent representa-  
1242 tion of circulation; conclusions from previous studies that used these reanalyses would not differ  
1243 significantly if redone with a *Demonstrated Suitable* reanalysis. However, absent a compelling  
1244 reason, these reanalyses should not be used for further research. *Use with Caution* has generally  
1245 been applied only to the surface-input reanalyses, and the older NCEP products, which exhibit  
1246 clear inconsistencies, particularly near their upper boundary at 10 hPa. Surface-input reanalyses  
1247 are severely handicapped when it comes to the representation of the stratosphere, but in some  
1248 cases could be used to explore variability on longer time scales. We also generally recommend to  
1249 use caution when evaluating trends since reanalysis data is affected by artificial jumps caused by  
1250 discontinuities in assimilated observations (Lu et al., 2015; Long et al., 2017, see also Chapter 3).

1251 Finally, as the name would imply, *Demonstrated Unsuitable* indicates the presence of clear

<sup>2</sup>The new European Space Agency Aeolus mission, launched in 2018 is an exception, designed to provide direct wind measurements.

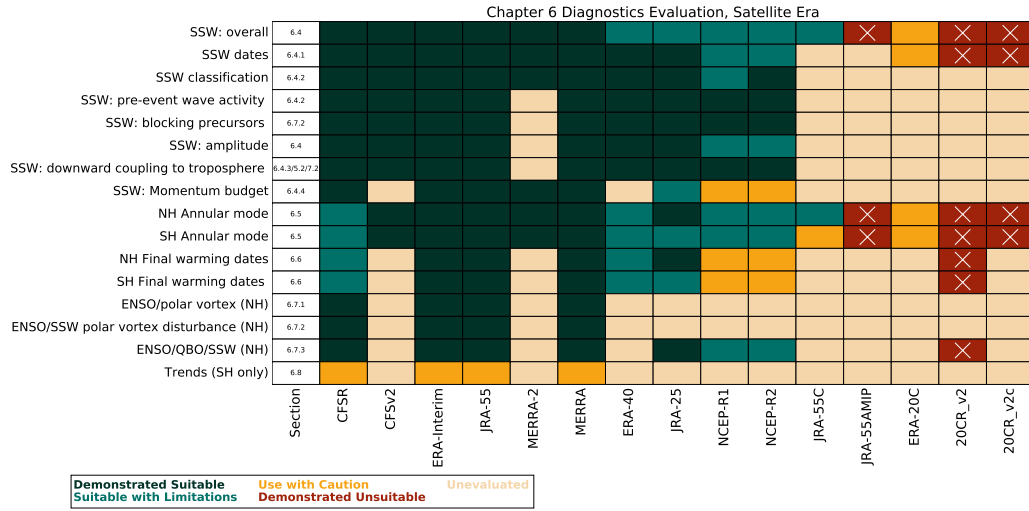


**Figure 6.23:** Metric based evaluation of the reanalyses during the satellite era, 1979 onward. Please see text for further details.

problems in a reanalysis product. In particular, all of the full-input reanalyses show clear sign of divergence from basic measurements in the Southern Hemisphere before 1979. This is not to say, however, that there is no useful information in them. We also found significant biases in the mean state and variability of the polar vortex in the NOAA 20CR surface-input reanalysis, such that we do not recommend it for the purpose of investigating stratosphere-troposphere coupling.

We find that nearly all measures of large scale coupling between the extratropical stratosphere and the troposphere are dominated by sampling uncertainty, as opposed to uncertainty in the reanalyses. As a result, conclusions based on any full (or conventional-input) reanalysis during the satellite era are generally valid. To put this more precisely, differences between the reanalyses are always smaller than the sampling uncertainty. One would not obtain results that are significantly different if you picked one reanalysis over another. The dominance of sampling uncertainty implies that our characterization of stratosphere-troposphere coupling is limited by the length of record; in a sense, we have a “small data” problem.

In the Northern Hemisphere, there is evidence that conventional observations are sufficient to constrain reanalyses from at least 1958 onward, as indicated in Figure 6.24. Given the dominance of sampling uncertainty, the longer record available in the boreal hemisphere is important. An additional two decades of high quality reanalysis, as provided by JRA-55, reduces uncertainty in stratosphere-coupling processes by about 20%. This reduction in uncertainty dwarfs the differences between the modern reanalysis over the satellite period, and makes a case for using JRA-55. We are excited that ERA5 will provide a reanalysis of the atmosphere from 1950, and it is a high priority for future work to more fully assess and compare this reanalysis.

The dominance of sampling uncertainty has implications for event based diagnostics, notably SSWs. Results based on different reanalyses may appear to diverge from one another more substantively if one does not compare the same events, i.e., use the same dates. This divergence, however, is really sampling uncertainty, aliasing into the signal.

All this said, we find that the modern reanalyses, ERA-Interim, JRA-55, MERRA 1 and 2, and to a slightly lesser extent, CFSR/CFSv2, are demonstrably superior to earlier reanalyses, providing

Chap 6 Diagnostics Eval, Pre-Satellite Era						
	6.4				X	X
SSW: overall						
SSW dates					X	X
SSW classification						
SSW: pre-event wave activity						
SSW: blocking precursors						
SSW: amplitude						
SSW: downward coupling to troposphere						
NH Annular modes					X	X
SH Annular modes	X	X	X		X	X
Section	JRA-55	ERA-40	NCEP-R1	ERA-20C	20CR-v2	20CR-v2c
	Demonstrated Suitable Suitable with Limitations	Use with Caution Demonstrated Unsuitable	Unevaluated			

**Figure 6.24:** Metric based evaluation of the reanalyses during the pre-satellite era from 1958-1978.

1279 a more dynamically consistent representation of the circulation. Over the limited period for which  
 1280 it is available, ERA5 also appears to be equally high quality as well. *As a matter of best practice,*  
 1281 *we would urge all users to avoid earlier reanalyses unless there is specific need for them.* As a  
 1282 practical note, modern reanalyses are available at reduced resolution. Based largely on anecdotal  
 1283 evidence, this appears to be a common reason why NCEP-R1 is still used widely: it is smaller,  
 1284 and thus simply easier to download. Reduced resolution is appropriate for many analyses of the  
 1285 large scale circulation, but it is recommended to use a modern reanalysis with a reduced resolution  
 1286 instead of NCEP-R1. An exception is when real-time data availability is required but we note that  
 1287 by mid 2020, ERA5 will be provided five days behind real time.

1288 The surface-input reanalyses are generally inferior in their representation of stratospheric vari-  
 1289 ability, but may still provide research value. We do not find evidence that NOAA-20CR reanalyses  
 1290 accurately capture stratospheric variability; they are therefore not recommended for use. There is  
 1291 evidence that ERA-20C has accurate climatological variability in the stratosphere, and substantial  
 1292 skill in recent decades of capturing the actual variability. It is not recommended for use if restricted  
 1293 to periods where other reanalyses are available, but could be valuable for analysis of stratosphere-  
 1294 troposphere coupling on longer time scales. It should, however, be viewed as a mixture of a high  
 1295 quality free running model and a reanalysis, as stratospheric variability is only partially constrained  
 1296 by observations.

1297 To conclude, we provide an overall, albeit more subjective, assessment of the reanalyses in  
 1298 Table 6.3. Full-input reanalyses, which make use of all available observations at a given time,  
 1299 have been marked recommended, consistent, or inconsistent. *Recommended* does not necessarily  
 1300 mean error-free, but indicates a self-consistent representation of the coupled variability, and consis-  
 1301 tency with other recommended reanalyses and observational constraints where available. We have  
 1302 marked other reanalyses *consistent* when differences between them and the recommended reanal-  
 1303 yses are small relative to sampling uncertainty. Hence published results based on these reanalyses  
 1304 would not be significantly different if they were redone with a recommended reanalysis. A mark of  
 1305 *inconsistent* indicates that the reanalysis differs substantially with respect to other reanalysis data  
 1306 sets and/or available observational constraints. While “inconsistent” is meant to convey a clear  
 1307 warning, it does not imply that there is no useful information in these reanalysis products.

1308 Given the dominance of sampling uncertainty, we may be able to glean additional confidence  
 1309 in stratosphere-troposphere coupling by careful use of earlier records and limited input reanalyses

**Table 6.3:** Recommendations on the use of atmospheric reanalyses to evaluate the large scale coupling between the stratospheric polar vortex and the tropospheric circulation on synoptic to interannual time scales. *This endorsement does not include the analysis of trends, where greater caution must be employed, as discussed in Section 6.8.*

reanalysis	post-satellite era, 1979 - present		pre-satellite era, 1958-1979	
	NH	SH	NH	SH
ERA-40	consistent	consistent	consistent*	inconsistent
ERA-Interim <sup>†</sup>	recommended use w/ caution	recommended use w/ caution	n.a. use w/ caution	n.a. use w/ caution
ERA-20C				
JRA-25	consistent	consistent	n.a.	n.a.
JRA-55	recommended	recommended	recommended*	inconsistent
JRA-55C	consistent*	use w/ caution	n.a.	n.a.
JRA-55AMIP	inconsistent	inconsistent	inconsistent	inconsistent
MERRA	consistent	consistent	n.a.	n.a.
MERRA-2	recommended	recommended	n.a.	n.a.
NCEP-R1	consistent*	consistent*	consistent*	inconsistent
NCEP-R2	consistent*	consistent*	n.a.	n.a.
CFSR	recommended	recommended	n.a.	n.a.
CFSv2	recommended	recommended	n.a.	n.a.
20CR v2	inconsistent	inconsistent	inconsistent	inconsistent
20CR v2c	inconsistent	inconsistent	inconsistent	inconsistent

\*There are few conventional observations above 10 hPa, and caution must be employed above this level (or the reanalysis itself does not extend past 10 hPa).

<sup>†</sup>ERA-Interim is being supplanted by the ERA5 reanalysis. Tentative analysis suggests that ERA5 is as good as ERA-Interim, if not better, but we do not have sufficient evidence to make a full recommendation. It will be particularly important to evaluate its performance in the Northern Hemisphere during the pre-satellite era.

1310 (Hitchcock, 2019). *Use w/ caution* has been applied to alternative reanalyses (JRA-55C and ERA-  
 1311 20C), the latter of which can be used to explore variability on longer time scales. NOAA-20CR  
 1312 may be suitable for analysis of the troposphere, but exhibits clear biases in the variability of the  
 1313 stratosphere. ERA-20C, while clearly not as accurate as modern, full-input reanalysis, does appear  
 1314 capable of capturing information about the variability of the stratosphere given only surface data.  
 1315 This feat alone establishes the remarkably tight coupling between the troposphere and stratosphere  
 1316 in our atmosphere.

## 1317 Appendix: Detection and classification of major SSW events

1318 The onset dates of SSW events identified independently for each reanalysis data sets are listed in  
 1319 Table 6.4. Then, for the common dates whose identification is described in Section 6.2, events  
 1320 are classified as to whether they are splits or displacements according a method adapted from  
 1321 Seviour et al. (2013) (Table 6.5), the Shibata method (Table 6.6) and the method of Lehtonen and  
 1322 Karpechko (2016) (Table 6.7). These methods are described in more detail in Section 6.4.2.

**Table 6.4:** Identification of major SSW events in reanalyses. The criterion for the detection is a reversal of zonal-mean zonal wind at 60°N and 10 hPa (see Section 6.4.1 for more details). Cases where the reanalysis deviates from the “common” events are highlighted in bold. Events that do not show a positive meridional temperature gradient at the same level within ± 5 days of the zonal wind reversal are highlighted in green.

common	NCEP-R1	CFSR	ERA-40	ERA-Interim	JRA-25	JRA-55	MERRA	MERRA-2	NCEP-R2
30-Jan-58	30-Jan-58		<b>31-Jan-58</b>			30-Jan-58			
—	<b>30-Nov-58</b>		—			—			
17-Jan-60	<b>16-Jan-60</b>		17-Jan-60			17-Jan-60			
29-Jan-63	***		<b>28-Jan-63</b>			<b>30-Jan-63</b>			
—	<b>23-Mar-65</b>		—			—			
17-Dec-65	<b>8-Dec-65</b>		<b>16-Dec-65</b>			<b>18-Dec-65</b>			
23-Feb-66	<b>24-Feb-66</b>		23-Feb-66			23-Feb-66			
7-Jan-68	***		7-Jan-68			7-Jan-68			
28-Nov-68	<b>27-Nov-68</b>		28-Nov-68			<b>29-Nov-68</b>			
13-Mar-69	13-Mar-69		13-Mar-69			***			
2-Jan-70	2-Jan-70		2-Jan-70			2-Jan-70			
18-Jan-71	17-Jan-71		18-Jan-71			18-Jan-71			
20-Mar-71	<b>20-Mar-71</b>		20-Mar-71			20-Mar-71			
31-Jan-73	<b>2-Feb-73</b>		31-Jan-73			31-Jan-73			
9-Jan-77	***		9-Jan-77			9-Jan-77			
22-Feb-79	22-Feb-79	22-Feb-79	22-Feb-79	22-Feb-79	22-Feb-79	22-Feb-79			22-Feb-79
29-Feb-80	29-Feb-80	29-Feb-80	29-Feb-80	29-Feb-80	29-Feb-80	29-Feb-80	29-Feb-80	29-Feb-80	29-Feb-80
—	—	—	—	—	<b>6-Feb-81</b>	<b>6-Feb-81</b>	—	—	—
4-Mar-81	***	<b>3-Mar-81</b>	4-Mar-81	4-Mar-81	4-Mar-81	<b>4-Mar-81</b>	4-Mar-81	***	***
4-Dec-81	4-Dec-81	4-Dec-81	4-Dec-81	4-Dec-81	4-Dec-81	4-Dec-81	4-Dec-81	4-Dec-81	4-Dec-81
24-Feb-84	24-Feb-84	24-Feb-84	24-Feb-84	24-Feb-84	24-Feb-84	24-Feb-84	24-Feb-84	24-Feb-84	24-Feb-84
1-Jan-85	<b>2-Jan-85</b>	1-Jan-85	1-Jan-85	1-Jan-85	1-Jan-85	1-Jan-85	1-Jan-85	01-Jan-85	<b>31-Dec-84</b>
23-Jan-87	23-Jan-87	23-Jan-87	23-Jan-87	23-Jan-87	23-Jan-87	23-Jan-87	23-Jan-87	23-Jan-87	23-Jan-87
8-Dec-87	8-Dec-87	8-Dec-87	8-Dec-87	8-Dec-87	8-Dec-87	8-Dec-87	8-Dec-87	8-Dec-87	8-Dec-87
14-Mar-88	14-Mar-88	14-Mar-88	14-Mar-88	14-Mar-88	14-Mar-88	14-Mar-88	14-Mar-88	14-Mar-88	14-Mar-88
21-Feb-89	<b>22-Feb-89</b>	21-Feb-89	21-Feb-89	21-Feb-89	21-Feb-89	21-Feb-89	21-Feb-89	21-Feb-89	<b>22-Feb-89</b>
—	—	—	—	—	—	—	—	—	<b>5-Feb-95</b>
15-Dec-98	15-Dec-98	15-Dec-98	15-Dec-98	15-Dec-98	15-Dec-98	15-Dec-98	15-Dec-98	15-Dec-98	15-Dec-98
26-Feb-99	<b>25-Feb-99</b>	26-Feb-99	26-Feb-99	26-Feb-99	26-Feb-99	26-Feb-99	26-Feb-99	26-Feb-99	26-Feb-99
20-Mar-00	20-Mar-00	20-Mar-00	20-Mar-00	20-Mar-00	20-Mar-00	20-Mar-00	20-Mar-00	20-Mar-00	20-Mar-00
11-Feb-01	11-Feb-01	11-Feb-01	11-Feb-01	11-Feb-01	11-Feb-01	11-Feb-01	11-Feb-01	11-Feb-01	<b>12-Feb-01</b>
31-Dec-01	<b>2-Jan-02</b>	<b>30-Dec-01</b>	31-Dec-01	<b>30-Dec-01</b>	31-Dec-01	31-Dec-01	<b>30-Dec-01</b>	<b>30-Dec-01</b>	<b>1-Jan-02</b>
—	—	<b>17-Feb-02</b>		<b>18-Feb-02</b>	—	—	—	<b>17-Feb-02</b>	—
18-Jan-03	18-Jan-03	18-Jan-03	18-Jan-03	18-Jan-03	18-Jan-03	18-Jan-03	18-Jan-03	18-Jan-03	18-Jan-03
5-Jan-04	<b>7-Jan-04</b>	5-Jan-04	5-Jan-04	<b>6-Jan-04</b>	5-Jan-04	5-Jan-04	5-Jan-04	5-Jan-04	<b>6-Jan-04</b>
21-Jan-06	21-Jan-06	21-Jan-06	21-Jan-06	21-Jan-06	21-Jan-06	21-Jan-06	21-Jan-06	21-Jan-06	21-Jan-06
24-Feb-07	24-Feb-07	24-Feb-07	24-Feb-07	24-Feb-07	24-Feb-07	24-Feb-07	24-Feb-07	24-Feb-07	24-Feb-07
22-Feb-08	22-Feb-08	22-Feb-08	22-Feb-08	22-Feb-08	22-Feb-08	22-Feb-08	22-Feb-08	22-Feb-08	22-Feb-08
24-Jan-09	24-Jan-09	24-Jan-09	24-Jan-09	24-Jan-09	24-Jan-09	24-Jan-09	24-Jan-09	24-Jan-09	24-Jan-09
9-Feb-10	9-Feb-10	9-Feb-10	9-Feb-10	9-Feb-10	9-Feb-10	9-Feb-10	9-Feb-10	9-Feb-10	9-Feb-10
24-Mar-10	24-Mar-10	24-Mar-10		24-Mar-10	24-Mar-10	24-Mar-10	24-Mar-10	24-Mar-10	24-Mar-10

**Table 6.5:** Classification of SSW events into splits and displacements adapted from the method described in Seviour et al. (2013). D and S denote displacement and split events, respectively. U denotes unclassifiable events. Bold text highlights disagreement from the “common” classification. Asterisks indicate that there was substantial disagreement on the classification of the 15-Dec-98, 20-Mar-00, and 09-Feb-10 events.

Shared Dates	common	NCEP-R1	CFSR	ERA-40	ERA-Interim	JRA-25	JRA-55	MERRA	MERRA2	NCEP-R2
30-Jan-58	D	D		D			D			
17-Jan-60	S	S		<b>D</b>			S			
29-Jan-63	S	S		S			S			
17-Dec-65	D	D		D			D			
23-Feb-66	D	D		D			<b>U</b>			
07-Jan-68	S	S		S			S			
28-Nov-68	D	D		D			D			
13-Mar-69	S	<b>U</b>		S			S			
02-Jan-70	S	S		S			S			
18-Jan-71	S	S		S			S			
20-Mar-71	D	D		D			D			
31-Jan-73	S	S		S			S			
09-Jan-77	S	S		S			S			
22-Feb-79	S	S	S	S	S	S	S	S		S
29-Feb-80	D	D	D	D	D	D	D	D		D
04-Mar-81	D	D	D	D	D	D	D	D		D
04-Dec-81	U	U	U	U	U	U	U	U		U
24-Feb-84	D	D	D	D	D	D	D	D		D
01-Jan-85	S	S	S	S	S	S	S	S		S
23-Jan-87	D	D	D	D	D	D	D	D		D
08-Dec-87	S	S	S	S	S	S	S	S		S
14-Mar-88	S	S	S	S	S	S	S	S		S
21-Feb-89	S	<b>D</b>	S	S	S	S	S	S		S
15-Dec-98	D*	D	<b>U</b>	D	D	<b>U</b>	D	D	<b>U</b>	D
26-Feb-99	S	S	S	S	S	S	S	S		S
20-Mar-00	U*	U	<b>D</b>	U	<b>D</b>	U	<b>D</b>	U		U
11-Feb-01	S	S	S	S	S	S	S	S		S
31-Dec-01	S	S	S	S	S	S	S	S		S
18-Jan-03	S	S	S		S	S	S	S		S
05-Jan-04	D	D	D		D	D	D	D		D
21-Jan-06	D	D	D		D	D	D	D		D
24-Feb-07	D	D	D		D	D	D	D		D
22-Feb-08	D	D	D		D	D	D	D		D
24-Jan-09	S	S	S		S	S	S	S		S
09-Feb-10	U*	<b>S</b>	U		<b>D</b>	<b>D</b>	<b>S</b>	U	<b>D</b>	<b>S</b>
24-Mar-10	D	D	D		D	D	D	D		D

**Table 6.6:** Classification of major SSW events into splits and displacements using the Shibata technique (Ayarzagüena et al., 2019). S and D denote split and displacement events, respectively.

Shared Dates common	NCEP-R1	CFSR	ERA-40	ERA-Interim	JRA-25	JRA-55	MERRA	MERRA-2	NCEP-R2
30-Jan-58	S	S	S			S			
17-Jan-60	D	D	D			S			
29-Jan-63	S	S	S			S			
17-Dec-65	D	<b>S</b>	D			D			
23-Feb-66	D	D	D			D			
07-Jan-68	S	S	S			S			
28-Nov-68	D	D	D			D			
13-Mar-69	D	D	D			D			
02-Jan-70	D	D	D			D			
18-Jan-71	S	S	S			S			
20-Mar-71	D	D	D			D			
31-Jan-73	S	S	S			S			
09-Jan-77	D	D	D			D			
22-Feb-79	S	S	S	S	S	S	S		S
29-Feb-80	D	D	D	D	D	D	D	D	D
04-Mar-81	D	D	D	D	D	D	D	D	D
04-Dec-81	D	D	D	D	D	D	D	D	<b>S</b>
24-Feb-84	D	D	D	D	D	D	D	D	D
01-Jan-85	S	S	S	<b>D</b>	S	<b>D</b>	S	S	S
23-Jan-87	D	D	D	D	D	D	D	D	D
08-Dec-87	S	<b>D</b>	S	S	<b>D</b>	S	S	S	S
14-Mar-88	S	S	S	S	S	S	S	S	S
21-Feb-89	S	S	S	S	S	S	S	S	S
15-Dec-98	S	S	S	S	S	S	S	S	S
26-Feb-99	S	S	S	S	S	S	S	S	S
20-Mar-00	D	D	D	D	D	D	D	<b>S</b>	D
11-Feb-01	D	D	D	D	D	D	D	<b>S</b>	D
31-Dec-01	D	D	D	D	D	D	D	D	D
18-Jan-03	S	S	S	S	S	S	S	S	<b>D</b>
05-Jan-04	D	D	D	D	D	D	D	D	D
21-Jan-06	D	D	D	D	D	D	D	D	D
24-Feb-07	D	D	D	D	D	D	D	D	D
22-Feb-08	D	D	D	D	D	D	D	D	D
24-Jan-09	S	S	S	S	S	S	S	S	S
09-Feb-10	S	S	S	S	S	S	S	S	S
24-Mar-10	D	D	D	D	D	D	D	D	D

**Table 6.7:** Classification of major SSW events into splits and displacements using the Lehtonen and Karpechko (2016) method. S and D denote split and displacement events, respectively.

Shared Dates common	NCEP-R1	CFSR	ERA-40	ERA-Interim	JRA-25	JRA-55	MERRA	MERRA-2	NCEP-R2
30-Jan-58	S	S	S			S			
17-Jan-60	D	D	D			S			
29-Jan-63	D	D	S			D			
17-Dec-65	D	D	D			D			
23-Feb-66	S	S	S			S			
7-Jan-68	S	S	S			S			
28-Nov-68	D	D	D			D			
13-Mar-69	D	D	D			D			
2-Jan-70	D	D	D			S			
18-Jan-71	S	S	S			S			
20-Mar-71	D	D	D			D			
31-Jan-73	S	S	S			S			
9-Jan-77	S	S	S			S			
22-Feb-79	S	S	S	S	S	S	S		S
29-Feb-80	D	D	D	D	D	D	D	D	D
4-Mar-81	D	D	D	D	D	D	D	D	D
4-Dec-81	D	D	D	D	D	D	D	D	D
24-Feb-84	D	D	D	D	D	D	D	D	D
1-Jan-85	S	S	S	S	S	S	S	S	S
23-Jan-87	D	D	D	D	D	D	D	D	D
8-Dec-87	S	S	S	S	S	S	S	S	S
14-Mar-88	S	S	S	S	S	S	S	S	S
21-Feb-89	S	S	S	S	S	S	S	S	S
15-Dec-98	D	D	D	D	D	D	D	D	D
26-Feb-99	S	S	S	S	S	S	S	S	S
20-Mar-00	D	D	D	D	D	D	D	D	D
11-Feb-01	S	S	D	S	D	S	S	S	S
31-Dec-01	D	D	D	D	D	D	D	D	D
18-Jan-03	S	S	S	S	S	S	S	S	S
5-Jan-04	D	D	D	D	D	D	D	D	D
21-Jan-06	D	D	D	D	D	D	D	D	D
24-Feb-07	D	D	D	D	D	D	D	D	D
22-Feb-08	D	D	D	D	D	D	D	D	D
24-Jan-09	S	S	S	S	S	S	S	S	S
9-Feb-10	S	S	S	S	S	S	S	S	S
24-Mar-10	D	D	D	D	D	D	D	D	D

1323 **List of Acronyms**

- 1324 ENSO: El Niño-Southern Oscillation  
1325 EP Flux: Eliassen-Palm Flux  
1326 NAM: Northern Annular Mode  
1327 NAO: North Atlantic Oscillation  
1328 QBO: Quasi-biennial Oscillation  
1329 SAM: Southern Annular Mode  
1330 SFW: Stratospheric Final Warming  
1331 SSW: Sudden Stratospheric Warming

1332

1333 **Acknowledgements**

1334 We thank Ilari Lehtonen for providing the classification of the split/displacement events shown  
1335 in Table A4. EPG acknowledges support from the US NSF through grants AGS-1546585 and  
1336 AGS-1852727. PM is a Japan Society for the Promotion of Science (JSPS) international research  
1337 fellow. BA was funded by “Ayudas para la contratación de personal postdoctoral de formación en  
1338 docencia e investigación en los departamentos de la UCM”. BA, DB, NC, FMP and MI were sup-  
1339 ported by the European Project 603557-STRATOCLIM under program FP7-ENV.2013.6.1-2 and  
1340 the Spanish Government through the PALEOSTRAT (CGL2015-69699-R) and JEDiS (RTI2018-  
1341 096402-B-I00) projects. The work of SCH was supported by the Met Office Hadley Centre Cli-  
1342 mate Programme funded by BEIS and Defra. The work by MT was supported by JSPS KAK-  
1343 ENHI Grant Number JP24224011. Figures 6.1, 6.3, 6.4, and 6.16 are reproduced or adapted from  
1344 Ayarzagüena et al. (2019). Figures 6.5, 6.6, and 6.7 are reproduced from Hitchcock (2018). Fig-  
1345 ures 6.8 and 6.9 are reproduced from Martineau et al. (2018b). Figures 6.10 and 6.11 are adapted  
1346 from Gerber and Martineau (2018). Figure 6.17 was adapted from Barriopedro and Calvo (2014).  
1347 All these reproductions are made under a creative commons attribution 4.0 license ([https://www.  
atmospheric-chemistry-and-physics.net/about/licence\\_and\\_copyright.html](https://www.atmospheric-chemistry-and-physics.net/about/licence_and_copyright.html)).

1349 **Bibliography**

- 1350 Andrews, D. G., Holton, J. R., and Leovy, C. B.: Middle Atmosphere Dynamics, Academic Press,  
1351 1987.
- 1352 Ayarzagüena, B. and Serrano, E.: Monthly Characterization of the Tropospheric Circulation over  
1353 the Euro-Atlantic Area in Relation with the Timing of Stratospheric Final Warmings, *J. Climate*,  
1354 22, 6313–6324, doi: [10.1175/2009JCLI2913.1](https://doi.org/10.1175/2009JCLI2913.1), 2009.
- 1355 Ayarzagüena, B., Palmeiro, F. M., Barriopedro, D., Calvo, N., Langematz, U., and Shibata, K.:  
1356 On the representation of major stratospheric warmings in reanalyses, *Atmos. Chem. Phys.*, 19,  
1357 9469–9484, doi: [10.5194/acp-19-9469-2019](https://doi.org/10.5194/acp-19-9469-2019), 2019.
- 1358 Badin, G. and Domeisen, D. I.: A Search for chaotic behavior in Northern Hemisphere strato-  
1359 spheric variability, *J. Atmos. Sci.*, 71, 1494–1507, doi: [10.1175/JAS-D-13-0225.1](https://doi.org/10.1175/JAS-D-13-0225.1), 2014.
- 1360 Baldwin, M. P. and Dunkerton, T. J.: Stratospheric Harbingers of Anomalous Weather Regimes,  
1361 *Science*, 294, 581–584, 2001.
- 1362 Baldwin, M. P. and Thompson, D. W. J.: A critical comparison of stratosphere-troposphere cou-  
1363 pling indices, *Quart. J. Roy. Meteor. Soc.*, 135, 1661–1672, 2009.
- 1364 Baldwin, M. P., Gray, L. J., Dunkerton, T. J., Hamilton, K., Haynes, P. H., Randel, W. J., Holton,  
1365 J. R., Alexander, M. J., Hirota, I., Horinouchi, T., Jones, D. B. A., Kinnear, J. S., Marquardt,  
1366 C., Sato, K., and Takahashi, M.: The Quasi-Biennial Oscillation, *Rev. Geophys.*, 39, 179–229,  
1367 2001.
- 1368 Baldwin, M. P., Stephenson, D. B., Thompson, D. W. J., Dunkerton, T. J., Charlton, A. J., and  
1369 O'Neill, A.: Stratospheric Memory and Skill of Extended-Range Weather Forecasts, *Science*,  
1370 301, 636–640, 2003.
- 1371 Bancalá, S., Krüger, K., and Giorgi, M.: The preconditioning of major sudden stratospheric  
1372 warmings, *J. Geophys. Res. Atm.*, 117, 4101–, doi: [10.1029/2011JD016769](https://doi.org/10.1029/2011JD016769), 2012.
- 1373 Barriopedro, D. and Calvo, N.: On the Relationship between ENSO, Stratospheric Sudden Warm-  
1374 ings, and Blocking, *J. Climate*, 27, 4704–4720, doi: [10.1175/JCLI-D-13-00770.1](https://doi.org/10.1175/JCLI-D-13-00770.1), 2014.
- 1375 Black, R. X.: Stratopsheric Forcing of Surface Climate in the Arctic Oscillation, *J. Clim.*, 15,  
1376 268–277, 2002.
- 1377 Black, R. X. and McDaniel, B. a.: The Dynamics of Northern Hemisphere Stratospheric Final  
1378 Warming Events, *J. Atmos. Sci.*, 64, 2932–2946, doi: [10.1175/JAS3981.1](https://doi.org/10.1175/JAS3981.1), 2007.
- 1379 Brönnimann, S.: Impact of El Niño-Southern Oscillation on European climate, *Rev. Geophys.*, 45,  
1380 RG3003—, doi: [10.1029/2006RG000199.1.INTRODUCTION](https://doi.org/10.1029/2006RG000199.1.INTRODUCTION), 2007.

- 1381 Butler, A. H. and Polvani, L. M.: El Niño, La Niña, and stratospheric sudden warmings: A reevaluation in light of the observational record, *Geophys. Res. Lett.*, 38, 1–5,  
 1382 doi: [10.1029/2011GL048084](https://doi.org/10.1029/2011GL048084), 2011.
- 1383
- 1384 Butler, A. H., Seidel, D. J., Hardiman, S. C., Butchart, N., Birner, T., and Match, A.: Defining Sud-  
 1385 den Stratospheric Warmings, *Bull. Am. Meteorol. Soc.*, 96, 1913–1928, doi: [10.1175/BAMS-D-13-00173.1](https://doi.org/10.1175/BAMS-D-13-00173.1), 2015a.
- 1386
- 1387 Butler, A. H., Seidel, D. J., Hardiman, S. C., Butchart, N., Birner, T., and Match, A.: Defining Sud-  
 1388 den Stratospheric Warmings, *Bull. Am. Meteorol. Soc.*, 96, 1913–1928, doi: [10.1175/BAMS-D-13-00173.1](https://doi.org/10.1175/BAMS-D-13-00173.1), 2015b.
- 1389
- 1390 Butler, A. H., Sjoberg, J. P., Seidel, D. J., and Rosenlof, K. H.: A sudden stratospheric warming  
 1391 compendium, *Earth Syst. Sci. Data*, 9, 63–76, doi: [10.5194/essd-9-63-2017](https://doi.org/10.5194/essd-9-63-2017), 2017.
- 1392
- 1393 Butler, A. H., Charlton-Perez, A., Domeisen, D. I., Simpson, I. R., and Sjoberg, J.: Predictability  
 1394 of Northern Hemisphere Final Stratospheric Warmings and Their Surface Impacts, *Geophys. Res. Lett.*, 46, 10 578–10 588, doi: [10.1029/2019GL083346](https://doi.org/10.1029/2019GL083346), 2019.
- 1395
- 1396 Byrne, N. J. and Shepherd, T. G.: Seasonal persistence of circulation anomalies in the Southern  
 1397 Hemisphere stratosphere, and its implications for the troposphere, *J. Clim.*, pp. JCLI-D-17–0557.1, doi: [10.1175/JCLI-D-17-0557.1](https://doi.org/10.1175/JCLI-D-17-0557.1), 2018.
- 1398
- 1399 Cagnazzo, C. and Manzini, E.: Impact of the stratosphere on the winter tropospheric teleconnec-  
 1400 tions between ENSO and the North Atlantic and European Region, *J. Clim.*, 22, 1223–1238, doi: [10.1175/2008JCLI2549.1](https://doi.org/10.1175/2008JCLI2549.1), 2009.
- 1401
- 1402 Cagnazzo, C., Manzini, E., Calvo, N., Douglass, A., Akiyoshi, H., Bekki, S., Chipperfield, M.,  
 1403 Dameris, M., Deushi, M., Fischer, A. M., Garny, H., Gettelman, A., Giorgi, M. A., Plummer, D.,  
 1404 Rozanov, E., Shepherd, T. G., Shibata, K., Stenke, A., Struthers, H., and Tian, W.: Northern  
 1405 winter stratospheric temperature and ozone responses to ENSO inferred from an ensemble of  
 Chemistry Climate Models, *Atmos. Chem. Phys.*, 9, 8935–8948, doi: [10.5194/acp-9-8935-2009](https://doi.org/10.5194/acp-9-8935-2009),  
 1406 URL <http://www.atmos-chem-phys.net/9/8935/2009/>, 2009.
- 1407
- 1408 Calvo, N., Giorgi, M. A., Garcia-Herrera, R., and Manzini, E.: Nonlinearity of the combined  
 1409 warm ENSO and QBO effects on the Northern Hemisphere polar vortex in MAECHAM5 simu-  
 lations, *J. Geophys. Res.*, 114, D13 109, doi: [10.1029/2008JD011445](https://doi.org/10.1029/2008JD011445), 2009.
- 1410
- 1411 Calvo, N., Iza, M., Hurwitz, M. M., Manzini, E., Peña-Ortiz, C., Butler, A. H., Cagnazzo, C.,  
 1412 Ineson, S., and Garfinkel, C. I.: Northern Hemisphere Stratospheric Pathway of different  
 1413 El Niño flavors in stratosphere-resolving CMIP5 models, *J. Clim.*, pp. JCLI-D-16–0132.1, doi: [10.1175/JCLI-D-16-0132.1](https://doi.org/10.1175/JCLI-D-16-0132.1), 2017.
- 1414
- 1415 Castanheira, J. M. and Barriopedro, D.: Dynamical connection between tropospheric blockings  
 and stratospheric polar vortex, *Geophys. Res. Lett.*, 37, 1–5, doi: [10.1029/2010GL043819](https://doi.org/10.1029/2010GL043819), 2010.
- 1416
- 1417 Charlton, A. J. and Polvani, L. M.: A New Look at Stratospheric Sudden Warmings. Part I: Clima-  
 tology and Modeling Benchmarks, *J. Climate*, 20, 449–469, 2007.

- 1418 Charney, J. G. and Drazin, P. G.: Propagation of Planetary-Scale Disturbances from the Lower into  
1419 the Upper Atmosphere, *J. Geophys. Res.*, 66, 83–109, 1961.
- 1420 Cohen, J. and Jones, J.: Tropospheric Precursors and Stratospheric Warmings, *J. Clim.*, 24, 6562–  
1421 6572, doi: [10.1175/2011JCLI4160.1](https://doi.org/10.1175/2011JCLI4160.1), 2011.
- 1422 Compo, G. P., Whitaker, J. S., Sardeshmukh, P. D., Matsui, N., Allan, R. J., Yin, X., Gleason,  
1423 B. E., Vose, R. S., Rutledge, G., Bessemoulin, P., Brönnimann, S., Brunet, M., Crouthamel,  
1424 R. I., Grant, A. N., Groisman, P. Y., Jones, P. D., Kruk, M. C., Kruger, A. C., Marshall, G. J.,  
1425 Maugeri, M., Mok, H. Y., Nordli, Ø., Ross, T. F., Trigo, R. M., Wang, X. L., Woodruff, S. D.,  
1426 and Worley, S. J.: The Twentieth Century Reanalysis Project, *Q. J. R. Meteorol. Soc.*, 137, 1–28,  
1427 doi: [10.1002/qj.776](https://doi.org/10.1002/qj.776), 2011.
- 1428 Dee, D. P., Uppala, S. M., Simmons, A. J., Berrisford, P., Poli, P., Kobayashi, S., Andrae,  
1429 U., Balmaseda, M. A., Balsamo, G., and Bauer, P.: The ERA-Interim reanalysis: configura-  
1430 tion and performance of the data assimilation system, *Q. J. R. Meteorol. Soc.*, 137, 553–597,  
1431 doi: [10.1002/qj.828](https://doi.org/10.1002/qj.828), 2011.
- 1432 Domeisen, D. I., Garfinkel, C. I., and Butler, A. H.: The Teleconnection of El Niño Southern  
1433 Oscillation to the Stratosphere, *Rev. Geophys.*, 57, 5–47, doi: [10.1029/2018RG000596](https://doi.org/10.1029/2018RG000596), 2019a.
- 1434 Domeisen, D. I. V., Butler, A. H., Charlton-Perez, A. J., Ayarzagüena, B., Baldwin, M. P., Dunn-  
1435 Sigouin, E., Furtado, J. C., Garfinkel, C. I., Hitchcock, P., Karpechko, A. Y., Kim, H., Knight,  
1436 J., Lang, A. L., Lim, E., Marshall, A., Roff, G., Schwartz, C., Simpson, I. R., Son, S., and  
1437 Taguchi, M.: The Role of the Stratosphere in Subseasonal to Seasonal Prediction: 2. Pre-  
1438 dictability Arising From Stratosphere-Troposphere Coupling, *J. Geophys. Res. Atmos.*, 125,  
1439 doi: [10.1029/2019JD030923](https://doi.org/10.1029/2019JD030923), 2019b.
- 1440 Esler, J. G. and Matthewman, N. J.: Stratospheric Sudden Warmings as Self-Tuning Resonances.  
1441 Part II: Vortex Displacement Events, *J. Atmos. Sci.*, 68, 2505–2523, doi: [10.1175/JAS-D-11-08.1](https://doi.org/10.1175/JAS-D-11-08.1), 2011.
- 1443 Eyring, V., Butchart, N., Waugh, D. W., Akiyoshi, H., Bekki, J. A. S., Bodeker, G. E., Boville,  
1444 B. A., Bruhl, C., Chipperfield, M. P., Cordero, E., Dameris, M., Deushi, M., Fioletov, V. E.,  
1445 Frith, S. M., Garcia, R. R., Gettelman, A., Giorgi, M. A., Grewe, V., Jourdain, L., Kinnison,  
1446 D. E., Manzini, E., Marchand, M., Marsh, D. R., Nagashima, T., Newman, P. A., Nielsen, J. E.,  
1447 Pawson, S., Pitari, G., Plummer, D. A., Rozanov, E., Schraner, M., Shepherd, T. G., Shibata,  
1448 K., Stolarski, R. S., Struthers, H., Tian, W., and Yoshiki, M.: Assessment of temperature, trace  
1449 species, and ozone in chemistry-climate model simulations of the recent past, *J. Geophys. Res.*,  
1450 111, D22 308, doi: [10.1029/2006JD007327](https://doi.org/10.1029/2006JD007327), 2006.
- 1451 Fujiwara, M., Wright, J. S., Manney, G. L., Gray, L. J., Anstey, J., Birner, T., Davis, S., Gerber,  
1452 E. P., Harvey, V. L., Hegglin, M. I., Homeyer, C. R., Knox, J. A., Krüger, K., Lambert, A., Long,  
1453 C. S., Martineau, P., Molod, A., Monge-Sanz, B. M., Santee, M. L., Tegtmeier, S., Chabriat, S.,  
1454 Tan, D. G. H., Jackson, D. R., Polavarapu, S., Compo, G. P., Dragani, R., Ebisuzaki, W., Harada,  
1455 Y., Kobayashi, C., McCarty, W., Onogi, K., Pawson, S., Simmons, A., Wargan, K., Whitaker,  
1456 J. S., and Zou, C.-Z.: Introduction to the SPARC Reanalysis Intercomparison Project (S-RIP)

- 1457 and overview of the reanalysis systems, *Atmos. Chem. Phys.*, 17, 1417–1452, doi: [10.5194/acp-17-1417-2017](https://doi.org/10.5194/acp-17-1417-2017), 2017.
- 1459 Garfinkel, C. I. and Hartmann, D. L.: Effects of the El Niño–Southern Oscillation and the Quasi-  
1460 Biennial Oscillation on polar temperatures in the stratosphere, *J. Geophys. Res.*, 112, D19 112,  
1461 doi: [10.1029/2007JD008481](https://doi.org/10.1029/2007JD008481), URL <http://doi.wiley.com/10.1029/2007JD008481>, 2007.
- 1462 Garfinkel, C. I. and Hartmann, D. L.: Tropospheric Precursors of Anomalous Northern Hemisphere  
1463 Stratospheric Polar Vortices, *J. Clim.*, 23, 3282–3299, doi: [10.1175/2010JCLI3010.1](https://doi.org/10.1175/2010JCLI3010.1), 2010.
- 1464 Garfinkel, C. I., Butler, A. H., Waugh, D. W., Hurwitz, M. M., and Polvani, L. M.: Why might  
1465 stratospheric sudden warmings occur with similar frequency in El Niño and La Niña winters?, *J.  
1466 Geophys. Res. Atmos.*, 117, 1–11, doi: [10.1029/2012JD017777](https://doi.org/10.1029/2012JD017777), 2012a.
- 1467 Garfinkel, C. I., Shaw, T. a., Hartmann, D. L., and Waugh, D. W.: Does the Holton-Tan Mechanism  
1468 Explain How the Quasi-Biennial Oscillation Modulates the Arctic Polar Vortex?, *J. Atmos. Sci.*,  
1469 69, 1713–1733, doi: [10.1175/JAS-D-11-0209.1](https://doi.org/10.1175/JAS-D-11-0209.1), 2012b.
- 1470 Gelaro, R., McCarty, W., Suárez, M. J., Todling, R., Molod, A., Takacs, L., Randles, C. A., Dar-  
1471 menov, A., Bosilovich, M. G., Reichle, R., Wargan, K., Coy, L., Cullather, R., Draper, C.,  
1472 Akella, S., Buchard, V., Conaty, A., da Silva, A. M., Gu, W., Kim, G.-K., Koster, R., Lucchesi,  
1473 R., Merkova, D., Nielsen, J. E., Partyka, G., Pawson, S., Putman, W., Riendecker, M., Schubert,  
1474 S. D., Sienkiewicz, M., and Zhao, B.: The Modern-Era Retrospective Analysis for Research and  
1475 Applications, Version 2 (MERRA-2), *J. Clim.*, 30, 5419–5454, doi: [10.1175/JCLI-D-16-0758.1](https://doi.org/10.1175/JCLI-D-16-0758.1),  
1476 2017.
- 1477 Gerber, E. P. and Martineau, P.: Quantifying the variability of the annular modes: Reanalysis  
1478 uncertainty vs. sampling uncertainty, *Atmos. Chem. Phys.*, 18, 17 099–17 117, doi: [10.5194/acp-18-17099-2018](https://doi.org/10.5194/acp-18-17099-2018), 2018.
- 1480 Gerber, E. P., Baldwin, M. P., Akiyoshi, H., Austin, J., Bekki, S., Braesicke, P., Butchart, N.,  
1481 Chipperfield, M., Dameris, M., Dhomse, S., Frith, S. M., Garcia, R. R., Garny, H., Gettelman,  
1482 A., Hardiman, S. C., Karpechko, A., Marchand, M., Morgenstern, O., Nielsen, J. E., Pawson, S.,  
1483 Peter, T., Plummer, D. A., Pyle, J. A., Rozanov, E., Scinocca, J. F., Shepherd, T. G., and Smale,  
1484 D.: Stratosphere-Troposphere Coupling and Annular Mode Variability in Chemistry-Climate  
1485 Models, *J. Geophys. Res.*, 115, D00M06, doi: [10.1029/2009JD013770](https://doi.org/10.1029/2009JD013770), 2010.
- 1486 Gómez-Escalor, M., Fueglistaler, S., Calvo, N., and Barriopedro, D.: Changes in polar strato-  
1487 spheric temperature climatology in relation to stratospheric sudden warming occurrence, *Geo-  
1488 phys. Res. Lett.*, 39, n/a–n/a, doi: [10.1029/2012GL053632](https://doi.org/10.1029/2012GL053632), 2012.
- 1489 Gray, L. J., Anstey, J. A., Kawatani, Y., Lu, H., Osprey, S., and Schenzinger, V.: Surface impacts  
1490 of the Quasi Biennial Oscillation, *Atmos. Chem. Phys.*, 18, 8227–8247, doi: [10.5194/acp-18-8227-2018](https://doi.org/10.5194/acp-18-8227-2018), 2018.
- 1492 Hardiman, S. C., Butchart, N., Charlton-Perez, A. J., Shaw, T. a., Akiyoshi, H., Baumgaertner, A.,  
1493 Bekki, S., Braesicke, P., Chipperfield, M., Dameris, M., Garcia, R. R., Michou, M., Pawson,  
1494 S., Rozanov, E., and Shibata, K.: Improved predictability of the troposphere using stratospheric  
1495 final warmings, *J. Geophys. Res. Atmos.*, 116, 1–11, doi: [10.1029/2011JD015914](https://doi.org/10.1029/2011JD015914), 2011.

- 1496 Haynes, P. H., Marks, C. J., McIntyre, M. E., Shepherd, T. G., and Shine, K. P.: On the "Downward  
1497 Control" of Extratropical Diabatic Circulations by Eddy-Induced Mean Zonal Forces, *J. Atmos.*  
1498 *Sci.*, 48, 651–678, 1991.
- 1499 Hitchcock, P.: On the value of reanalyses prior to 1979 for dynamical studies, *Atmos. Chem. Phys.*  
1500 *Discuss.*, pp. 1–27, doi: [10.5194/acp-2018-879](https://doi.org/10.5194/acp-2018-879), 2018.
- 1501 Hitchcock, P.: On the value of reanalyses prior to 1979 for dynamical studies of strato-  
1502 sphere–troposphere coupling, *Atmos. Chem. Phys.*, 19, 2749–2764, doi: [10.5194/acp-19-2749-2019](https://doi.org/10.5194/acp-19-2749-2019), 2019.
- 1504 Holton, J. R. and Tan, H.-C.: The Influence of the Equatorial Quasi-Biennial Oscillation  
1505 on the Global Circulation at 50 mb, *J. Atmos. Sci.*, 37, 2200–2208, doi: [10.1175/1520-0469\(1980\)037;2200:TIOTEQ;2.0.CO;2](https://doi.org/10.1175/1520-0469(1980)037;2200:TIOTEQ;2.0.CO;2), 1980.
- 1507 Horel, J. D. and Wallace, J. M.: Planetary-Scale Atmospheric Phenomena Associated with the  
1508 Southern Oscillation, *Mon. Wea. Rev.*, 109, 813–829, 1981.
- 1509 Huck, P. E., Tilmes, S., Bodeker, G. E., Randel, W. J., McDonald, A. J., and Nakajima, H.: An im-  
1510 proved measure of ozone depletion in the Antarctic stratosphere, *J. Geophys. Res.*, 112, D11 104,  
1511 doi: [10.1029/2006JD007860](https://doi.org/10.1029/2006JD007860), URL <http://doi.wiley.com/10.1029/2006JD007860>, 2007.
- 1512 Iza, M. and Calvo, N.: Role of Stratospheric Sudden Warmings on the response to Central Pacific  
1513 El Niño, *Geophys. Res. Lett.*, 42, 2482–2489, doi: [10.1002/2014GL062935](https://doi.org/10.1002/2014GL062935), 2015.
- 1514 Iza, M., Calvo, N., and Manzini, E.: The Stratospheric Pathway of La Niña, *J. Clim.*, 29, 8899–  
1515 8914, doi: [10.1175/JCLI-D-16-0230.1](https://doi.org/10.1175/JCLI-D-16-0230.1), 2016.
- 1516 Kalnay, E., Kanamitsu, M., Kistler, R., Collins, W., Deaven, D., Gandin, L., Iredell, M., Saha, S.,  
1517 White, G., Woollen, J., Zhu, Y., Chelliah, M., Ebisuzaki, W., Higgins, W., Janowiak, J., Mo,  
1518 K. C., Ropelewski, C., Wang, J., Leetmaa, A., Reynolds, R., Jenne, R., and Joseph, D.: The  
1519 NCEP/NCAR 40-Year Reanalysis Project, *Bull. Am. Meteorol. Soc.*, 77, 437–471, 1996.
- 1520 Kanamitsu, M., Ebisuzaki, W., Woollen, J., Yang, S.-K., Hnilo, J. J., Fiorino, M., and Potter,  
1521 G. L.: NCEP–DOE AMIP-II Reanalysis (R-2), *Bull. Am. Meteorol. Soc.*, 83, 1631–1644,  
1522 doi: [10.1175/BAMS-83-11-1631](https://doi.org/10.1175/BAMS-83-11-1631), URL <http://journals.ametsoc.org/doi/10.1175/BAMS-83-11-1631>, 2002.
- 1524 Karpechko, A. Y., Hitchcock, P., Peters, D. H., and Schneidereit, A.: Predictability of Down-  
1525 ward Propagation of Major Sudden Stratospheric Warmings, *Q. J. R. Meteorol. Soc.*, 60,  
1526 doi: [10.1002/QJ.3017](https://doi.org/10.1002/QJ.3017), 2017.
- 1527 Kim, J., Son, S.-W., Gerber, E. P., and Park, H.-S.: Defining Sudden Stratospheric Warming  
1528 in Climate Models: Accounting for Biases in Model Climatologies, *J. Clim.*, 30, 5529–5546,  
1529 doi: [10.1175/JCLI-D-16-0465.1](https://doi.org/10.1175/JCLI-D-16-0465.1), 2017.
- 1530 Kobayashi, C., Endo, H., Ota, Y., Kobayashi, S., Onoda, H., Harada, Y., Onogi, K., and Kamahori,  
1531 H.: Preliminary Results of the JRA-55C, an Atmospheric Reanalysis Assimilating Conventional  
1532 Observations Only, *SOLA*, 10, 78–82, doi: [10.2151/sola.2014-016](https://doi.org/10.2151/sola.2014-016), 2014.

- 1533 Kobayashi, S., Ota, Y., Harada, Y., Ebita, A., Moriya, M., Onoda, H., Onogi, K., Kamahori,  
1534 H., Kobayashi, C., Endo, H., Miyaoka, K., and Takahashi, K.: The JRA-55 Reanalysis:  
1535 General Specifications and Basic Characteristics, *J. Meteorol. Soc. Japan. Ser. II*, 93, 5–48,  
1536 doi: [10.2151/jmsj.2015-001](https://doi.org/10.2151/jmsj.2015-001), 2015.
- 1537 Kushner, P. J.: Annular modes of the troposphere and stratosphere, *Geophys. Monogr. Ser.*, 190,  
1538 59–91, doi: [10.1029/2009GM000924](https://doi.org/10.1029/2009GM000924), 2010.
- 1539 Kushner, P. J. and Polvani, L. M.: Stratosphere-Troposphere Coupling in a Rela-  
1540 tively Simple AGCM: The Role of Eddies, *J. Clim.*, 17, 629–639, doi: [10.1175/1520-0442\(2004\)017;0629:SCIARS;2.0.CO;2](https://doi.org/10.1175/1520-0442(2004)017;0629:SCIARS;2.0.CO;2), 2004.
- 1541 Labitzke, K.: Interannual Variability of the Winter Stratosphere in the Northern Hemisphere, *Mon.  
1542 Weather Rev.*, 105, 762–770, doi: [10.1175/1520-0493\(1977\)105;0762:IVOTWS;2.0.CO;2](https://doi.org/10.1175/1520-0493(1977)105;0762:IVOTWS;2.0.CO;2),  
1543 1977.
- 1544 Lehtonen, I. and Karpechko, A. Y.: Observed and modeled tropospheric cold anomalies as-  
1545 sociated with sudden stratospheric warmings, *J. Geophys. Res. Atmos.*, 121, 1591–1610,  
1546 doi: [10.1002/2015JD023860](https://doi.org/10.1002/2015JD023860), 2016.
- 1547 Lim, E., Hendon, H. H., and Thompson, D. W. J.: Seasonal Evolution of Stratosphere-Troposphere  
1548 Coupling in the Southern Hemisphere and Implications for the Predictability of Surface Climate,  
1549 *J. Geophys. Res. Atmos.*, 123, 12,002–12,016, doi: [10.1029/2018JD029321](https://doi.org/10.1029/2018JD029321), 2018.
- 1550 Limpasuvan, V., Thompson, D. W. J., and Hartmann, D. L.: The Life Cycle of the Northern  
1551 Hemisphere Sudden Stratospheric Warmings, *J. Clim.*, 17, 2584–2596, doi: [10.1175/1520-0442\(2004\)017;2584:TLCCOTN;2.0.CO;2](https://doi.org/10.1175/1520-0442(2004)017;2584:TLCCOTN;2.0.CO;2), 2004.
- 1552 Long, C. S., Fujiwara, M., Davis, S., Mitchell, D. M., and Wright, C. J.: Climatology and interan-  
1553 nual variability of dynamic variables in multiple reanalyses evaluated by the SPARC Reanalysis  
1554 Intercomparison Project (S-RIP), *Atmos. Chem. Phys.*, 17, 14 593–14 629, doi: [10.5194/acp-17-14593-2017](https://doi.org/10.5194/acp-17-14593-2017), 2017.
- 1555 Lu, H., Bracegirdle, T. J., Phillips, T., and Turner, J.: A Comparative Study of Wave Forcing  
1556 Derived from the ERA-40 and ERA-Interim Reanalysis Datasets, *J. Clim.*, 28, 2291–2311, 2015.
- 1557 Marshall, G. J.: Trends in the Southern Annular Mode from Observations and Reanalyses, *J.  
1558 Climate*, 16, 4134–4143, 2003.
- 1559 Martineau, P.: S-RIP: Zonal-mean dynamical variables of global atmospheric  
1560 reanalyses on pressure levels., Centre for Environmental Data Analysis,  
1561 doi: [10.5285/b241a7f536a244749662360bd7839312](https://doi.org/10.5285/b241a7f536a244749662360bd7839312), URL <http://dx.doi.org/10.5285/b241a7f536a244749662360bd7839312>, 2017.
- 1562 Martineau, P. and Son, S.-W.: Quality of reanalysis data during stratospheric vortex weakening  
1563 and intensification events, *Geophys. Res. Lett.*, 37, doi: [10.1029/2010GL045237](https://doi.org/10.1029/2010GL045237), 2010.
- 1564
- 1565
- 1566
- 1567

- 1568 Martineau, P. and Son, S.-W.: Onset of Circulation Anomalies during Stratospheric Vortex Weak-  
1569 ening Events: The Role of Planetary-Scale Waves, *J. Clim.*, 28, 7347–7370, doi: [10.1175/JCLI-D-14-00478.1](https://doi.org/10.1175/JCLI-D-14-00478.1), 2015.
- 1570
- 1571 Martineau, P., Son, S.-W., and Taguchi, M.: Dynamical Consistency of Reanalysis Datasets in the  
1572 Extratropical Stratosphere, *J. Clim.*, 29, 3057–3074, doi: [10.1175/JCLI-D-15-0469.1](https://doi.org/10.1175/JCLI-D-15-0469.1), 2016.
- 1573 Martineau, P., Chen, G., Son, S.-W., and Kim, J.: Lower-Stratospheric Control of the Fre-  
1574 quency of Sudden Stratospheric Warming Events, *J. Geophys. Res. Atmos.*, 123, 3051–3070,  
1575 doi: [10.1002/2017JD027648](https://doi.org/10.1002/2017JD027648), 2018a.
- 1576 Martineau, P., Son, S.-W., Taguchi, M., and Butler, A. H.: A comparison of the momentum budget  
1577 in reanalysis datasets during sudden stratospheric warming events, *Atmos. Chem. Phys.*, 18,  
1578 7169–7187, doi: [10.5194/acp-18-7169-2018](https://doi.org/10.5194/acp-18-7169-2018), 2018b.
- 1579 Martineau, P., Wright, J. S., Zhu, N., and Fujiwara, M.: Zonal-mean data set of global atmospheric  
1580 reanalyses on pressure levels, *Earth Syst. Sci. Data*, 10, 1925–1941, doi: [10.5194/essd-10-1925-2018](https://doi.org/10.5194/essd-10-1925-2018), 2018c.
- 1581
- 1582 Martius, O., Polvani, L. M., and Davies, H. C.: Blocking precursors to stratospheric sudden warm-  
1583 ing events, *Geophys. Res. Lett.*, 36, doi: [10.1029/2009GL038776](https://doi.org/10.1029/2009GL038776), 2009.
- 1584 Matsuno, T.: A Dynamical Model of the Stratospheric Sudden Warming, *J. Atmos. Sci.*, 28, 1479–  
1585 1491, 1971.
- 1586 Matthewman, N. J. and Esler, J. G.: Stratospheric Sudden Warmings as Self-Tuning Resonances.  
1587 Part I: Vortex Splitting Events, *J. Atmos. Sci.*, 68, 2481–2504, doi: [10.1175/JAS-D-11-071](https://doi.org/10.1175/JAS-D-11-071),  
1588 2011.
- 1589 Matthewman, N. J., Esler, J. G., Charlton-Perez, a. J., and Polvani, L. M.: A New Look at Strato-  
1590 spheric Sudden Warmings. Part III: Polar Vortex Evolution and Vertical Structure, *J. Clim.*, 22,  
1591 1566–1585, doi: [10.1175/2008JCLI2365.1](https://doi.org/10.1175/2008JCLI2365.1), 2009.
- 1592 Maycock, A. C. and Hitchcock, P.: Do split and displacement sudden stratospheric warm-  
1593 ings have different annular mode signatures?, *Geophys. Res. Lett.*, 42, 10,943–10,951,  
1594 doi: [10.1002/2015GL066754](https://doi.org/10.1002/2015GL066754), 2015.
- 1595 McDaniel, B. A. and Black, R. X.: Intraseasonal Dynamical Evolution of the Northern Annular  
1596 Mode, *J. Clim.*, 18, 3820–3839, doi: [10.1175/JCLI3467.1](https://doi.org/10.1175/JCLI3467.1), 2005.
- 1597 McInturff, R. M.: Stratospheric warmings: Synoptic, dynamic and general-circulation aspects,  
1598 NASA Reference Publ. NASA-RP-1017, p. 174, URL <https://ntrs.nasa.gov/archive/nasa/casi.ntrs.nasa.gov/19780010687.pdf>, 1978.
- 1600 McIntyre, E.: How well do we Understand the Dynamics of Stratospheric Warmings, *J. Meteorol.*  
1601 Soc. Japan, pp. 37–65, 1982.
- 1602 McIntyre, M. and Palmer, T.: The 'surf zone' in the stratosphere, *J. Atmos. Terr. Phys.*, 46, 1984.

- 1603 McIntyre, M. E. and Palmer, T. N.: Breaking planetary waves in the stratosphere, *Nature*, 305,  
1604 593–600, doi: [10.1038/305593a0](https://doi.org/10.1038/305593a0), 1983.
- 1605 Mitchell, D. M., Charlton-Perez, A. J., and Gray, L. J.: Characterizing the variability and extremes  
1606 of the stratospheric polar vortices using 2D moment analysis, *J. Atmos. Sci.*, 68, 1194–1213,  
1607 2011.
- 1608 Mitchell, D. M., Gray, L. J., Anstey, J., Baldwin, M. P., and Charlton-Perez, A. J.: The Influence of  
1609 Stratospheric Vortex Displacements and Splits on Surface Climate, *J. Climate*, 26, 2668–2682,  
1610 doi: [10.1175/JCLI-D-12-00030.1](https://doi.org/10.1175/JCLI-D-12-00030.1), 2013.
- 1611 Mitchell, D. M., Gray, L. J., Fujiwara, M., Hibino, T., Anstey, J. a., Ebisuzaki, W., Harada, Y.,  
1612 Long, C., Misios, S., Stott, P. a., and Tan, D.: Signatures of naturally induced variability in  
1613 the atmosphere using multiple reanalysis datasets, *Q. J. R. Meteorol. Soc.*, 141, 2011–2031,  
1614 doi: [10.1002/qj.2492](https://doi.org/10.1002/qj.2492), 2015.
- 1615 Nishii, K., Nakamura, H., and Miyasaka, T.: Modulations in the planetary wave field induced  
1616 by upward-propagating Rossby wave packets prior to stratospheric sudden warming events: A  
1617 case-study, *Quart. J. Roy. Meteor. Soc.*, 135, 39–52, doi: [10.1002/qj.359](https://doi.org/10.1002/qj.359), 2009.
- 1618 Nishii, K., Nakamura, H., and Orsolini, Y. J.: Geographical Dependence Observed in Blocking  
1619 High Influence on the Stratospheric Variability through Enhancement and Suppression of Up-  
1620 ward Planetary-Wave Propagation, *J. Clim.*, 24, 6408–6423, doi: [10.1175/JCLI-D-10-05021.1](https://doi.org/10.1175/JCLI-D-10-05021.1),  
1621 2011.
- 1622 Omrani, N. E., Keenlyside, N. S., Bader, J., and Manzini, E.: Stratosphere key for winter-  
1623 time atmospheric response to warm Atlantic decadal conditions, *Clim. Dyn.*, 42, 649–663,  
1624 doi: [10.1007/s00382-013-1860-3](https://doi.org/10.1007/s00382-013-1860-3), 2014.
- 1625 Onogi, K., Tsutsui, J., Koide, H., Sakamoto, M., Kobayashi, S., Hatsushika, H., Matsumoto, T.,  
1626 Yamazaki, N., Kamahori, H., Takahashi, K., Kadokura, S., Wada, K., Kato, K., Oyama, R., Ose,  
1627 T., Mannaji, N., and Taira, R.: The JRA-25 Reanalysis, *J. Meteor. Soc. Japan*, 85, 369–432,  
1628 2007.
- 1629 Orr, A., Bracegirdle, T. J., Hosking, J. S., Jung, T., Haigh, J. D., Phillips, T., and Feng, W.:  
1630 Possible Dynamical Mechanisms for Southern Hemisphere Climate Change due to the Ozone  
1631 Hole, *J. Atmos. Sci.*, 69, 2917–2932, doi: [10.1175/JAS-D-11-0210.1](https://doi.org/10.1175/JAS-D-11-0210.1), 2012.
- 1632 Palmeiro, F. M., Barriopedro, D., García-Herrera, R., and Calvo, N.: Comparing Sudden Strato-  
1633 spheric Warming Definitions in Reanalysis Data\*, *J. Clim.*, 28, 6823–6840, doi: [10.1175/JCLI-D-15-0004.1](https://doi.org/10.1175/JCLI-D-15-0004.1), 2015.
- 1635 Plumb, R. A.: On the seasonal cycle of stratospheric planetary waves, *Pure Appl. Geophys. PA-*  
1636 *GEOPH*, 130, 233–242, doi: [10.1007/BF00874457](https://doi.org/10.1007/BF00874457), 1989.
- 1637 Plumb, R. A.: Planetary Waves and the Extratropical Winter Stratosphere, *Geophys. Monogr. Ser.*,  
1638 pp. 23–41, doi: [10.1002/9781118666630.ch2](https://doi.org/10.1002/9781118666630.ch2), 2010.

- 1639 Poli, P., Hersbach, H., Dee, D. P., Berrisford, P., Simmons, A. J., Vitart, F., Laloyaux, P., Tan,  
1640 D. G. H., Peubey, C., Thépaut, J. N., Trémolet, Y., Hólm, E. V., Bonavita, M., Isaksen, L.,  
1641 and Fisher, M.: ERA-20C: An atmospheric reanalysis of the twentieth century, *J. Clim.*, 29,  
1642 4083–4097, doi: [10.1175/JCLI-D-15-0556.1](https://doi.org/10.1175/JCLI-D-15-0556.1), 2016.
- 1643 Polvani, L. M. and Waugh, D. W.: Upward Wave Activity Flux as a Precursor to Extreme Strato-  
1644 spheric Events and Subsequent Anomalous Surface Weather Regimes, *J. Clim.*, 17, 3548–3554,  
1645 doi: [10.1175/1520-0442\(2004\)017;3548:UWAFAA;2.0.CO;2](https://doi.org/10.1175/1520-0442(2004)017;3548:UWAFAA;2.0.CO;2), 2004.
- 1646 Polvani, L. M., Sun, L., Butler, A. H., Richter, J. H., and Deser, C.: Distinguishing stratospheric  
1647 sudden warmings from ENSO as key drivers of wintertime climate variability over the North  
1648 Atlantic and Eurasia, *J. Clim.*, doi: [10.1175/JCLI-D-16-0277.1](https://doi.org/10.1175/JCLI-D-16-0277.1), 2017.
- 1649 Ramaswamy, V., Chanin, M.-L., Angell, J., Barnett, J., Gaffen, D., Gelman, M., Keckhut, P.,  
1650 Koshelkov, Y., Labitzke, K., Lin, J.-J. R., O'Neill, A., Nash, J., Randel, W., Rood, R., Shine,  
1651 K., Shiotani, M., and Swinbank, R.: Stratospheric temperature trends: Observations and model  
1652 simulations, *Rev. Geophys.*, 39, 71–122, doi: [10.1029/1999RG000065](https://doi.org/10.1029/1999RG000065), 2001.
- 1653 Randel, W. J.: The seasonal evolution of planetary waves in the Southern Hemisphere stratosphere  
1654 and troposphere, *Q. J. R. Meteorol. Soc.*, 587, 1385–1409, doi: [10.1002/qj.49711448403](https://doi.org/10.1002/qj.49711448403), 1988.
- 1655 Rao, J., Garfinkel, C. I., and Ren, R.: Modulation of the Northern Winter Stratospheric El  
1656 Niño–Southern Oscillation Teleconnection by the PDO, *J. Clim.*, pp. JCLI-D-19-0087.1,  
1657 doi: [10.1175/JCLI-D-19-0087.1](https://doi.org/10.1175/JCLI-D-19-0087.1), 2019.
- 1658 Richter, J. H., Matthes, K., Calvo, N., and Gray, L. J.: Influence of the quasi-biennial oscilla-  
1659 tion and El Niño–Southern Oscillation on the frequency of sudden stratospheric warmings, *J.  
1660 Geophys. Res.*, 116, D20 111, doi: [10.1029/2011JD015757](https://doi.org/10.1029/2011JD015757), 2011.
- 1661 Rienecker, M. M., Suarez, M. J., Gelaro, R., Todling, R., Bacmeister, J., Liu, E., Bosilovich, M. G.,  
1662 Schubert, S. D., Takacs, L., Kim, G. K., Bloom, S., Chen, J., Collins, D., Conaty, A., Da Silva,  
1663 A., Gu, W., Joiner, J., Koster, R. D., Lucchesi, R., Molod, A., Owens, T., Pawson, S., Pegion, P.,  
1664 Redder, C. R., Reichle, R., Robertson, F. R., Ruddick, A. G., Sienkiewicz, M., and Woollen, J.:  
1665 MERRA: NASA's modern-era retrospective analysis for research and applications, *J. Clim.*, 24,  
1666 3624–3648, 2011.
- 1667 Saha, S., Moorthi, S., Pan, H.-L., Wu, X., Wang, J., Nadiga, S., Tripp, P., Kistler, R., Woollen,  
1668 J., Behringer, D., Liu, H., Stokes, D., Grumbine, R., Gayno, G., Wang, J., Hou, Y.-T., Chuang,  
1669 H.-Y., Juang, H.-M. H., Sela, J., Iredell, M., Treadon, R., Kleist, D., Van Delst, P., Keyser, D.,  
1670 Derber, J., Ek, M., Meng, J., Wei, H., Yang, R., Lord, S., Van Den Dool, H., Kumar, A., Wang,  
1671 W., Long, C., Chelliah, M., Xue, Y., Huang, B., Schemm, J.-K., Ebisuzaki, W., Lin, R., Xie, P.,  
1672 Chen, M., Zhou, S., Higgins, W., Zou, C.-Z., Liu, Q., Chen, Y., Han, Y., Cucurull, L., Reynolds,  
1673 R. W., Rutledge, G., and Goldberg, M.: The NCEP Climate Forecast System Reanalysis, *Bull.  
1674 Am. Meteorol. Soc.*, 91, 1015–1057, doi: [10.1175/2010BAMS3001.1](https://doi.org/10.1175/2010BAMS3001.1), 2010.
- 1675 Saha, S., Moorthi, S., Wu, X., Wang, J., Nadiga, S., Tripp, P., Behringer, D., Hou, Y.-T., ya Chuang,  
1676 H., Iredell, M., Ek, M., Meng, J., Yang, R., Mendez, M. P., van den Dool, H., Zhang, Q., Wang,

- 1677 W., Chen, M., and Becker, E.: The NCEP Climate Forecast System Version 2, *J. Climate*, 27,  
1678 2185–2208, doi: [10.1175/JCLI-D-12-00823.1](https://doi.org/10.1175/JCLI-D-12-00823.1), 2014.
- 1679 Scherhag, R.: Die Explosionsartige Stratosphärenerwärmung des Spätwinters 1951/52, *Ber. Dtsch.  
1680 Wetterdienstes U.S. Zone*, 6, 51–63, 1952.
- 1681 Seviour, W. J. M., Mitchell, D. M., and Gray, L. J.: A practical method to identify dis-  
1682 placed and split stratospheric polar vortex events, *Geophys. Res. Lett.*, 40, 5268–5273,  
1683 doi: [10.1002/grl.50927](https://doi.org/10.1002/grl.50927), 2013.
- 1684 Sigmond, M., Scinocca, J. F., Kharin, V. V., and Shepherd, T. G.: Enhanced seasonal forecast skill  
1685 following stratospheric sudden warmings, *Nat. Geosci.*, 6, 1–5, doi: [10.1038/ngeo1698](https://doi.org/10.1038/ngeo1698), 2013.
- 1686 Smith, K. L. and Kushner, P. J.: Linear interference and the initiation of extratropical stratosphere-  
1687 troposphere interactions, *J. Geophys. Res.*, 117, doi: [10.1029/2012JD017587](https://doi.org/10.1029/2012JD017587), 2012.
- 1688 Son, S.-W., Gerber, E. P., Perlitz, J., Polvani, L. M., Gillet, N., Seo, K.-Y., Eyring, V., Shepherd,  
1689 T. G., Waugh, D., Akiyoshi, H., Austin, J., Baumgaertner, A., Bekki, S., Braesicke, P., Brühl,  
1690 C., Butchart, N., Chipperfield, M. P., Cugnet, D., Dameris, M., Dhomse, S., Frith, S., Garny, H.,  
1691 Garcia, R., Hardiman, S. C., Jöckel, P., Lamarque, J. F., Mancini, E., Marchand, M., Michou,  
1692 M., Nakamura, T., Morgenstern, O., Pitari, G., Plummer, D. A., Pyle, J., and J. F. Scinocca, E. R.,  
1693 Shibata, K., Smale, D., Teyssèdre, H., Tian, W., and Yamashita, Y.: The Impact of Stratospheric  
1694 Ozone on Southern Hemisphere Circulation Change: A Multimodel Assessment, *J. Geophys.  
1695 Res.*, 115, D00M07, doi: [10.1029/2010JD014271](https://doi.org/10.1029/2010JD014271), 2010.
- 1696 Son, S.-W., Han, B.-R., Garfinkel, C. I., Kim, S.-Y., Park, R., Abraham, N. L., Akiyoshi, H.,  
1697 Archibald, A. T., Butchart, N., Chipperfield, M. P., Dameris, M., Deushi, M., Dhomse, S. S.,  
1698 Hardiman, S. C., Jöckel, P., Kinnison, D., Michou, M., Morgenstern, O., O'Connor, F. M.,  
1699 Oman, L. D., Plummer, D. A., Pozzer, A., Revell, L. E., Rozanov, E., Stenke, A., Stone, K.,  
1700 Tilmes, S., Yamashita, Y., and Zeng, G.: Tropospheric jet response to Antarctic ozone depletion:  
1701 An update with Chemistry-Climate Model Initiative (CCMI) models, *Environ. Res. Lett.*, 13,  
1702 054024, doi: [10.1088/1748-9326/aabf21](https://doi.org/10.1088/1748-9326/aabf21), 2018.
- 1703 Song, K. and Son, S. W.: Revisiting the ENSO-SSW relationship, *J. Clim.*, 31, 2133–2143,  
1704 doi: [10.1175/JCLI-D-17-0078.1](https://doi.org/10.1175/JCLI-D-17-0078.1), 2018.
- 1705 Song, Y. and Robinson, W. A.: Dynamical Mechanisms for Stratospheric Influences on the Tropo-  
1706 sphere, *J. Atmos. Sci.*, 61, 1711–1725, 2004.
- 1707 Sun, L. and Robinson, W. a.: Downward influence of stratospheric final warming events in an  
1708 idealized model, *Geophys. Res. Lett.*, 36, L03819, doi: [10.1029/2008GL036624](https://doi.org/10.1029/2008GL036624), URL <http://doi.wiley.com/10.1029/2008GL036624>, 2009.
- 1709 Taguchi, M.: Changes in Frequency of Major Stratospheric Sudden Warmings with El  
1710 Niño/Southern Oscillation and Quasi-Biennial Oscillation, *J. Meteorol. Soc. Japan. Ser. II*, 93,  
1711 99–115, doi: [10.2151/jmsj.2015-007](https://doi.org/10.2151/jmsj.2015-007), 2015.
- 1712 Taguchi, M. and Hartmann, D. L.: Increased Occurrence of Stratospheric Sudden Warmings during  
1713 El Niño as Simulated by WACCM, *J. Clim.*, 19, 324–332, doi: [10.1175/JCLI3655.1](https://doi.org/10.1175/JCLI3655.1), 2006.

- 1715 Thiéblemont, R., Ayarzagüena, B., Matthes, K., Bekki, S., Abalichin, J., and Langematz, U.:  
1716 Drivers and Surface Signal of Interannual Variability of Boreal Stratospheric Final Warmings, J.  
1717 Geophys. Res. Atmos., p. 2018JD029852, doi: [10.1029/2018JD029852](https://doi.org/10.1029/2018JD029852), 2019.
- 1718 Thompson, D. W. J. and Solomon, S.: Interpretation of recent Southern Hemisphere Climate  
1719 Change, Science, 296, 895–899, 2002.
- 1720 Thompson, D. W. J. and Wallace, J. M.: The Arctic Oscillation signature in the wintertime geopo-  
1721 tential height and temperature fields., Geophys. Res. Lett., 25, 1297–1300, 1998.
- 1722 Thompson, D. W. J. and Wallace, J. M.: Annular modes in the extratropical circulation. Part I:  
1723 Month-to-month variability., J. Climate, 13, 1000–1016, 2000.
- 1724 Thompson, D. W. J., Solomon, S., Kushner, P. J., England, M. H., Grise, K. M., and Karoly, D. J.:  
1725 Signatures of the Antarctic ozone hole in Southern Hemisphere surface climate change, Nat.  
1726 Geosci., 4, 741–749, doi: [10.1038/ngeo1296](https://doi.org/10.1038/ngeo1296), 2011.
- 1727 Tripathi, O. P., Charlton-Perez, A., Sigmond, M., and Vitart, F.: Enhanced long-range forecast  
1728 skill in boreal winter following stratospheric strong vortex conditions, Environ. Res. Lett., 10,  
1729 doi: [10.1088/1748-9326/10/10/104007](https://doi.org/10.1088/1748-9326/10/10/104007), 2015.
- 1730 Uppala, S. M., Kallberg, P. W., Simmons, A. J., Andrae, U., Bechtold, V. D. C., Fiorino, M.,  
1731 Gibson, J. K., Haseler, J., Hernandez, A., Kelly, G. A., Li, X., Onogi, K., Saarinen, S., Sokka,  
1732 N., Allan, R. P., Andersson, E., Arpe, K., Balmaseda, M. A., Beljaars, A. C. M., Berg, L. V. D.,  
1733 Bidlot, J., Bormann, N., Caires, S., Chevallier, F., Dethof, A., Dragosavac, M., Fisher, M.,  
1734 Fuentes, M., Hagemann, S., Holm, E., Hoskins, B. J., Isaken, L., Janssen, P. A. E. M., Jenne,  
1735 R., McNally, A. P., Mahfouf, J. F., Morcrette, J. J., Rayner, N. A., Saunders, R. W., Simon, P.,  
1736 Sterl, A., Trenberth, K. E., Untch, A., Vasiljevic, D., Viterbo, P., and Woollen, J.: The ERA-40  
1737 re-analysis, Q. J. R. Meteorol. Soc., 131, 2961–3012, 2005.
- 1738 Waugh, D. W.: Elliptical diagnostics of stratospheric polar vortices, Q. J. R. Meteorol. Soc., 123,  
1739 1725–1748, 1997.
- 1740 Waugh, D. W. and Randel, W. J.: Climatology of Arctic and Antarctic Polar Vor-  
1741 tices Using Elliptical Diagnostics, J. Atmos. Sci., 56, 1594–1613, doi: [10.1175/1520-0469\(1999\)056;1594:COAAAP;2.0.CO;2](https://doi.org/10.1175/1520-0469(1999)056;1594:COAAAP;2.0.CO;2), 1999.
- 1743 Waugh, D. W., Sobel, A. H., and Polvani, L. M.: What Is the Polar Vortex and How Does It  
1744 Influence Weather?, Bull. Am. Meteorol. Soc., 98, 37–44, doi: [10.1175/BAMS-D-15-00212.1](https://doi.org/10.1175/BAMS-D-15-00212.1),  
1745 2017.
- 1746 Weinberger, I., Garfinkel, C. I., White, I. P., and Oman, L. D.: The salience of nonlinear-  
1747 ities in the boreal winter response to ENSO: Arctic stratosphere and Europe, Clim. Dyn.,  
1748 doi: [10.1007/s00382-019-04805-1](https://doi.org/10.1007/s00382-019-04805-1), 2019.
- 1749 White, I., Garfinkel, C. I., Gerber, E. P., Jucker, M., Aquila, V., and Oman, L. D.: The downward  
1750 influence of sudden stratospheric warmings: Association with tropospheric precursors, J. Clim.,  
1751 32, 85–108, doi: [10.1175/JCLI-D-18-0053.1](https://doi.org/10.1175/JCLI-D-18-0053.1), 2019.

- 1752 Woo, S.-H., Sung, M.-K., Son, S.-W., and Kug, J.-S.: Connection between weak stratospheric vor-  
1753 tex events and the Pacific Decadal Oscillation, *Clim. Dyn.*, pp. 3481–3492, doi: [10.1007/s00382-015-2551-z](https://doi.org/10.1007/s00382-015-2551-z), 2015.
- 1755 Woollings, T., Hannachi, A., Hoskins, B., and Turner, A.: A regime view of the North  
1756 Atlantic oscillation and its response to anthropogenic forcing, *J. Clim.*, 23, 1291–1307,  
1757 doi: [10.1175/2009JCLI3087.1](https://doi.org/10.1175/2009JCLI3087.1), 2010.
- 1758 Woollings, T., Barriopedro, D., Methven, J., Son, S.-W., Martius, O., Harvey, B., Sillmann, J.,  
1759 Lupo, A. R., and Seneviratne, S.: Blocking and its Response to Climate Change, *Curr. Clim.  
1760 Chang. Reports*, 4, 287–300, doi: [10.1007/s40641-018-0108-z](https://doi.org/10.1007/s40641-018-0108-z), 2018.
- 1761 Yoden, S., Taguchi, M., and Naito, Y.: Numerical Studies on Time Variations of the Troposphere-  
1762 Stratosphere Coupled System., *J. Meteorol. Soc. Japan*, 80, 811–830, doi: [10.2151/jmsj.80.811](https://doi.org/10.2151/jmsj.80.811),  
1763 2002.